Carbonate formation in the ocean crust as a proxy for water-rock interactions

Dissertation
zur Erlangung des Doktorgrades
der Naturwissenschaften
– Dr. rer. nat. –

Am Fachbereich Geowissenschaften
der Universität Bremen

vorgelegt von

Benjamin Eickmann

Bremen, März 2009

Tag des öffentlichen Kolloquiums

06.04.2009

Gutachter der Dissertation

Prof. Dr. Jörn Peckmann

Prof. Dr. Wolfgang Bach

Prüfer

Prof. Dr. Kai-Uwe Hinrichs

Prof. Dr. Reinhard X. Fischer

Weitere Mitglieder des Prüfungsausschusses

PD Dr. Sabine Kasten

Matthias Kellermann

TABLE OF CONTENTS

ABSTRACT 1

KURZFASSUNG 3

I. INTRODUCTION 6

1. General aspects of carbonate formation in the ocean crust 6

1.1. Carbonate formation in ultramafic environments and the influence of serpentinization ... 8

2. Carbonate geochemistry as a proxy for sub seafloor mixing 13

2.1. Stable O and C isotope geochemistry 13

2.2. Sr isotopes 15

2.3. Rare earth elements 17

2.4. Mg/Ca and Sr/Ca ratios 19

II. SCIENTIFIC OBJECTIVES AND OUTLINE OF THIS THESIS 21

III. MANUSCRIPTS 23

3. Authigenesis of carbonate minerals in modern and Devonian ocean-floor hard rocks 23

3.1. Introduction 24

3.2. Geological setting 26

3.3. Materials and methods 28

3.4. Carbonate petrography 31

3.5. Stable Isotope Geochemistry 37

3.6. Carbonate Formation in Ultramafic Rocks: Mid-Ocean Ridge and Frankenwald 38

3.7. Hints for Biogenicity of Mineral Phases from the Logatchev Hydrothermal Field 41

3.8. Conclusions 43

Acknowledgments 45

4. Geochemical constraints on the modes of carbonate formation in peridotites from the Logatchev Hydrothermal Vent Field and Gakkel Ridge 46

4.1. Introduction 47

4.2. Geological background 49

4.3. Samples and analytical methods 51

4.3.1. Samples 51

4.3.2. Analytical methods 51

4.3.3. Mixing model 53

4.4. Results 54

4.4.1. Strontium isotope ratios 54

4.4.2. Minor and trace element contents 56

4.5. Discussion 58
4.5.1. Basement fluid evolution inferred from Sr isotope ratios and stable isotopes 58
4.5.2. Rare earth elements of carbonates at mid-ocean ridges 62
4.5.3. Compositional evolution of carbonates and calculated composition of sub seafloor fluids 65
4.6. Conclusions 67
Acknowledgments 68
5. Widespread cryptoendolithic life in Devonian pillow basalts 69
5.1. Introduction 70
5.2. Geological setting 72
5.3. Methods 73
5.4. Results 73
5.5. Discussion 77
5.5.1. Volcanic rocks as a niche of life 77
5.5.2. How widespread were basalt-hosted ecosystems? 80
5.6. Conclusions 80
Acknowledgements 81
IV. GENERAL CONCLUSIONS AND OUTLOOK 82
General conclusions 83
Outlook 85
V. REFERENCES 88
ACKNOWLEDGEMENTS 99
ERKLÄRUNG 101

ABSTRACT

The main objective of this thesis was to elucidate the authigenesis of carbonate minerals in modern and Devonian ocean-floor volcanic rocks and to demonstrate that Late Devonian (Frasnian) pillow basalts from the Saxothuringian zone once harbored microbial life. The ultramafic-hosted Logatchev hydrothermal field (LHF) at the Mid-Atlantic Ridge, the Arctic Gakkel Ridge (GR) and the Late Devonian Frankenwald feature carbonate precipitates (aragonite, calcite, dolomite) in voids and fractures of different types of rocks. Carbonate veins cut the rock texture, postdating the emplacement and serpentinization of the upper mantle rocks. Petrographic and stable isotope ($\delta^{13}C$, $\delta^{18}O$) patterns were compared in an attempt to understand the genesis of carbonate minerals in these settings. Specifically, were the carbonate sample from the modern seafloor settings and the Devonian analogue of hydrothermal origin, low-temperature abiogenic or biogenic origin? Aragonite is the most abundant carbonate mineral in serpentnites from the LHF and GR and occurs within massive sulfides of the LHF. $\delta^{18}O$ values of aragonite hosted in serpentinites and sulfides are consistent with precipitation from cold seawater. Most of the corresponding $\delta^{13}C$ values indicate a marine carbon source, while $\delta^{13}C$ values of sulfide-hosted aragonite as high as +3.6‰ may reflect residual carbon dioxide in the zone of methanogenesis. Calcite veins from LHF, by contrast, have low $\delta^{18}O$ values (as low as −20.0‰) and $\delta^{13}C$ values (as low as −5.8‰) indicative of precipitation from hydrothermal solutions dominated by magmatic carbon dioxide. To gain deeper insights in the formation of carbonates in hydrothermal environments, chemical and strontium isotopic composition of these different carbonates were analyzed to examine the conditions that led to their formation. Seawater-like $^{87}Sr/^{86}Sr$ ratios of aragonite in serpentinites from LHF are similar to those of aragonite from the GR, indicating aragonite formation from seawater at ambient conditions at both sites. Aragonite veins in sulfides from LHF also have seawater-like $^{87}Sr/^{86}Sr$ ratios, however, the rare earth element (REE) patterns show a clear positive europium (Eu) anomaly indicative of small (<1%) proportions of hydrothermal fluids. In contrast to aragonite, dolomite and calcite from the LHF precipitated at much higher temperatures, indicative of formation from evolved hydrothermal fluids. A simple mixing model based on strontium mass balance and enthalpy conservation indicates strongly variable conditions of fluid mixing and heat transfers involved in carbonate formation. Aragonite

samples corroborate the stable isotope patterns and formed at low temperatures form pure seawater. Dolomite precipitated from a mixture of 97% seawater and 3% hydrothermal fluid that indicate conductive heating, probably of seawater prior to mixing. Hydrothermal serpentinite-hosted calcite formed from a mixture of 67% hydrothermal fluid and 33% seawater due to conductive cooling of hydrothermal fluid effusing a fault. REE patterns corroborate the results of the mixing model; since the calcite that formed from waters with the greatest hydrothermal contribution have REE that closely resemble those of vent fluids from the LHF.

$\delta^{13}C$ values of Late Devonian (Frasnian) calcite hosted in basalts indicate precipitation from seawater, while $\delta^{13}C$ values of serpentinite-hosted calcite agree with mantle-derived carbon dioxide with a contribution of amagmatic carbon (for values low as −8.6‰), presumably methane. Low $\delta^{18}O$ values reflect diagenetic and metamorphic overprinting. Furthermore, Late Devonian pillow basalts from the Saxothuringian zone were found to contain abundant putative biogenic filaments, indicating that the volcanic rocks once harbored microbial life. The mineralized filaments are found in carbonate-filled vesicles, where they start to form on internal surfaces after seawater ingress. A biogenic origin of filaments is indicated by their size and morphology resembling modern microorganisms, their independence of crystal faces and cleavage plans, complex branching patterns, and internal segmentation. They became preserved upon microbial clay authigenesis similar to the encrustation of modern prokaryotes in iron-rich environments.

The results presented in this thesis give rise to a new and better understanding of carbonate formation in the ocean crust, especially in ultramafic-hosted hydrothermal environments. Further, the results highlight the important of mixing processes in the subseafloor of hydrothermal systems that led to the formation of carbonates and highlights that seafloor basalt may thus represent a common, perhaps universal niche for life in the oceanic crust.

KURZFASSUNG

Der Schwerpunkt dieser Arbeit liegt auf der Analyse authigener Karbonatminerale in rezenter und devonischer ozeanischer Kruste sowie der Beschreibung mikrobieller Habitate in devonischen Pillowbasalten. Karbonateminerale (Aragonit, Calcit, Dolomit) bildeten sich in verschiedenen Gesteinen (Serpentinite, Basalte, Sulfidbrekzien, Talusbrekzien) des Logatchev Hydrothermalfeldes (LHF) am Mittelatlantischen Rücken, des arktischen Gakkelrückens (GR) sowie des Frankenwaldes. Sie bildeten sich bevorzugt in Klüften und durchgzogen als Karbonatadern das Gestein, oder verfüllten Hohlräume. Die Bildung der Karbonate ist ein später Prozess, der sich dem Herausheben ehemaliger Gesteine des oberen Erdmantels und der darauffolgenden Serpentinisierung anschließt. Sowohl petrographische Untersuchungen als auch die Analyse stabiler Isotope ($\delta^{13}C$, $\delta^{18}O$) wurden herangezogen, um die genaue Genese der Karbonatminerale zu klären. Hierbei ging es in erster Linie um die Fragestellung, ob es sich bei den rezenten Karbonaten und deren devonischen Äquivalenten um hydrothermale Bildungen oder um Niedrigtemperaturbildungen abiogenen oder biogenen Ursprungs handelt. Das häufigste Karbonatmineral in Serpentiniten des LHF und des GR, sowie in massiven Sulfiden des LHF ist Aragonit. $\delta^{18}O$-Werte für Aragonit in Serpentiniten als auch in Sulfiden deuten daraufhin, dass der Aragonit bei niedrigen Temperaturen aus dem Meerwaser ausgefällt wurde. Diese Annahme wird durch dadurch gestützt, dass die meisten $\delta^{13}C$-Werte eine marine Kohlenstoffquelle anzeigen. Jedoch deuten hohe $\delta^{13}C$-Werte (Aragonit in den Sulfiden) auf residualen Kohlenstoff als Quelle hin, der durch Methanogenese an ^{13}C angereichert wird. Im Gegensatz dazu zeigt der Calcit niedrige $\delta^{18}O$- (−20.0‰) und $\delta^{13}C$-Werte (−5.8‰), welche eine Fällung aus hydrothermalen Fluiden und magmatischen Kohlenstoff anzeigen. Um ein tieferes Verständnis über die genauen Blidungsmechanismen zu bekommen, wurden die chemische Zusammensetzung und die Strontiumisotopie der unterschiedlichen Karbonate bestimmt. Die $^{87}Sr/^{86}Sr$-Verhältnisse im Aragonit (Serpentinit), sowohl im LHF als auch am GR gleichen sich, welches zum einen für eine Fällung aus Meerwasser und zum anderen für gleiche Bedingungen in den beiden Gebieten spricht. Auch das $^{87}Sr/^{86}Sr$-Verhältnis des Aragonits in den Sulfiden im LHF zeigt eine Meerwassersignatur, doch die Muster der Seltenen Erden (REE) weisen eine positive Europiumanomalie (Eu) auf. Dies spricht für eine geringe (<1%) Beeinflussung durch hydrothermale Fluide. Im Gegensatz

dazu wurden der Calcit und der Dolomit unter deutlich höheren Temperaturen gebildet, ein eindeutiges Anzeichen für eine veränderte Fluidzusammensetzung. Ein auf Strontiummassenbilanz und der Konservierung der Enthalpie basierendes Mischungsmodel deutet auf stark veränderte Bedingungen und Wärmetransport während der Karbonatbildung hin. Die Ergebnisse des Mischungsmodels bestätigen die geochemischen Analysen und zeigen ebenfalls, dass der Aragonit bei niedrigen Temperaturen aus dem Meerwasser ausgefällt wurde. Der Dolomit entstand durch die Mischung von 97% Meerwasser und 3% Hydrothermalfluid infolge einer konduktiven Aufheizung, möglicherweise von Meerwasser vor der anschließenden Mischung mit dem hydrothermalen Fluid. Der hydrothermale Calcit bildete sich aus der Mischung von 67% Hydrothermalfluid und 33% Meerwasser aufgrund konduktiver Abkühlung des hydrothermalen Fluids, welches entlang einer Störung austritt. REE-Muster spiegeln die Ergebnisse des Mischungsmodels wieder. Der Calcit zeigt die eindeutigste hydrothermale Signatur und dessen REE-Muster gleichen denen der hydrothermalen Fluid im LHF.

Spät devonischer Calcit im Serpentinit und im Basalt weist unterschiedliche Kohlenstoffquellen auf. $\delta^{13}C$-Werte für den Calcit im Basalt sprechen für eine Ausfällung aus Meerwasser. Im Gegensatz dazu zeigen die $\delta^{13}C$-Werte für den Calcit im Serpentinit zwei Kohlenstoffquellen an: Mantel-CO_2 mit einer Beimischung amagmatischen Kohlenstoffs, vermutlich Methan. Niedrige $\delta^{18}O$-Werte in beiden Lithologien deuten eine diagenetische und metamorphe Überprägung an. Des Weiteren wurden in den Pillowbasalten des Saxothüringikums vermeintlich biogene Filamente gefunden, ein Anzeichen für mikrobielles Leben in vulkanischen Gesteinen. Die Filamente befinden sich in Karbonat gefüllten Blasen, in denen ihr Wachstum an den internen Oberflächen der Blasen begann, nachdem die Basalte im Kontakt mit Meerwasser kamen und das Wasser hindurch zirkulierte. Der biogene Ursprung der Filamente stützt sich auf verschiedene Befunde. Die Größe und Morphologie gleicht denen moderner Mikroorganismen, ihr Auftreten ist unabhängig von mineralogischen Grenzflächen (Klüfte oder Korngrenzen), Bildung komplexer Netzwerke, und die interne Segmentierung. Ihre Erhaltung beruht auf der Tatsache, dass Mikroorganismen imstande sind Tonminerale zu bilden. Diese Erhaltungsform gleicht modernen Prokaryoten in Eisen-reichen Habitaten.

Die Ergebnisse, die in dieser Arbeit vorgestellt werden, führen zu einem detaillierteren Verständnis der Karbonatbildung in der ozeanischen Kruste und tragen wesentlich zum besseren Verständnis besonders der Karbonatbildung in ultramafisch-dominierten Hydrothermalsystemen bei. Es wird zum einen deutlich, dass Mischungsprozesse in hydrothermalen Systemen bei der Karbonatbildung eine entscheidende Rolle spielen und zum anderen, dass Pillowbasalte eine wichtige und möglicherweise sogar globale Nische für mikrobielles Leben in ozeanischer Kruste repräsentieren.

I. INTRODUCTION

1. General aspects of carbonate formation in the ocean crust

Seawater circulation through the oceanic crust begins immediately after its formation at mid-ocean ridges (von Damm, 1995). This circulation is divided into high-temperature (up to ~400°C) active axial systems and low-temperature (0 to ~100°C) passive and diffuse off-axis flank systems (Elderfield and Schultz, 1996). As more than one third of the present oceanic crust is actively involved in low-temperature hydrothermal alteration within flank setting, low-temperature alteration plays an important role in controlling the global distribution of elements and heat in the Earth's geochemical and thermal budget (Hunter et al., 1999). According to the four-stage alteration model by Staudigel et al. (1981), carbonate formation within the oceanic crust is defined as a late stage alteration process, postdating the formation of clay minerals (stage 3). This model indicates that the carbonate minerals precipitate from fluids which do not contain significant amounts of basaltic Sr. Abundances of carbonate minerals is greater in older than in younger crust (Fig. I.1), suggesting progressive uptake of carbon by the upper ocean crust, with an annual storage rate of 1.5 to 2.4 × 10^{12} mol C y^{-1} and thus represents an important part of the global carbon cycle (Alt and Teagle, 1999). Most of the carbon in altered ocean crust is taken up in the upper portion of the volcanic section, via formation of carbonate minerals at low temperatures (0 to 60°C) during aging of the crust (Alt and Teagle, 1999). The carbonate minerals either occur in veins cross-cutting the primary silicate mineralogy or in vesicles (amygdules) within pillow basalts. Carbonate-filled amygdules represent former gas-filled (carbon dioxide) vesicles formed upon extrusion of volatile-rich basaltic lava on the sea floor. These amygdules were found to contain putative cryptoendolithic filaments fossilized by microbial clay authigenesis, reflecting that even volcanic rocks harbor microbial life.

Tracing chemical fluxes associated with hydrothermal circulation in the oceanic crust is a central issue to our understanding of sweater chemistry (Elderfield et al., 1999; Hardie, 2003). The chemical input to the oceans associated with hydrothermal venting is dependent on the flux and composition of hydrothermal fluids. Approximately one third of convective heat loss occurs at crustal ages greater than 1 Ma (Stein and Stein, 1994), accomplished by seawater circulation through ridge flanks at significantly lower temperatures than axial black smoker venting. Here, the direct sampling of fluids is

limited to the high-temperature vent fluids issuing from black smokers (e.g., Von Damm, 1990). Estimates of low-temperature fluid compositions have largely been inferred from direct study of upper crustal rocks subsequent to their interaction with low-temperature fluids (Staudigel et al., 1981; Elderfield and Schultz, 1996).

It is the aim of this thesis to study alteration processes at high and low temperatures in ultramafic-hosted hydrothermal environments to provide more detailed insights in the carbonate formation in such systems. Thus, the studies are based on carbonate minerals in different host rocks.

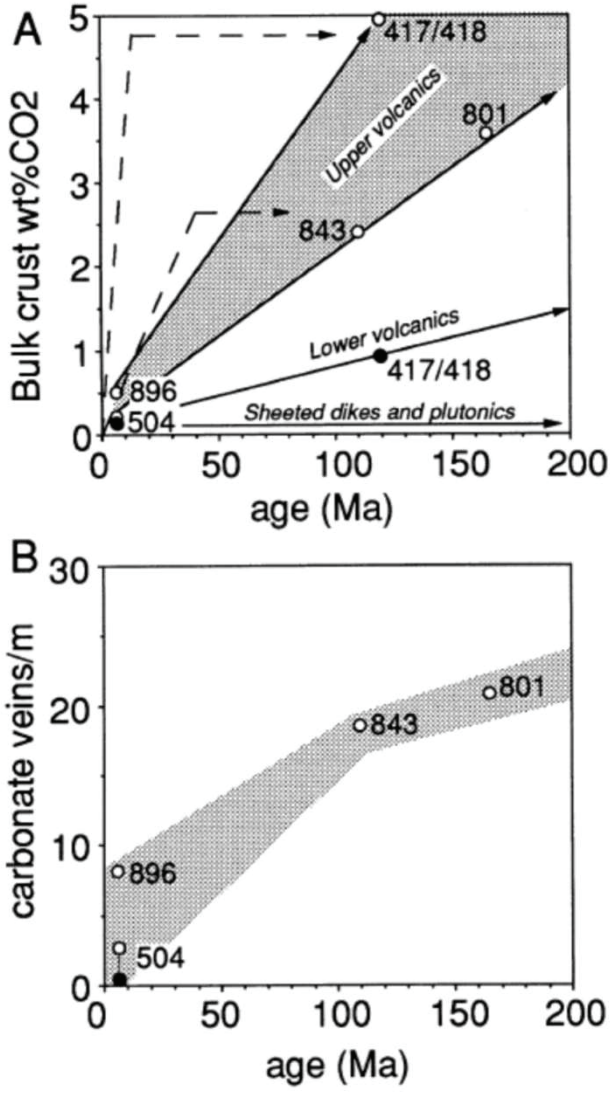

Fig. I.1. Carbonate data for the upper section of the oceanic crust illustrates the greater CO_2 content of older crust and the continued carbonate formation and additions of CO_2 during aging. The open and solid circles represent different ODP sites (from Alt and Teagle, 1999).

1.1. Carbonate formation in ultramafic environments and the influence of serpentinization

Carbonate formation in ultramafic settings is documented in fracture zones (Bonatti et al., 1980), in hydrothermal systems (Ribeiro da Costa et al., 2008), and off-axis at the Mid-Atlantic ridge (Kelley et al., 2001), at the Mariana and Izu Bonin forearc (Haggerty, 1991; Alt and Shanks, 2006), as well as on passive continental margins (Agrinier et al., 1996). Nevertheless, this thesis focuses on carbonate formation in ultramafic environments at slow to ultra-slow spreading ridges. Ultramafic rocks represent sections of the upper mantle which are exposed on the seafloor due to tectonic faulting associated with extension and crustal thinning (Cannat, 1993; Tucholke and Lin, 2004). These faults provide permeable pathways for hydrothermal circulation (Karson et al., 2006). Since mid-ocean ridges with a spreading rate less than 20 mm yr^{-1} comprise about one third of the global ridge system (Dick et al., 2003), the characterization and geochemistry of carbonates in these environments is still poorly constraint. Furthermore, almost 20% of the ocean crust at slow-spreading ridges consists of ultramafic rocks including peridotites (Früh-Green et al., 2004), for which the carbon uptake budgets derived for volcanic crust are not valid (Alt and Teagle, 1999). Understanding the carbonate formation in ultramafics will help to illuminate the still unknown role of slow-spreading ridges in the global carbon cycle.

Since many carbonate samples collected from ultramafic environments at water depth were the seawater is undersaturated with respect to calcium carbonate (Li et al., 1969; Ridgwell and Zeeebe, 2005), it is of great interests which mechanism favors the carbonate precipitation. Although the surface of the ocean is everywhere oversaturated with respect to the solid carbonate phases, with a mean value for saturation state ($\Omega = [Ca^{2+}] \times [CO_3^{2-}]/K_{sp}$, where K_{sp} is a solubility constant; Zeebe and Wolf-Gladrow, 2005) of calcite of 4.8, the spontaneous precipitation of calcite from the water column is not observed in the ocean (Ridgwell and Zeebe, 2005; Morse et al., 2007). This is because the initial step of crystal nucleation is kinetically unfavorable, and experimentally, spontaneous nucleation does not occur in seawater solutions until $\Omega_{calcite} > \sim 20$ to 25 (Morse et al., 2003). The reason for carbonate formation in ultramafic rocks at water depth were the seawater is undersaturated with respect to calcium carbonate is due to enhanced interaction between circulating seawater and the ultramafic rocks (Ludwig et al., 2006; Ribeiro da Costa et al., 208). In the presence of water and due to their exposure

to the seafloor, olivine and pyroxene became thermodynamically unstable when exposed to lower temperatures in the near-surface environment and undergo reaction with water. This reaction results in a mineral assemblage dominated by serpentine minerals, with magnetite and brucite or talc (Früh-Green et al., 2004; Bach et al., 2006). In addition, serpeninization generates fluids with high concentrations of hydrogen and methane (Charlou et al., 2001; Chalou et al., 2002). Conversion of Fe^{2+} in olivine to Fe^{3+} in magnetite during serpentinization leads to the production of hydrogen and conversion of carbon dioxide to reduced carbon species, including methane (Berndt et al., 1996). Here, the Fischer-Tropsch like reaction (Eqn. 1) which is catalyzed by iron- and chromium-bearing minerals is a well known process for converting carbon dioxide to hydrocarbons by reaction with hydrogen (Berndt et al., 1996; Foustoukos and Seyfried, 2004).

$$CO_2 + 4H_2 \rightarrow CH_4 + 2H_2O \quad (1)$$

Apart from that and to explain the carbonate formation in such environments, reactions between ultramafic rocks and seawater at temperatures below 200 to 250°C lead furthermore to the development of high Ca^{2+} concentrations and high pH values of the interacting fluids (Allen and Seyfried, 2003; Palandri and Reed, 2004; Kelley et al., 2005). High dissolved Ca^{2+} concentrations have been reported for the Logatchev field vent fluids (Amini et al., 2008) as well as for the ultramafic-hosted Rainbow field at the Mid-Atlantic ridge almost certainly resulting from the reaction of seawater-derived Mg^{2+} with Ca-bearing silicates (Eqn. 2; Allen and Seyfried, 2003).

$$6CaMgSi_2O_6 + 6MgSiO_3 + 5Mg^{2+} + 9H_2O \rightarrow 3Mg_3Si_2O_5(OH)_4 + Mg_3Si_4O_{10}(OH)_2 + CaMg_5Si_8O_{22}(OH)_2 + 4Ca^{2+}\ 2H^+ \quad (2)$$

The dissolution of CaO in protoliths minerals such as olivine or pyroxene provides an additional source of OH^-, driving the fluid to higher pH values (Eqn. 3).

$$CaO + 2H_2O \rightarrow Ca^{2+} + 2OH^- \quad (3)$$

The calcium incorporated into the carbonate minerals is derived primarily from the vent fluid, because the cold seawater serves only to dilute the high concentration of calcium in the initial hot fluid (Palandri and Reed, 2004).

Experimental results indicate that the aqeous phase during water-rock interactions evolves with decreasing water-rock interaction to increased concentrations of Ca^{2+} and OH^-, and becomes hyperalkaline and highly reducing (Allen and Seyfried, 2003; Palandri and Reed, 2004). The fundamental reason that reaction of seawater with ultramafic rock produces hyperalkaline fluid is that OH^- produced by dissolution of olivine (Eqn. 4) and pyroxene (Eqn. 5) is not counterbalanced by OH^- consumption by precipitation of serpentine minerals until the OH^- concentrations becomes quite large (Palandri and Reed, 2004). In other words, there are no insoluble alteration minerals that form in the neutral pH range.

$$Mg_2SiO_4\ (fo) + 2H_2O \rightarrow 2Mg^{2+} + SiO_2\ (aq) + 4OH^- \quad (4)$$

$$MgSiO_3\ (en) + H_2O \rightarrow Mg^{2+} + SiO_2\ (aq) + 2OH^- \quad (5)$$

The resulting alkaline or hyperalkaline fluids control which carbonate species is thermodynamically stable. Thus, the carbonate ion (CO_3^{2-}), not the bicarbonate (HCO_3^-) ion in seawater (Fig. I.2), is the dominant species of dissolved inorganic carbon in these fluids.

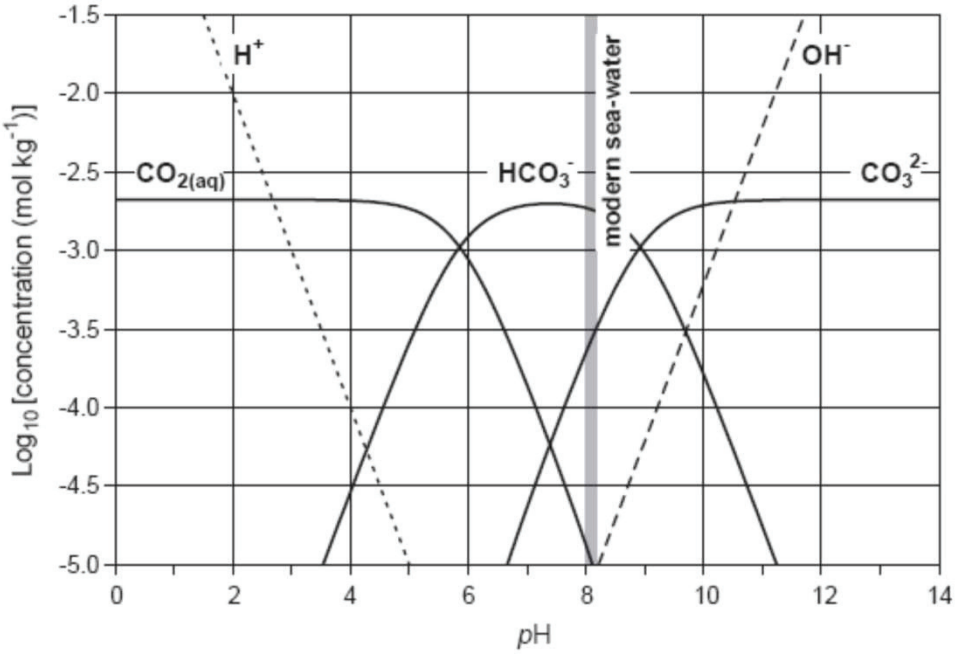

Fig. I.2. Bjerrum diagram showing the concentrations of the dissolved carbonate species as a function of pH values (from Ridgwell and Zeebe, 2005).

Despite low inorganic carbon contents (Proskurowski et al., 2008), the high hydroxide alkalinity of serpentinization fluids causes carbonate precipitation, similar to the carbonate chimneys at the Lost City field (Ludwig et al., 2006) and the Mariana forearc (Hagerty, 1991). However, if these alkaline fluids mix with relatively acidic seawater, the carbonate ions combine with Ca^{2+} from the vent fluids to form carbonate minerals (Eqn. 6).

$$Ca^{2+} + HCO_3^- + OH^- \rightarrow CaCO_3(s) + H_2O \quad (6)$$

The dominant carbonate mineral in almost all ultramafic environments is aragonite, but calcite hosted serpentinites were also found in the Logatchev hydrothermal field and in ODP Hole 1271A (Amini et al., 2008). Although aragonite is the major carbonate mineral in serpentinites (Bonatti et al., 1980; Ribeiro da Costa et al., 2008); in carbonate chimneys along the Mariana forearc (Haggerty, 1991) and the in the Lost City field forming above serpentinites (Ludwig et al., 2006), it is only metastable in these environments in these environments and may convert to calcite (Berndt and Seyfried,

1999). Factors controlling the precipitation of either aragonite or calcite are the fluid chemistry; in particular Mg^{2+} and sulfate concentrations and the Mg/Ca ratio influence carbonate precipitation (Burne, 1993). Calcite precipitation is hindered by the fact that Mg^{2+} ions are preferentially introduced into the crystal lattice of calcite. This so-called 'poisoning effect' of Mg^{2+} ions is caused by the strong hydration of the small Mg^{2+} ion, which results in a kinetical barrier for precipitation, making Mg^{2+} a selective factor favoring aragonite instead of calcite precipitation (Mucci and Morse, 1983; Morse et al., 2007). Additionally, elevated Sr^{2+} concentrations in fluids may also inhibit calcite precipitation (Wasylenki et al., 2005). Although aragonite is metastable, the sluggish conversion to calcite by dissolution and re-precipitation at low temperatures like those characterizing bottom seawater in contact with exposed serpentinites is responsible for their preservation (Berndt and Seyfried, 1999). Thus, high Mg^{2+} concentration of seawater and the stabilizing effect of Sr^{2+} ion in aragonite inhibit conversion to calcite (Katz et al., 1972).

Fluids that favored calcite precipitation, on the other hand, supposedly had low Mg^{2+} and sulfate concentrations. Such fluids are typically generated by serpentinization (Charlou et al., 2002). Additionally, the fact that serpentinite-hosted calcite from the Logatchev hydrothermal field precipitated from high-temperature hydrothermal fluids can be reconciled by considering the low solubility of calcite at high temperatures. Although the hydrothermal fluids from LHF display extremely low carbonate activities, the solubility of calcite is much lower or at least equal to the respective CO_3^{2-} concentrations indicating a remarkably high saturation level of the hydrothermal fluids (Amini et al., 2008). Thus, the hydrothermal fluids are oversaturated ($\Omega_{calcite}$ = 40 to 49 at 170°C) with respect to calcite.

2. Carbonate geochemistry as a proxy for sub seafloor mixing

2.1. Stable O and C isotope geochemistry

Commonly used proxies to reconstruct the temperature at which carbonate minerals were formed and to verify the carbon sources are the ratios of stable oxygen and carbon isotopes. Isotopes are atoms whose nuclei contain the same number of protons but different number of neutrons. Oxygen has three stable isotopes with the following abundances: ^{16}O (99.763%), ^{17}O (0.0375%), ^{16}O (0.1995%), while the abundances of the two carbon isotopes are: ^{12}C (98.89%), ^{13}C (1.11%; Hoefs, 2004). Based on thermodynamics and reaction kinetics, the light isotopes are partially separated from the heavier isotopes in a process called isotope fractionation. Typically, the lighter isotopes reactants react faster and as a result the products are isotopically depleted. For practical reasons, the accepted unit of isotope ratios measurements is the delta value (δ) given in per mill (‰), which is defined as (Eqn. 7):

$$\delta[X] = \frac{R_{(sample)} - R_{(standard)}}{R_{(standard)}} \times 1000 \quad (7)$$

In this equation [X] is the less-abundant isotope, and R is the isotopic ratio measured for sample and standard ($^{18}O/^{16}O$ and $^{13}C/^{12}C$).

Since the thermodynamic properties of isotopes have been concerned (Urey, 1946), the first temperature scale for biogenic carbonate minerals was introduced by McCrea (1950). Experimental studies on the oxygen isotope fractionation of calcite (Eqn. 8; Kim and O'Neil, 1997), aragonite (Eqn. 9; Kim et al., 2007) and dolomite (Eqn. 10; Vaconcelos et al., 2005) have been performed to refine the dependence on temperature (Fig. 3).

$$10^3 \ln\alpha(\text{calcite-water}) = 18.03(10^3 T^{-1}) - 32.42 \quad (8)$$

$$10^3 \ln\alpha(\text{aragonite-water}) = 17.88(10^3/T) - 31.14 \quad (9)$$

$$10^3 \ln\alpha(\text{dolomite-water}) = 2.73 \times 10^6 T^{-2} + 0.26 \quad (10)$$

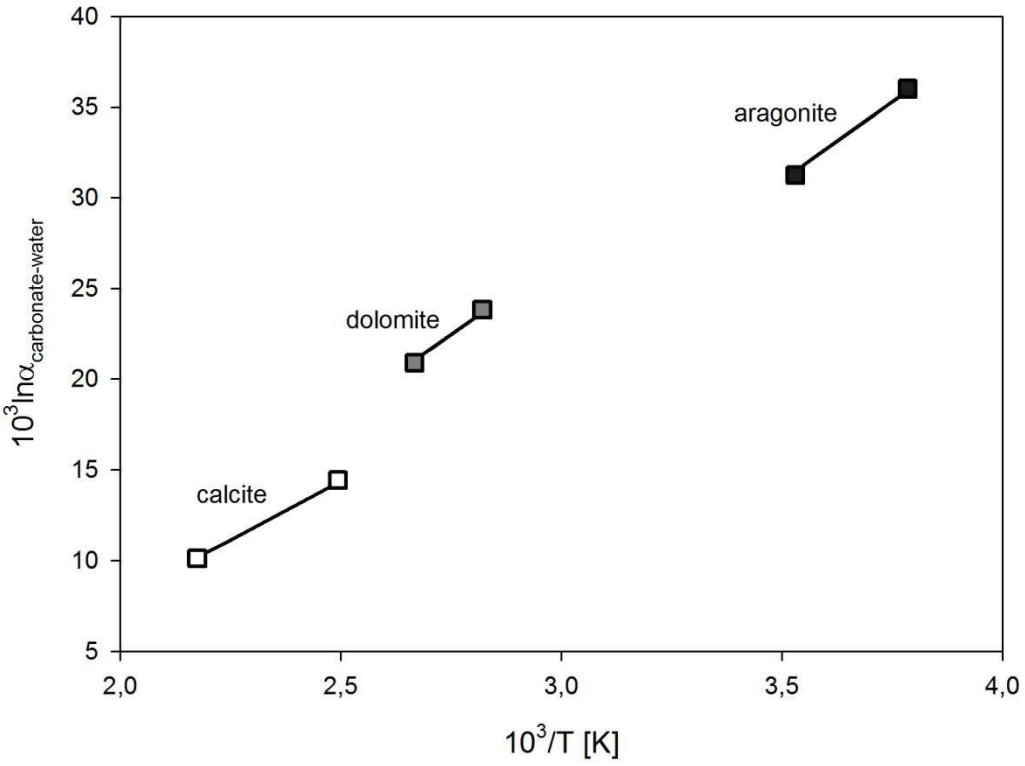

Fig. I.3. Comparison of fractionation factors for all studied carbonate minerals.

The carbon isotopic composition of carbonate minerals covering a wide range of $\delta^{13}C$ values, with marine carbonates yielding $\delta^{13}C$ values around 0‰, to $\delta^{13}C$ values as low as − 60‰ for methane-derived authigenic carbonates formed at cold methane-seeps (Peckman and Thiel, 2004). $\delta^{13}C$ values of marine carbonates are usually close the isotopic composition of the dissolved bicarbonate (HCO_3^-) in the ocean (Zeebe and Wolf-Gladrow, 2005). The vast majority of the $\delta^{13}C$ values of carbonates precipitated by marine organisms such as foraminifera, corals, and mollusca fall within the range from −2 to +2‰ (e.g., Wefer and Berger, 1991). Since the crystal structure of aragonite is rhombohedral and that of calcite is orthorhombic (Morse et al., 2007), the different structures lead to different physical and chemical properties such as density and solubility and also to different isotopic fractionation factors between the dissolved carbon in the water and the carbon in the carbonate mineral. Experimental studies

found an enrichment of ^{13}C in calcite and aragonite relative to HCO_3^- of 0.9‰ and 2.7‰, respectively (Rubinson and Clayton, 1969; Romanek et al., 1992). Furthermore, Romanek et al. (1992) concluded that this fractionation is essentially independent of temperature (over the 10 to 40°C) and precipitation rates (~$10^{2.5}$ to$10^{4.5}$ μmol m^{-2} h^{-1}). However, because carbonate minerals are known to record water-rock interaction in the ocean crust, their $\delta^{13}C$ values used to verify their carbon sources. Possible carbon sources in such systems include seawater ($\delta^{13}C$ = ~0‰), mantle-derived carbon ($\delta^{13}C$ = −7‰), and if serpentinization is considered, methane ($\delta^{13}C$ = <−20‰).

2.2. Sr isotopes

Strontium isotope ($^{87}Sr/^{86}Sr$) ratios of carbonate minerals is a very powerful indicator of hydrothermal alteration in the ocean crust, because fresh crust has an unradiogenic $^{87}Sr/^{86}Sr$ ratio of 0.7022 (Palmer, 1992), while seawater yield a radiogenic $^{87}Sr/^{86}Sr$ ratio of 0.70918 (Butterfield et al., 2001). Seawater $^{87}Sr/^{86}Sr$ ratio changes with time, as expressed in the classical 'Burke curve' (Fig. I.3) covering the Phanerozoic eon, which is constructed from analyses of marine carbonates and evaporates (Burke et al., 1982). The $^{87}Sr/^{86}Sr$ ratio of the present seawater, based on the marine carbonate record from 2.5 Ma to present, is increasing at a rate of ~0.000054 per million years (Hodell et al., 1990).

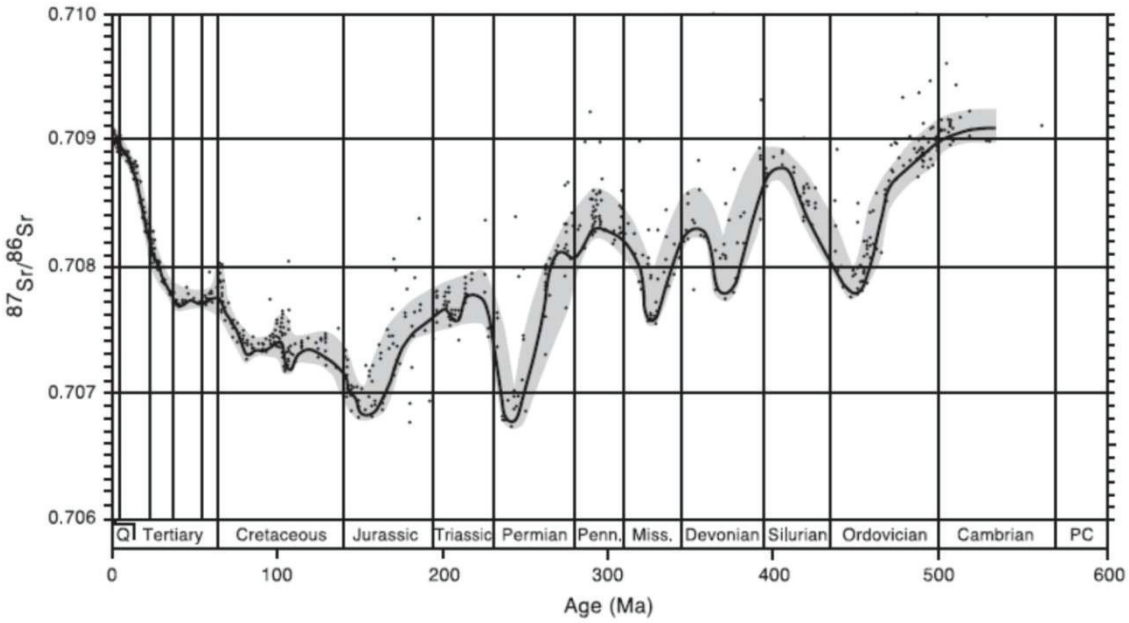

Fig. I.3. Burke curve for secular changes of seawater $^{87}Sr/^{86}Sr$ variations during the Phanerozoic. The shaded area around the curve is the error envelope of best estimate seawater value (from Burke et al., 1982).

These changes in the $^{87}Sr/^{86}Sr$ ratio of seawater reflects the shifting balance between input of radiogenic strontium dissolved in rivers ad unradiogenic strontium derived from the reaction of seawater with volcanic ocean crust (Butterfield et al., 2001). $^{87}Sr/^{86}Sr$ ratios of secondary minerals such as carbonate minerals in hydrothermal environments quantitatively reflect the Sr contributions from seawater and from basalt (Staudigel, 2003).

Based on $^{87}Sr/^{86}Sr$ ratios for carbonates in hydrothermal environments, most of them precipitated from almost pure seawater (Ribeiro da Costa et al., 2008) or with a minor hydrothermal contribution (Früh-Green et al., 2003). The only carbonates that have been found to have precipitated from hydrothermal fluids are from a shallow-water hydrothermal system in Papua New Guinea (Pichler and Veizer, 2004). Strontium isotopes and concentrations were used to determine the fraction of seawater (F_{SW}) in hypothetic mixtures (MIX) of seawater (SW) and vent fluids (HF) by simple mass balance (see 4.3.3). This simple mass balance allows us to determine the relative amounts of conductive cooling of hydrothermal solutions versus conductive heating of seawater.

2.3. Rare earth elements

Rare earth elements (REE) in mid-ocean ridge hydrothermal systems have elicited considerable interest because chondrite-normalized concentrations may provide insights into subseafloor alteration. REE pattern of basalt-hosted environments at the East Pacific Rise (Michard et al., 1983) and the Mid-Atlantic ridge (e.g., Douville et al., 1999) show obvious similarities. All of these studies reported that the chondrite-normalized REE patterns of hydrothermal fluids exhibit light-REE enrichment with a strong positive europium (Eu) anomaly, although the total REE abundances can vary widely, even in the same vent field. REE concentrations vary only as a function strong phase separation (Douville et al., 1999; Schmidt et al., 2007). Positive Eu anomalies in fluids point to a contribution of reduced hydrothermal fluids (Bau, 1991). Similar REE patterns have been reported for vent fluids issuing from ultramafic-hosted hydrothermal systems, indicating that the fractionation of REE in hydrothermal systems seems to be a characteristic signature independently from host-rock composition (Allen and Seyfried, 2005; Schmidt et al., 2007). REE fractionation in hydrothermal systems is mainly controlled by a combination of reducing conditions (see discussion below) at high temperatures, acidic pH, chloride complexation depending on ionic radii and temperature, and incorporation of REE in secondary alteration minerals (Bau, 1999; Douville et al., 1999; Allen and Seyfried, 2005).

Due to their equal ionic charges (REE^{3+}) and similar ionic radii, the REE constitute a coherent group of elements. However, since in natural systems Ce^{3+} can be oxidized to Ce^{4+} and Eu^{3+} can be reduced to Eu^{2+}, this argument holds only in specific redox environments (Wood, 1990). Decoupling of Eu from the other REE is confirmed by the development of an Eu anomaly, either negative or positive. This requires the reduction of Eu^{3+} to Eu^{2+}, because the change of valence state is accompanied by an increase in ionic radius (Wood, 1990). Eu reduction is extremely unlikely under standard conditions (25°C, 1 bar), because the Eu^{3+}/Eu^{2+} redox equilibrium (Fig. I.4) is located at very low oxygen fugacity (Bau, 1991).

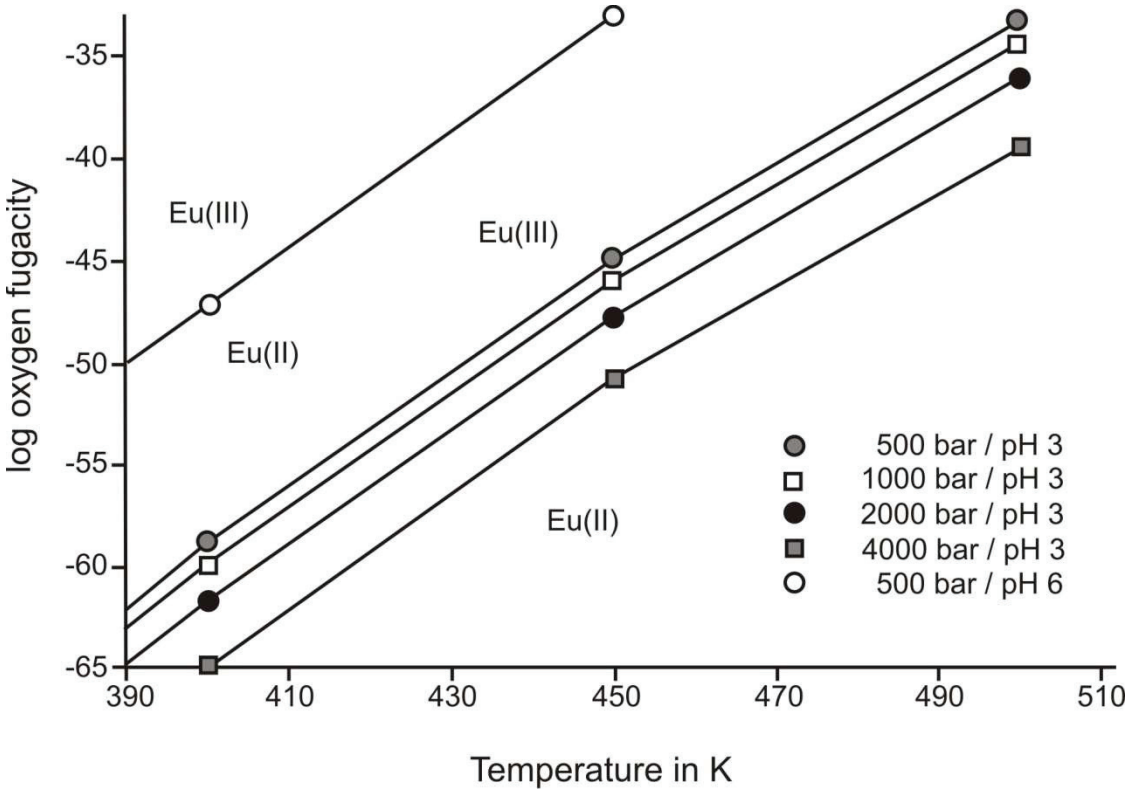

Fig. I.4. The Eu^{3+}/Eu^{2+} redox equilibrium as a function of oxygen fugacity, temperature, pressure and pH (redrawn after Bau, 1991).

The Eu^{3+}/Eu^{2+} redox equilibrium (Fig. I.4) depends on (1) the strong redox potential increase with temperature, (2) redox potential increase with increasing pH, and (3) redox potential decrease with increasing pressure (Bau, 1990; Sverjensky, 1984; Bilal, 1991). Hence, even under slightly reducing conditions Eu can occur in the divalent oxidation state, i.e. an Eu anomaly can develop, provided the temperature is high enough. In water-rock interactions the REE pattern of the fluid might be influenced by (1) the REE pattern of the host rock the fluid interacts, (2) sorption, and (3) chemical complexation (Bau, 1991). Since the REE patterns and abundances of seawater and hydrothermal fluids in the Logatchev hydrothermal field are distinct and well characterized (Schmidt et al., 2007; Amini et al., 2008), their concentrations can be used to calculate a mixing model. The high sensitivity of Eu^{3+}/Eu^{2+} redox equilibrium can be used as an indicator of hydrothermal input even when strontium isotopes, which are generally used to trace hydrothermal processes, do not show a hydrothermal signal.

2.4. Mg/Ca and Sr/Ca ratios

Changes in the trace element concentrations of carbonate minerals reflect the chemical development of the fluid from which they precipitated. During hydrothermal circulation, the precipitation of secondary minerals and the leaching of elements from igneous basement rocks affect the relative elemental concentration in the fluid and the resulting carbonate minerals (Hunter et al., 1999). Since Mg/Ca and Sr/Ca ratios of carbonate minerals are sensitive temperatures, they can be taken as proxy for the degree of fluid evolution (Coggon et al., 2004). Carbonates precipitated from hotter fluids, with a greater basaltic $^{87}Sr/^{86}Sr$ component, have lower Mg/Ca and Sr/Ca ratios. If the Mg/Ca and Sr/Ca ratios of the carbonates were determined and given suitable partition coefficients for Mg (Eqn. 11) and Sr (Eqn. 12), it is possible to calculate the Mg/Ca and Sr/Ca ratios of the fluids from which the carbonates precipitated.

$$K_D^{Sr-Ca} = \frac{[Sr/Ca]_{CaCO3}}{[Sr/Ca]_{fluid}} \quad (11)$$

$$K_D^{Mg-Ca} = \frac{[Mg/Ca]_{CaCO3}}{[Mg/Ca]_{fluid}} \quad (12)$$

It is important to note that the predictions of formation fluid composition are highly dependent on the choice of partition coefficients for Mg and Sr in carbonate minerals. To calculate the fluid compositions from which calcite precipitated, the partition coefficients for calcite given by Rimstidt et al. (1998) for both, Mg (Eqn. 13) and for Sr (Eqn. 14) were used.

$$LogK_{Cc}^{Mg-Ca} = 4.436 - \frac{1348}{T[K]} - 0.005339 \times T[K] \quad (13)$$

$$LogK_{Cc}^{Sr-Ca} = -1.874 + \frac{179.2}{T[K]} + 0.0006248 \times T[K] \quad (14)$$

Since minimal Mg can be incorporated into the aragonite lattice, there has been little work to date regarding the partitioning of Mg in aragonite. However, the small amount of Mg is not temperature-dependent (Oomori et al., 1987). A value of $K_{arag}^{Mg-Ca} = 0.001$ is cautiously selected here (Burns, 1979). In contrast, the partitioning of Sr (Eqn. 15) is far better constraint and similar to that of calcite, temperature-dependent (Kinsman and Holland, 1969).

$$K_{arag}^{Sr-Ca} = 1.455 - 0.0178 \times T[°C] \quad (15)$$

As seawater interacts with the ocean crust during hydrothermal circulation, Mg is removed and Ca is added to the fluids (e.g., von Damm, 1990). Even at temperatures of 60°C and lower, Mg concentrations approach concentrations of 2 mmol/kg, while Ca concentrations increase to 60 mmol/kg (Elderfield et al., 1999; Wheat and Mottle, 2000). It is hence likely that fluid evolution paths in the sub seafloor away from hydrothermal upflow and mixing zones deviates from simple mixing scenarios. Most Mg/ca ratios of carbonate minerals in hydrothermal environments are much lower than predicted for precipitation from seawater (Coggon et al., 2004; Ludwig et al., 2006), indicating that notable Mg loss and Ca gain of the seawater-derived fluids took place prior to precipitation (Amini et al., 2008). In contrast, calculated Mg/Ca and Sr/Ca ratios of fluids higher than seawater may also indicate prolonged exposure of the carbonates to seawater and subsequent incorporation of seawater-derived Sr and Mg, similar to carbonates from the Lost City field (Ludwig et al., 2006). The formation of carbonates at the Juan de Fuca ridge faithfully records the evolution of seawater during interaction with basaltic basement at temperatures below 65°C (Coggon et al., 2004).

II. SCIENTIFIC OBJECTIVES AND OUTLINE OF THIS THESIS

The main focus of this thesis was to understand the genesis of carbonate minerals in the ocean crust, especially in ultramafic-hosted hydrothermal environments along slow-spreading mid-ocean ridges and to use carbonate minerals as a proxy to model mixing processes in the sub seafloor basement within these systems. This thesis highlights the importance of mixing processes in hydrothermal systems leading to the formation of different carbonate minerals. Furthermore, it is demonstrated that carbonate-filled vesicles in Late Devonian (Frasnian) pillow basalts from the Saxothuringian zone in Germany were found to contain abundant putative biogenic filaments, indicating that basalts once harbored microbial life. The results arising from these studies are presented in the following three manuscripts.

Chapter 3: Authigenesis of carbonate minerals in modern and Devonian ocean-floor hard rocks

Benjamin Eickmann, Wolfgang Bach, Jörn Peckmann

The Journal of Geology; in press, doi:10.1086/597362

This manuscript introduces the petrography of carbonate minerals from two ultramafic-hosted hydrothermal sites at slow-spreading mid-ocean ridges, the Logatchev hydrothermal field (LHF) and the arctic Gakkel ridge (GR). The modern samples were compared to Late Devonian serpentinite- and basalt-hosted carbonates from the Frankenwald in an attempt to understand the genesis of carbonate minerals in modern and ancient marine volcanic rocks. Authigenic carbonates from the three sites reflect precipitation at different temperatures and from different fluids spanning from ambient temperatures and seawater to hydrothermal conditions.

Chapter 4: Geochemical constraints on the modes of carbonate formation in peridotites from the Logatchev Hydrothermal Vent Field and Gakkel Ridge

Benjamin Eickmann, Wolfgang Bach, Martin Rosner, Jörn Peckmann

Chemical Geology; in review

In this manuscript, mixing models using the chemical endmember composition of seawater and hydrothermal fluids within the Logatchev hydrothermal field were performed. These models gain a more detailed understanding of carbonate formation in hydrothermal environments. At least three different mixing trends leads to carbonate formation: (1) precipitation from seawater, (2) conductive heating of seawater, and (3) conductive cooling of hydrothermal fluids. REE of the different carbonate minerals corroborate the results of the mixing model. This is the first comprehensive study of carbonate precipitation over a wide temperature range due to various mixing processes in the sub seafloor basement within a single hydrothermal system.

Chapter 5: Widespread cryptoendolithic life in Devonian pillow basalts

Benjamin Eickmann, Wolfgang Bach, Steffen Kiel, Joachim Reitner, Jörn Peckmann

Palaeogeography, Palaeoclimatology, Palaeoecology; to be submitted

This manuscript presents the existence of microbial life within Late Devonian (Frasnian) pillow basalts from the Frankenwald and the Thüringer Wald, Germany. Abundant putative biogenic filaments are found in carbonate-filled amygdules, where they started to form on internal surfaces after seawater ingress. Thus, the filamentous microorganisms represent cryptoendoliths. Their mineralization by microbial clay authigenesis is similar to the encrustation of modern prokaryotes and to those found in Middle Devonian pillow basalts from the Rheinisches Schiefergebirge. This study suggests that this mode of life was widespread in the shallow subsurface of the Devonian seafloor.

III. MANUSCRIPTS

3. Authigenesis of carbonate minerals in modern and Devonian ocean-floor hard rocks

Benjamin Eickmann, Wolfgang Bach, Jörn Peckmann

MARUM – Center for Marine Environmental Sciences, Universität Bremen, 28334 Bremen, Germany

The Journal of Geology; in press, doi:10.1086/597362

Petrographic and stable isotope ($\delta^{13}C$, $\delta^{18}O$) patterns of carbonates from the Logatchev hydrothermal field (LHF), the Gakkel ridge (GR), and a Late Devonian outcrop from the Frankenwald (Germany) were compared in an attempt to understand the genesis of carbonate minerals in marine volcanic rocks. Specifically, were the carbonate samples from the modern seafloor settings and the Devonian analogue of hydrothermal origin, low-temperature abiogenic origin (as inferred for aragonite in serpentinites from elsewhere on the Mid-Atlantic ridge), or biogenic origin? Aragonite is the most abundant carbonate mineral in serpentinites from the two modern spreading ridges and occurs within massive sulfides of the LHF. The precipitation and preservation of aragonite suggests high Mg^{2+} and sulfate concentrations of fluids. $\delta^{18}O_{PDB}$ values of serpentinite-hosted aragonite as high as +5.3‰ and sulfide-hosted aragonite as high as +4.2‰ are consistent with precipitation from cold seawater. Most of the corresponding $\delta^{13}C$ values indicate a marine carbon source, whereas $\delta^{13}C$ values of sulfide-hosted aragonite as high as +3.6‰ may reflect residual carbon dioxide in the zone of methanogenesis. Calcite veins from LHF, by contrast, have low $\delta^{18}O_{PDB}$ (−20.0 to −16.1‰) and $\delta^{13}C$ values (−5.8 to −4.5‰) indicative of precipitation from hydrothermal solutions (~129 to 186°C) dominated by magmatic CO_2. Calcite formation was probably favored by fluid rock interactions at elevated temperatures, which tend to remove solutes that inhibit calcite precipitation in seawater (Mg^{2+} and sulfate). Devonian Frankenwald calcites show low $\delta^{18}O$ values reflecting diagenetic and metamorphic overprinting. $\delta^{13}C$ values of basalt-hosted calcite around 0‰ indicate seawater-derived inorganic carbon, whereas $\delta^{13}C$ values of serpentinite-hosted calcite agree with mantle-derived carbon dioxide

(for values as low as −6‰) with a contribution of amagmatic carbon (for values as low as −8.6‰), presumably methane. Secondary mineral phases from LHF for which a biogenic origin appears feasible include dolomite dumbbells, clotted carbonate, and a network of iron- and silica-rich filaments.

3.1. Introduction

Ultramafic rocks represent sections of the upper mantle, which are exposed on the seafloor in and near fracture zones and along slow and ultraslow-spreading ridges due to tectonic faulting associated with extension and crustal thinning (e.g., Tucholke and Lin 1994). Almost 20% of the ocean floor at slow-spreading ridges consists of ultramafic rocks including peridotites (Früh-Green et al. 2004) for which the carbon uptake budgets derived for volcanic crust (e.g., Alt and Teagle 1999) are not valid. Although much work has focused on sulfide mineralogy and sulfur geochemistry of ultramafic rocks (e.g., Alt and Shanks 1998), little is known about the genesis and petrography of authigenic carbonates found in these seafloor settings. Understanding the formation of authigenic carbonates in ultramafics will help illuminate the unknown role of slow-spreading ridges in the global carbon cycle.

Carbonate formation is a common process related to the low-temperature alteration of peridotites to serpentinites (Bonatti et al. 1980) and moderate-temperature hydrothermal activity as has been recognized at the Lost City hydrothermal field (Kelley et al. 2005). Reactions between ultramafic rocks and seawater at temperatures below approximately 200 to 250°C lead to the development of high Ca^{2+} concentrations and high pH values of the interacting fluids (Allen and Seyfried 2003; Palandri and Reed 2004; Kelley et al. 2005). The carbonate ion, not the bicarbonate ion as in seawater, is the dominant species of dissolved inorganic carbon in these fluids. Despite low dissolved inorganic carbon contents (Proskurowski et al. 2008), the high hydroxide alkalinity of serpentinization fluids causes carbonate precipitation (e.g., Ludwig et al. 2006); however, the precise mechanism of precipitation is not well understood. It has been suggested that dissolution of olivine in peridotites during weathering may cause interstitial waters to become alkaline, lowering carbonate solubility and promoting precipitation (Palandri and Reed 2004). Because seawater is undersaturated with respect to carbonates at ambient deep-sea conditions (~ 4°C, ~300 bar; Li et al. 1969),

carbonate formation is confined to insterstices of ultramafic rock where alteration of ultramafic rocks liberates Ca^{2+} ions and increases hydroxide alkalinity. Alternatively, carbonate precipitation at slow-spreading ridges can also be induced by high-temperature hydrothermal activity (Edmonds et al. 2003; Schmidt et al. 2007).

Here we describe serpentinite-hosted carbonates from the Logatchev hydrothermal field (LHF) at the Mid-Atlantic ridge and the Gakkel ridge (GR) in the Arctic Ocean, as well as Late Devonian serpentinite- and basalt-hosted carbonates from the Frankenwald, Germany (Fig. 3.1, 3.2).

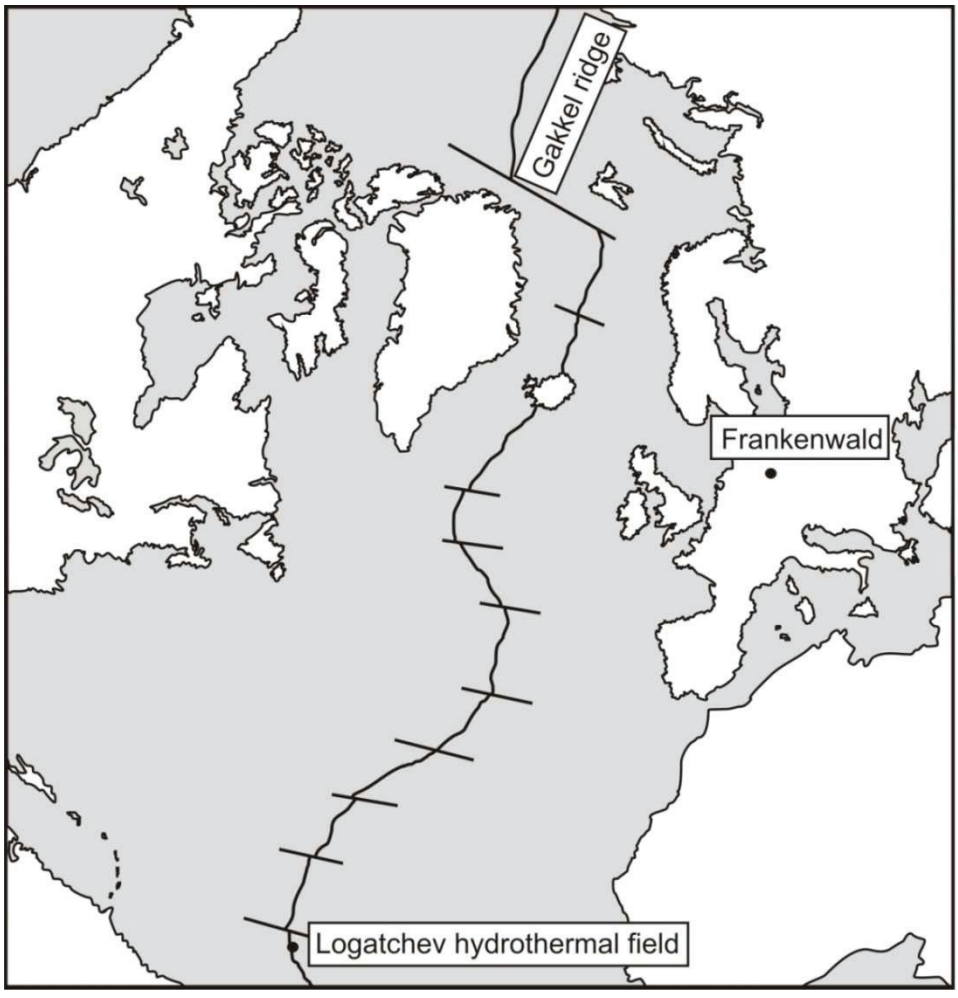

Fig. 3.1. Sketch map of the northern Atlantic and Arctic Oceans and adjacent continents with the three sample localities.

We investigate whether the apparently similar modern and ancient secondary carbonates have a hydrothermal origin similar to carbonate chimneys in the Lost City

hydrothermal field (Früh-Green et al. 2003), or a low-temperature origin as proposed for aragonite in serpentinites from the Mid-Atlantic ridge (Bonatti et al. 1980). A detailed petrographic examination of the carbonates, using standard optical and fluorescence microscopy combined with cathodoluminescence and FE-SEM was undertaken to obtain paragenetic sequences. Stable oxygen and carbon isotope signatures of carbonate phases were used to reconstruct (1) carbon sources, (2) formation temperatures, (3) interaction between seawater and basement rocks, and in the case of the Devonian samples, (4) metamorphic overprint.

3.2. Geological setting

Logatchev Hydrothermal Field. The Mid-Atlantic ridge south of the 15°20'N fracture zone is characterized by abundant exposure of peridotite and gabbroic rocks on both flanks along the spreading axis (Cannat et al. 1997; Fujiwara et al. 2003). Here, widespread fluid-peridotite interaction in the sub-seafloor is evident from extensive methane and hydrogen anomalies in the water column and high-temperature fluid discharge at the LHF (Charlou et al. 1998; 2002). The active LHF field is located at 14°45'N and 44°58'W on a plateau on the eastern rift valley wall at a water depth of 3060 to 2900 m (Schmidt et al. 2007). It comprises seven high-temperature sites, two black smokers (Irina II and Site 'A'), and five smoking craters (Quest, Site 'B', Irina, Anna-Louise and Candelabra). The smoking craters consist of a central depression surrounded by a rim with 1 to 2 m elevation above the seafloor (Schmidt et al. 2007). The basement at the LHF is mainly made of serpentinized peridotites, coarse-grained magmatic cumulates, and subordinate basalts and gabbros (Amini et al. 2008). Measured temperatures show a wide range (Schmidt et al. 2007) with a maximum temperature of 353°C (Douville et al. 2002).

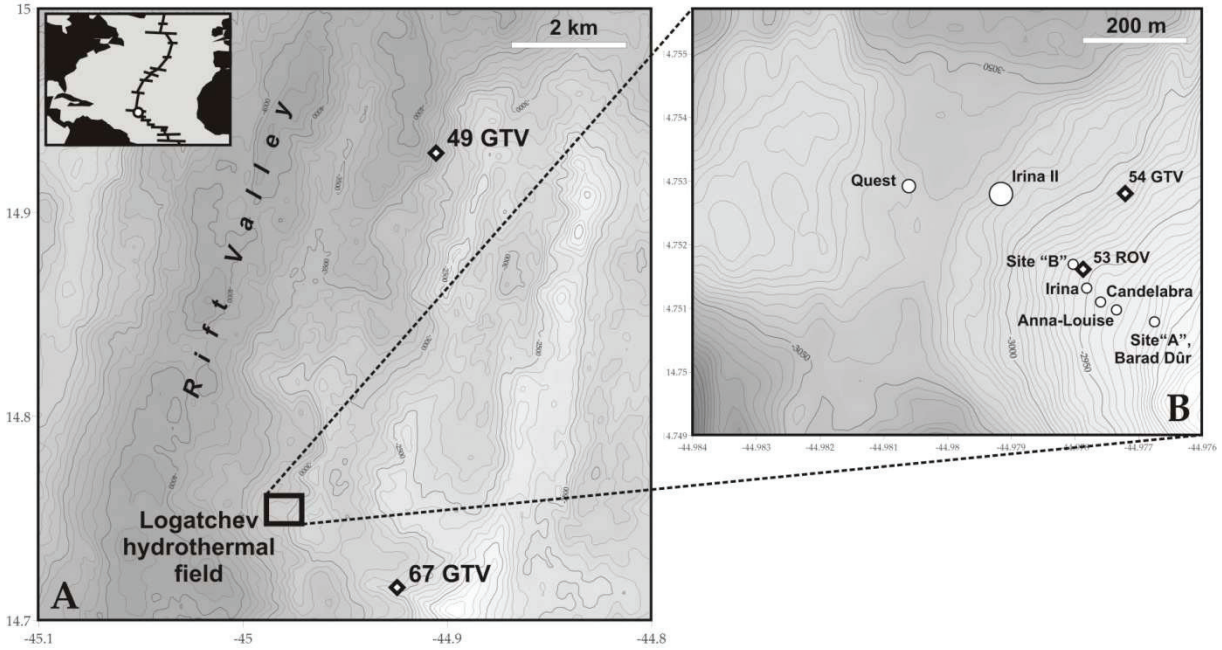

Fig. 3.2. Detailed bathymetric maps of the Mid-Atlantic ridge near the Logatchev hydrothermal field. (*A*) Bathymetric map of the Mid-Atlantic ridge south of the 15°20'N fracture zone including the two sampling sites for the serpentinite-hosted calcite (49GTV) and serpentinite-hosted aragonite (67GTV). (*B*) Detailed bathymetric map of vent sites in the ultramafic-hosted Logatchev hydrothermal field and sampling sites for the sulfide-hosted aragonite (54GTV) and dolomite (53ROV). Figure by Nico Augustin (Kiel).

Gakkel Ridge. The GR extends for 1800 km from the north coast of Greenland to the north coast of Russia and crosses the Eurasian basin of the Arctic Ocean (Hellebrand et al. 2002). It is the world's slowest spreading mid-ocean ridge. The fastest spreading part of GR is still slower than the slowest spreading part of the well-studied Southwest Indian ridge (Hellebrand et al. 2002). Dick et al. (2003) identified the GR as an ultraslow-spreading ridge, which is characterized by (1) an absence of transform faults, (2) rift valley walls defined by extremely long-lived low-angle faults, and (3) long stretches of seafloor where mantle peridotite is emplaced directly to the seafloor with little or no volcanic cover between widely spaced isolated magmatic centers. Axial valley depths can exceed 5000 m and valley width ranges from 10 to > 30 km (Baker et al. 2004).

The GR is divided into three magmato-tectonic domains, two of which are characterized by abundant volcanism (Michael et al. 2003). Our samples are from the middle segment (005°36.2''E to 005°44.0''E and 014°43.6''E to 014°59.7''E) that is volcanically starved. Edmonds et al. (2003) presented evidence for hydrothermal venting on the GR, which is localized near volcanic centers and, recently, even explosive volcanism was documented (Sohn et al. 2008).

Frankenwald. The studied serpentinite- and basalt-hosted calcites are from an active quarry in the northwestern part of the Frankenwald, northern Bavaria, Germany. The quarry is situated on the northern slope of the Grundberg Hill (50°10'09.07''N, 11°31'37.55''E), 2 km east-northeast (ENE) of the town of Stadtsteinach, and approximately 9 km NE of the city of Kulmbach. The Frankenwald, part of the Saxothuringian basin of the Variscan orogen, represents Paleozoic basin facies in southern Germany (Franke 1989). The Saxothuringian zone of Bavaria is a north-east trending belt of rocks situated at the north-western margin of the Bohemian Massif (Franke et al. 1995). Crustal extension associated with bimodal volcanism occurred mainly during the Cambrian and Ordovician (Franke 1989). Late Devonian (Frasnian) volcanism lead to the formation of pillow basalts locally reaching as much as 200 m in thickness in the study area, which records a brief, yet prominent interval of renewed rifting (Falk et al. 1995). The volcanic rocks can be assigned to an intraplate setting (Falk et al. 1995). The basalt is microcrystalline to fine-grained and relict glass is occasionally preserved. The greenish color of pillow basalt reflects a relatively low alteration stage, documented by the presence of chlorite. Because of alteration, the basalt has been named metabasalt, but is here referred to as pillow basalt. The serpentinites are highly altered, which is documented by the absence of primary silicate minerals and slight foliation.

3.3. Materials and methods

Material. We analyzed serpentinite-hosted carbonates, sulfide-hosted carbonates, and dolomite hosted in talus breccia from the LHF (Table 3.1). From the Arctic GR only serpentinite-hosted aragonite has been studied. From the Saxothuringian Frankenwald, Late Devonian pillow basalt-hosted and serpentinite-hosted vein calcites have been analyzed. Samples from the modern seafloor were dredged during METEOR cruise M60/3 (LHF) and POLARSTERN cruise AMORE 1 (GR).

Methods. Standard petrographic and fluorescence microscopy was done with thin sections using a Zeiss Axioskop 40 A Pol equipped with a Zeiss AxioCam MRc digital camera. For petrographical staining, a mixture of potassium ferricyanide and alizarin red, dissolved in 0.l% HCl, was used (Dickson 1966). Aragonite was stained with Feigl's solution (Feigl 1958).

Table 3.1. List of samples with carbonate mineralogy, stable isotopes (vs. V-PDB), and accessory mineral informarion.

Sample	Mineralogy	Host rock	$\delta^{13}C$ [VPDB]	$\delta^{18}O$ [VPDB]	Accessory minerals
Logatchev hydrothermal field					
Site 49GTV					
49GTV-1C-S2	calcite	serpentinite	−5.8	−20.0	
49GTV-1C-S3	calcite	serpentinite	−5.5	−19.1	
49GTV-1C-S4	calcite	serpentinite	−5.5	−19.3	
49GTV-1C-S5	calcite	serpentinite	−4.5	−16.1	
Site 53ROV					
53ROV-2-S1	dolomite	talus breccia	2.8	−9.2	
53ROV-2-S2	dolomite	talus breccia	2.9	−7.6	
53ROV-2-S3	dolomite	talus breccia	2.8	−8.6	
53ROV-2-S4	dolomite	talus breccia	2.7	−8.6	
53ROV-2-S5	dolomite	talus breccia	3.0	−7.0	
53ROV-2-S6	dolomite	talus breccia	3.0	−7.9	
53ROV-2-S7	dolomite	talus breccia	2.9	−7.2	
53ROV-2-S8	dolomite	talus breccia	2.6	−8.1	
Site 54GTV					
54GTV-2A-1-S1	aragonite	sulfide	3.3	2.0	clotted carbonate
54GTV-2A-1-S2	aragonite	sulfide	2.5	2.5	clotted carbonate
54GTV-2A-1-S3	aragonite	sulfide	2.8	4.0	clotted carbonate
54GTV-2A-1-S4	aragonite	sulfide	2.8	4.2	clotted carbonate
54GTV-2A-1-S5	aragonite	sulfide	2.7	3.8	clotted carbonate
54GTV-2A-1-S6	aragonite	sulfide	3.0	3.8	clotted carbonate
54GTV-2A-1-S7	aragonite	sulfide	2.8	3.0	clotted carbonate
54GTV-2A-4-S1	aragonite	sulfide	2.5	4.0	clotted carbonate
54GTV-2A-4-S2	aragonite	sulfide	3.4	2.0	clotted carbonate/filaments
54GTV-2A-4-S3	aragonite	sulfide	3.1	2.0	clotted carbonate/filaments
54GTV-2A-4-S4	aragonite	sulfide	3.4	1.3	clotted carbonate/filaments
54GTV-2A-4-S5	aragonite	sulfide	3.0	3.9	clotted carbonate/filaments
54GTV-2A-4-S6	aragonite	sulfide	3.0	3.7	clotted carbonate/filaments
54GTV-2B-S1	aragonite	sulfide	3.0	3.4	clotted carbonate
54GTV-2B-S2	aragonite	sulfide	3.2	3.0	clotted carbonate
54GTV-2B-S3	aragonite	sulfide	3.1	3.1	clotted carbonate
54GTV-2B-S4	aragonite	sulfide	3.6	1.6	clotted carbonate
54GTV-2C-S1	aragonite	sulfide	3.4	2.0	clotted carbonate
54GTV-2C-S2	aragonite	sulfide	3.4	2.2	clotted carbonate
54GTV-2C-S3	aragonite	sulfide	3.3	2.0	clotted carbonate
54GTV-2C-S4	aragonite	sulfide	2.7	3.3	clotted carbonate
54GTV-2C-S5	aragonite	sulfide	3.0	3.6	clotted carbonate
Site 67GTV					
67GTV-2C-S1	aragonite	serpentinite	−1.0	4.0	brown/opaque minerals
67GTV-2C-S2	aragonite	serpentinite	−1.6	4.8	brown/opaque minerals
67GTV-2C-S3	aragonite	serpentinite	−1.0	4.6	brown/opaque minerals
Gakkel ridge					
Site PS 59					
PS 59-238-75-S1	aragonite	serpentinite	0.7	4.7	opaque mineral
PS 59-238-75-S2	aragonite	serpentinite	0.7	4.9	opaque mineral
PS 59-238-75-S3	aragonite	serpentinite	2.7	5.3	opaque mineral
PS 59-249-A63-S1	aragonite	serpentinite	2.3	5.1	opaque mineral
Frankenwald					
FW-05-S-1-01	calcite	serpentinite	−4.7	−16.0	
FW-05-S-1-02	calcite	serpentinite	−4.3	−15.8	
FW-05-S-2-01	calcite	basalt	−0.2	−12.6	
FW-05-S-2-02	calcite	basalt	0.2	−12.9	
FW-05-S-3a-01	calcite	serpentinite	−5.0	−14.9	
FW-05-S-3a-02	calcite	serpentinite	−4.9	−14.6	
FW-05-S-3b-01	calcite	serpentinite	−5.0	−14.6	
FW-05-S-3b-02	calcite	serpentinite	−4.9	−14.7	
FW-05-S-5-01	calcite	serpentinite	−4.6	−15.8	
FW-05-S-5-02	calcite	serpentinite	−4.9	−15.4	
FW-05-S-6-01	calcite	basalt	−0.2	−12.0	
FW-05-S-6-02	calcite	basalt	−0.9	−9.2	
FW-05-S-7-01	calcite	serpentinite	−5.4	−15.8	
FW-05-S-7-02	calcite	serpentinite	−5.3	−15.9	
FW-05-S-8-01	calcite	serpentinite	−0.6	−15.5	
FW-05-S-8-02	calcite	serpentinite	−0.4	−15.5	
FW-05-S-9-01	calcite	serpentinite	−6.8	−15.9	
FW-05-S-9-02	calcite	serpentinite	−7.3	−15.6	
FW-05-S-10-01	calcite	serpentinite	−8.6	−16.0	
FW-05-S-10-02	calcite	serpentinite	−8.0	−16.0	

Field emission scanning electron microscopy (FE-SEM) was performed on broken subsamples that were etched with 1% HCl for 30 s and cleaned with distilled water. A LEO 1530 (Geoscience Department, Göttingen University) was used for FE-SEM. The LEO 1530 is equipped with an Oxford INCA 400 for energy-dispersive x-ray analyses. Cathodoluminescence investigations were carried out with a Citl 8200 MK3A cold cathode mounted on a Zeiss Axiolab microscope (Geoscience Department, Göttingen University). Micrographs were made at 20 kV using a cooled SPOT-CCD camera. The SPOT's CCD chip has a true resolution of 1315 × 1033 pixels. By exposing the CCD three times (for red, green and blue, respectively), each color was accurately recorded on every CCD pixel.

X-ray diffraction measurements have been performed in the Crystallography Department, Geosciences, Bremen University, on a Philips X'Pert Pro MD equipped with a Cu-tube (kalpha 1.541, 45 kV 40 mA), a fixed divergence slit (¼° 2theta), a 15 samples changer, a secondary monochromator and the X´Celerator detector system. Sample preparation with the Philips backloading system should provide random distribution of crystallites in the sample. Measurements were done as a continuous scan from 3 to 85 ° 2theta with a calculated step size of 0.016° 2theta. The calculated time per step was 100 seconds.
Mineral identification was done by means of the Philips software HiScore.
The mineralogy of opaque and brown phases in the serpentinite-hosted aragonite and the filamentous network in the sulfide-hosted aragonite was assessed with a JXA 8900 R electron microprobe (Geoscience Department, Kiel University). The electron microprobe is equipped with five WD spectrometers and an EDX system. Electron source parameter were an acceleration voltage of 15 keV, a beam current of 20 nA and a 1 micrometer beam diameter.

Carbon and oxygen isotope measurements were performed with a Finnigan MAT 251 mass spectrometer using the 'Kiel' carbonate device type 'Bremen' (Isotope Laboratory, Geoscience Department, Bremen University). Carbonates were converted into carbon dioxide and measured regarding their 45/44 and 46/44 mass ratios against a standard gas (Burgbrohl carbon dioxide gas). A Solnhofen limestone was used as standard, which was calibrated against NBS 19 as an internal standard. Analytical standard deviation was approximately ±0.07% for $\delta^{18}O$ values, and ±0.05% for $\delta^{13}C$ values. The $\delta^{18}O$ and $\delta^{13}C$ values are reported relative to the V-PDB standard. Formation temperatures for calcite

were calculated after Kim and O'Neil (1997), for dolomite after Veizer (1983), Zheng (1999), Vasconcelos et al. (2005), and for aragonite after Kim et al. (2007).

3.4. Carbonate petrography

Mid-Ocean Ridge Carbonates. Most serpentinite-hosted carbonates are aragonite (Fig. 3.3; Table 3.1), which was found at the LHF and at the GR, whereas serpentinite-hosted calcite was only observed in rocks from the LHF. At both sites, the aragonite occurs in transgranular veins, i.e. those that cross-cut the primary porphyroclastic rock fabric (Fig. 3.3a, 3.3b). Vein aragonite displays three distinct crystal habits, botryoidal crystal aggregates, acicular aragonite crystals, and microcrystalline aragonite (only GR). In samples from LHF, the first generation of botryoidal aragonite grows into the open fracture, whereas later aragonite cement fills the remaining void space (Fig. 3.3a, 3.3b). The long axes of crystals of this cement are preferentially oriented parallel to the walls of veins. In many veins, aragonite precipitation postdates the formation of unidentified brown minerals on fracture walls (Fig. 3.3b, 3.3d). The brown minerals are only found in samples from the LHF. The thickness of the brown, cryptocrystalline mineral aggregates is relatively constant (10 to 30 µm). Calcium and iron are the most abundant elements, followed by trace amounts of magnesium and silica (Table 3.2).

Table 3.2. Electron microprobe analyses of opaque minerals (LHF and GR), brown minerals (LHF), and filaments (LHF). All chemical analyses are given in weight percent (wt%) and represent average values.

	filaments	opaque minerals	brown minerals
Al_2O_3	0.1	4.0	0.1
MnO	0.1	35.7	0.1
SO_2	0.1	0.3	0.1
MgO	1.6	12.4	1.2
CuO	0.1	0.0	0.0
SiO_2	6.5	2.4	0.9
FeO	58.4	1.2	7.6
CoO	0.1	4.4	0.0
NiO	0.1	4.3	0.2
CaO	1.8	2.1	46.5
Total	**69.1**	**66.9**	**56.6**

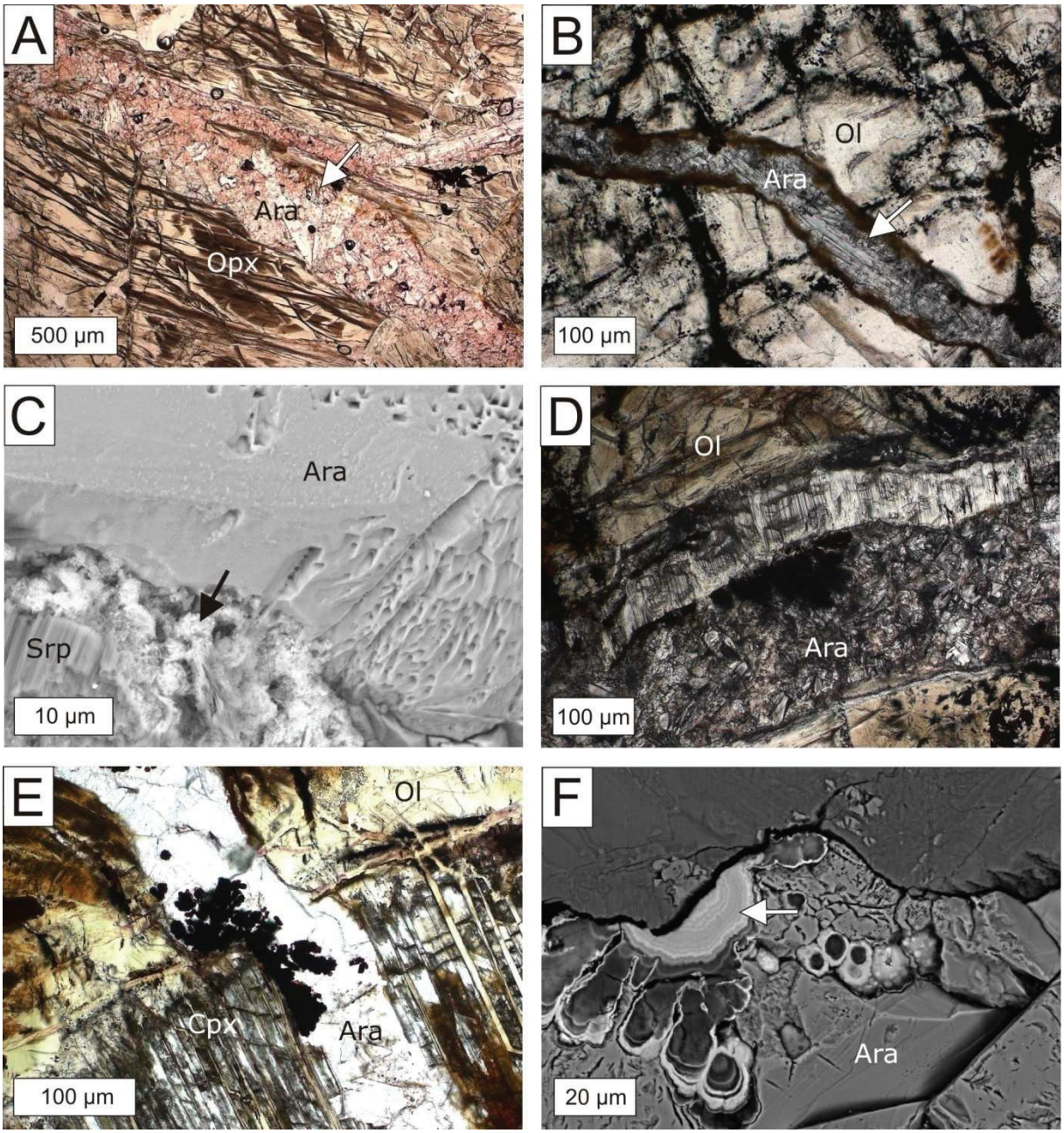

Fig. 3.3. Serpentinite-hosted aragonite phases. Ara = aragonite; Opx = orthopyroxene; Ol = olivine; Srp = serpentine minerals; Cpx = clinopyroxene. Plane polarized light. (*A*) Aragonite vein in fractured othopyroxene. The arrow indicates the first aragonite (stained pinkish) generation of radial fibrous crystals (LHF). (*B*) Aragonite vein coated by an unknown iron-rich phase, cross-cutting the silicate matrix. The arrow indicates the first aragonite generation (LHF). (*C*) FE-SEM image of a serpentinite-hosted aragonite vein. The arrow indicates the brown minerals representing the contact between the aragonite vein and the serpentinite host rock (LHF). (*D*) Vein-filling aragonite postdating talc formation (LHF). (*E*) Heavy metal rich opaque phase projecting into a vein (GR). (*F*) Electron microprobe image of an aragonite vein hosted in serpentinite. The white arrow indicates the opaque minerals revealing a concentric internal layering (GR).

In both LHF and GR samples, an opaque dendritic mineral aggregate is recognized that precipitated on vein walls (Fig. 3.3d, 3.3e). The layered opaque precipitate (Fig. 3.3f) is not found in the rock matrix. Its thickness is highly variable, ranging from 20 to almost 150 μm. The most abundant elements are manganese and magnesium, followed by trace amounts of copper, nickel, calcium, silica, and aluminum (Table 3.2). Only one serpentinite sample from the LHF was found to contain calcite (Fig. 3.4a, 3.4b). Calcite crystals show no zoning under fluorescence or cathodoluminescence.

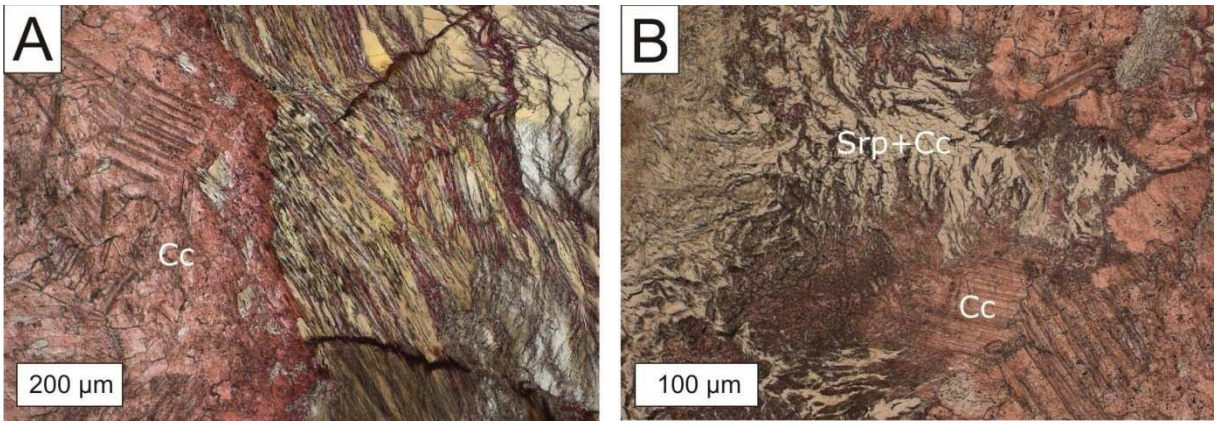

Fig. 3.4. Serpentinite-hosted calcite samples (LHF). Cc = calcite; Srp = serpentine minerals. (*A*) Calcite vein crosscutting an assemblage of finely laminated calcite (stained pinkish) and talc. (*B*) Secondary calcite (stained pinkish) within serpentinite.

The petrography of the LHF sulfide-hosted carbonates is more complex. The paragenetic sequence of the carbonates is represented by (1) microcrystalline aragonite, (2) botryoidal and isopachous aragonite, and (3) clotted microcrystalline aragonite (Fig. 3.5a). Aragonite occurs in veins and in cavities cementing sulfide minerals. Microcrystalline aragonite initiates on the surface of sulfide minerals and predates the growth of aragonite needles (Fig. 3.5b). Clotted microcrystalline aragonite often forms dense aggregates. Clots are a few 100 μm or smaller in diameter (Fig. 3.5c). A common feature in the sulfide-hosted aragonite is intense in-situ brecciation, which is followed by the precipitation of acicular aragonite cementing the open fractures (Fig. 3.5d).

Some aragonite veins contain atacamite, a product of sulfide weathering. Networks of unidentified filaments with diameters from 2 to 8 μm are found in LHF sulfides (Fig. 3.6). The length of individual filaments is variable, ranging from 5 to 40 μm. The networks resembling the hyperthermophilic archaeon *Pyrodictium*, which has been found at hot

vents off Vulcano, Italy (Stetter 2006), cover an overall area of 30 to 100 µm in width. The branching filaments form dense networks that are brownish under transmitted light. Individual filaments are connected with up to five other filaments (Fig. 3.6a). Based on electron microprobe analyses, the filaments predominantly consist of iron and silica (Table 3.2). The well-structured network, which is enclosed in microcrystalline aragonite, is independent of other crystals or cleavage plans (Fig. 3.6b).

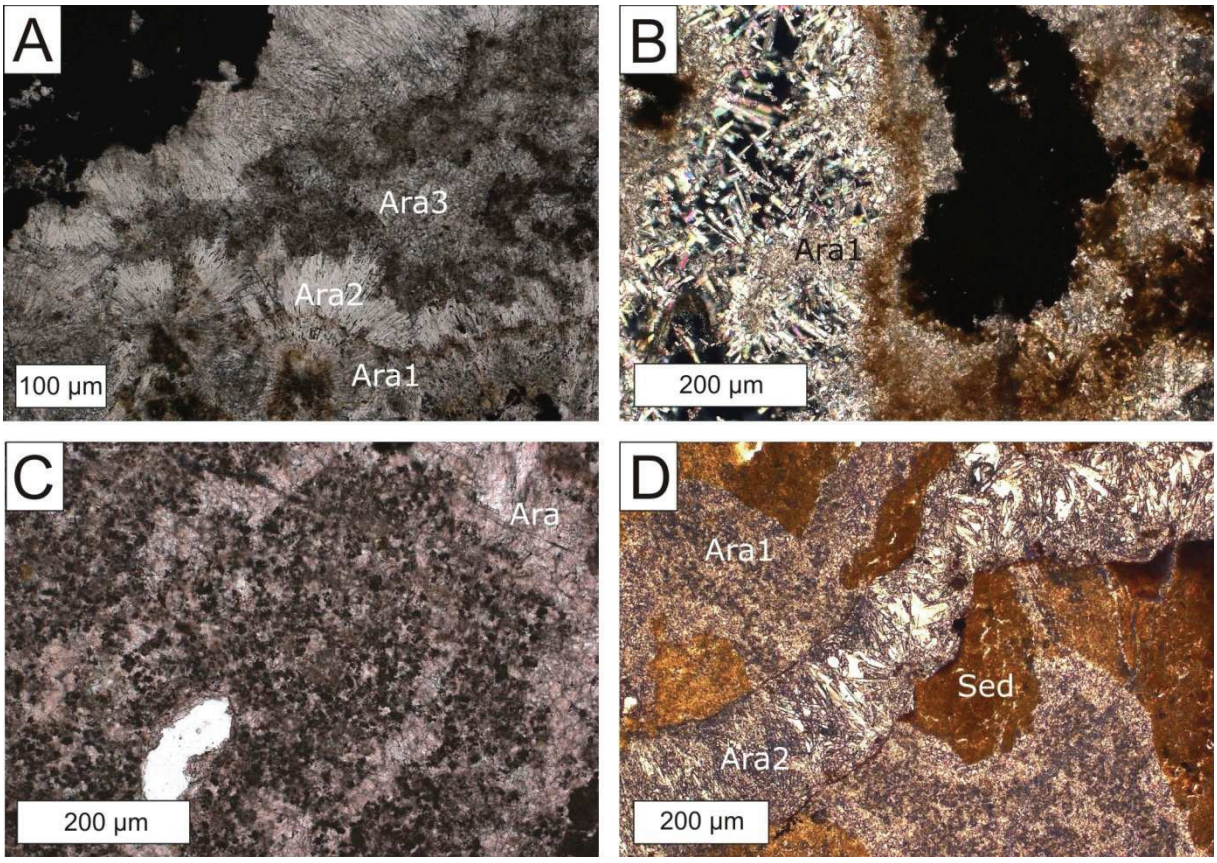

Fig. 3.5. Sulfide-hosted carbonates (LHF). Ara = aragonite; Ara1 = microcrystalline aragonite; Ara2 = acicular aragonite; Ara3 = late microcrystalline aragonite; Sed = sedimentary detritus. (*A*) Paragenetic sequence of sulfide-hosted carbonates with microcrystalline aragonite, isopachous aragonite, and later clotted aragonite. Plane polarized light. (*B*) Formation of microcrystalline aragonite and fibrous aragonite initiated on the surface of sulfide minerals. Crossed polarized light. (*C*) Clotted carbonate surrounded by aragonite (stained pinkish) cement (Ara). Plane polarized light. (*D*) In-situ brecciation of microcrystalline aragonite associated with sediments. The opened fractures are filled by acicular aragonite (stained pinkish). Plane polarized light.

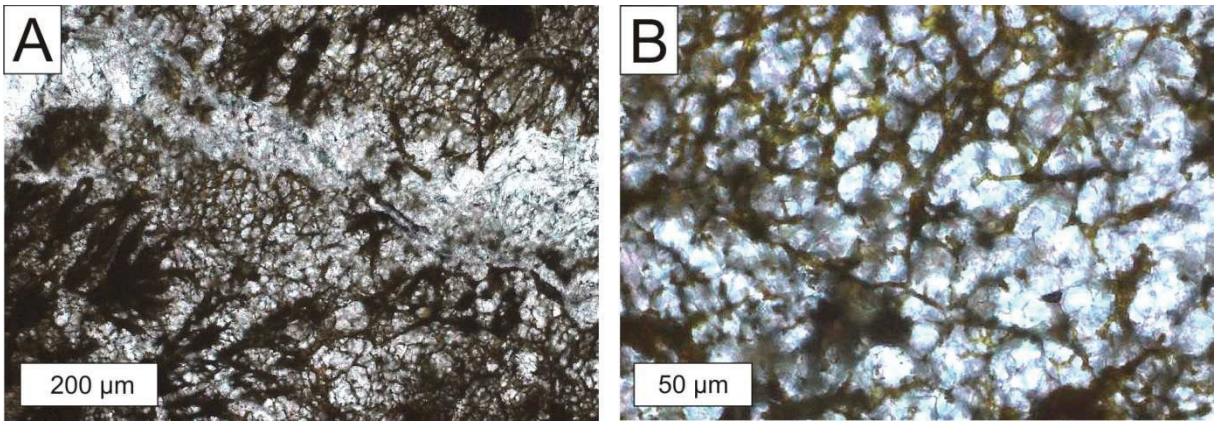

Fig. 3.6. Branching filaments in sulfide-hosted aragonite (LHF). Plane polarized light. (*A*) Dense accumulations of unidentified filaments within later aragonite. (*B*) Detail from (*A*).

Unusual dumbbell-shaped crystal aggregates of dolomite were found in talus breccia deposits from the LHF (Fig. 3.7). This is the first report of dumbbell-shaped dolomite in an active hydrothermal environment. The size of the dumbbells is relatively uniform (150 to 250 µm). Under fluorescence and cathodoluminescence internal zoning of individual crystals is evident (Fig. 3.7a, 3.7b).

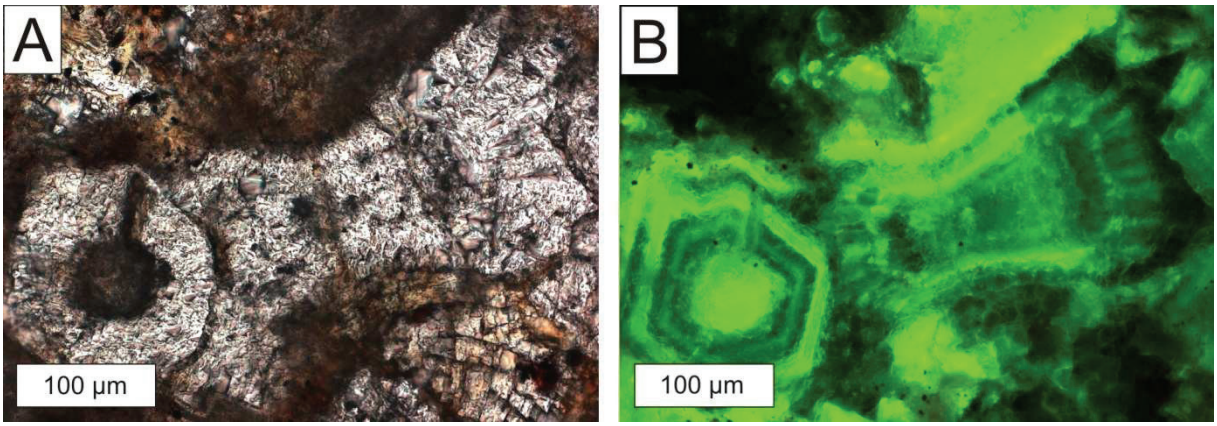

Fig. 3.7. Dolomite dumbbells (LHF). (*A*) Two dumbbells in transverse and longitudinal section; plane polarized light. (*B*) Same detail as (*A*); fluorescence photomicrograph.

Frankenwald Carbonates. Authigenic carbonates were found in pillow basalts and serpentinites (Fig. 3.8; Table 3.1). In contrast to most of the modern seafloor carbonates, all studied Late Devonian (Frasnian) carbonates are ferroan calcite. The pillow basalt-hosted calcite occurs in veins and amygdules (Fig. 3.8a). It exhibits rhombohedral cleavage planes. Some earlier botryoidal crystal aggregates of calcite in amygdules may

represent former aragonite (Fig. 3.8b). Calcite in the outer part of the pillow is accompanied by chlorite, which is consistent with seawater alteration. Some chlorite obviously predates calcite (Fig. 3.8a). Vein filling calcite is often accompanied by interstitial quartz. Some calcite veins are predated by an aggregation of chlorite and microcrystalline calcite (Fig. 3.8c).

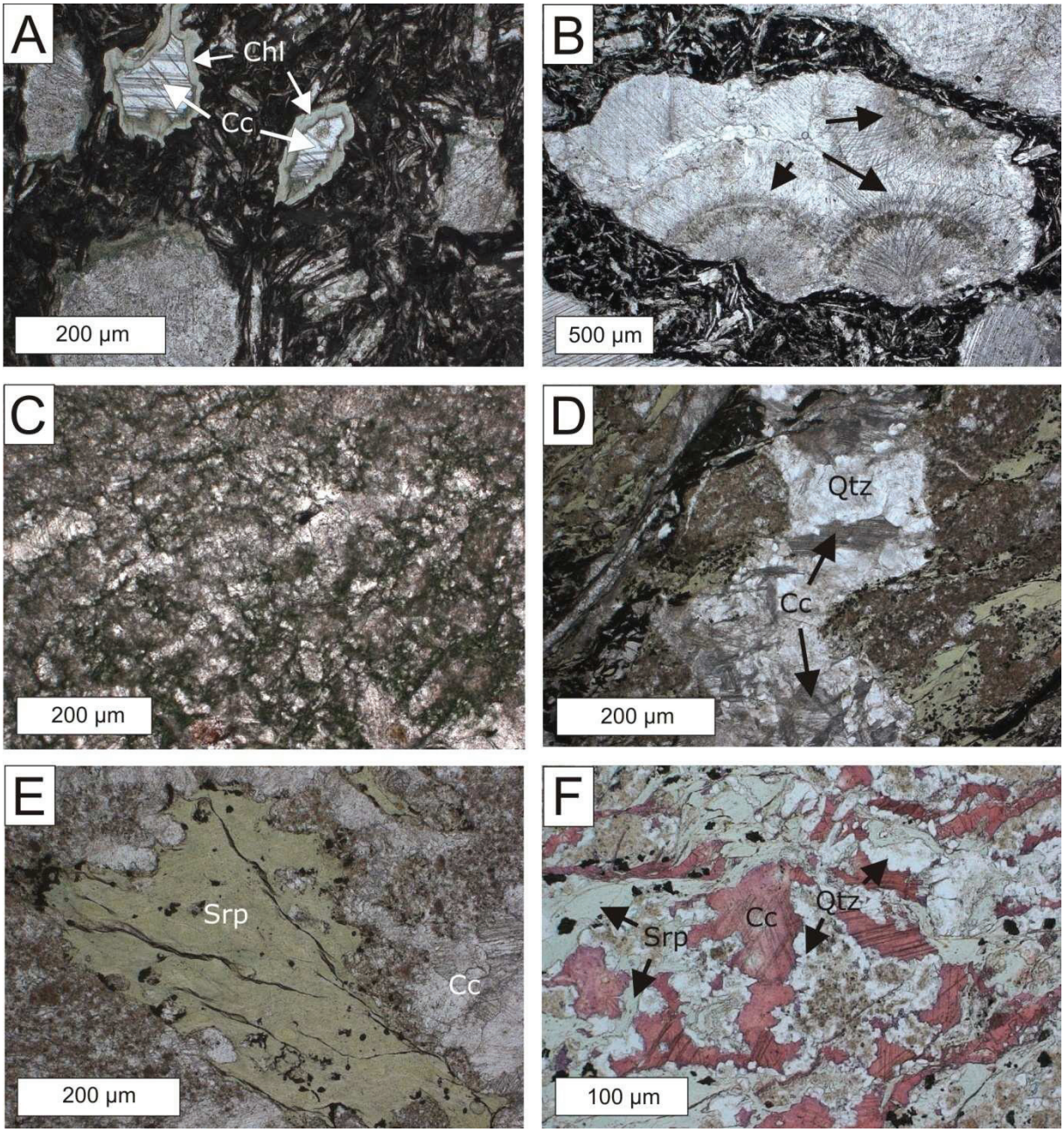

Figure 3.8. Basalt-hosted (*A* to *C*) and serpentinite-hosted (*D* to *F*) carbonates from the Frankenwald. Cc = ferroan calcite; Chl = chlorite; Qtz = quartz; Srp = serpentine mineral. Plane polarized light. (*A*) The basalt-hosted calcite occurs in vesicles. Calcite postdating chlorite. (*B*) Botryoidal crystal aggregates of calcite (arrows), probably representing former aragonite. (*C*) Aggregation of microcrystalline calcite and chlorite and calcite veins in basalt. (*D*) Calcite vein in serpentinite containing quartz. (*E*) Serpentine mineral surrounded by calcite. (*F*) Dispersed ferroan calcite in the serpentinite matrix. Ferroan calcite surrounded by microcrystalline quartz. Stained thin section.

The serpentinite-hosted equant ferroan calcite is found in veins and finely dispersed in the serpentinite matrix (Fig. 3.8d – 3.8f). Overall, the thickness of the calcite veins is highly variable, ranging from 50 µm to 1 mm. Crystal size of the finely dispersed ferroan calcite is also highly variable. Like vein filling calcite in the pillow basalt, the calcite veins contain later quartz (Fig. 3.8d). Ferroan calcite in the serpentinite matrix is surrounded by microcrystalline quartz (Fig. 3.8f). The ferroan calcite veins are postdated by later ferroan calcite and quartz veins, both cross-cutting veins with ferroan calcite.

3.5. Stable Isotope Geochemistry

Mid-Ocean Ridge Carbonates. The $\delta^{18}O$ values of LHF serpentinite-hosted calcite range from –20.0 to –16.1‰, serpentinite-hosted aragonite ranges from +4.0 to +4.8‰ (LHF) and +4.7 to +5.3‰ (GR), respectively (Fig. 3.9; Table 3.1). $\delta^{18}O$ values of the LHF sulfide-hosted aragonite range from +1.3 to +4.2‰. Dolomite in the talus breccia deposits yielded $\delta^{18}O$ values from –9.2 to –7.0‰.

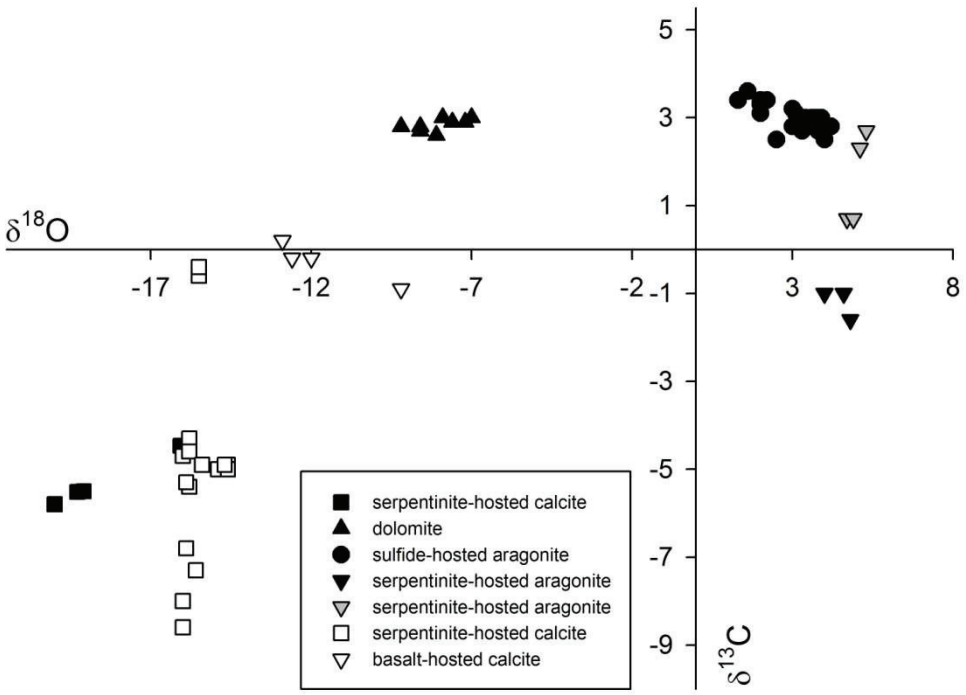

Fig. 3.9. $\delta^{18}O$ and $\delta^{13}C$ cross plot of carbonates from the Logatchev hydrothermal field (LHF), the Gakkel ridge (GR), and the Frankenwald. Black symbols represent LHF samples, gray symbols represent GR samples, whereas white symbols represent Frankenwald samples.

The $\delta^{13}C$ values of serpentinite-hosted calcite range from –5.8 to –4.5‰, those of serpentinite-hosted aragonite vary from –1.6 to –1.0‰ (LHF) and +0.7 to +2.7‰ (GR), respectively. $\delta^{13}C$ values of sulfide-hosted aragonite vary from +2.5 to +3.6‰, those of dolomite dumbbells range from +2.6 to +3.0‰.

For temperature estimates based on $\delta^{18}O$ values, the oxygen fractionation factors of the respective minerals are required. The inferred temperatures – based on the assumption that all carbonate phases precipitated from seawater ($\delta^{18}O$ = 0‰) – are highest for the serpentinite-hosted calcite (129 to 186°C), and lowest for the serpentinite- and sulfide-hosted aragonite (ambient seawater). Formation temperatures for the dolomite samples range from 83 to 101°C. However, if a $\delta^{18}O_{water}$ value close to a measured value of LHF vent fluid is assumed ($\delta^{18}O_{SMOW}$ = +1.5‰; pers. comm. M. Peters, Münster) the formation temperature of the LHF carbonates is higher by 6 to 29°C. Low-temperature alteration of silicate minerals leads to higher $\delta^{18}O_{silicate}$ values and lower $\delta^{18}O_{water}$ values, whereas high-temperature alteration leads to lower $\delta^{18}O_{silicate}$ values and higher $\delta^{18}O_{water}$ values (Muehlenbachs and Clayton 1976), indicating that the LHF vent fluid was affected by high-temperature alteration (cf. Schmidt et al. 2007).

Frankenwald Carbonates. The $\delta^{18}O$ values of the serpentinite-hosted calcite range from –16.0 to –14.6‰ (Fig. 3.9; Table 3.1). $\delta^{18}O$ values of the basalt-hosted calcite vary from –12.9 to –9.2‰. The corresponding $\delta^{13}C$ values of the serpentinite-hosted calcite exhibits values between –8.6 and –0.4‰. $\delta^{13}C$ values for the basalt-hosted calcite range from –0.9 to +0.2‰.

3.6. Carbonate Formation in Ultramafic Rocks: Mid-Ocean Ridge and Frankenwald

Mid-Ocean Ridge Carbonates. The studied samples reveal that aragonite constitutes a significant proportion of the vein-filling carbonates in many of the serpentinites recovered from the LHF and the GR. Sulfide breccia from the LHF contains exclusively aragonite. Although aragonite is a major carbonate mineral in weathered serpentinites (Bonatti et al. 1980; Ribeiro da Costa et al. 2008), as well as in carbonate chimneys along the Mariana forearc (Haggerty 1991) and the Mid-Atlantic ridge at 30°N (Ludwig et al. 2006) forming above serpentinites, it is only metastable in these environments and may convert to calcite (Berndt and Seyfried 1999). The presence of serpentinite-hosted

calcite and aragonite with variable stable carbon and oxygen compositions from the LHF reveal the influence of fluids with different chemical compositions on the mineralogy of calcium carbonates. Besides temperature, additional factors play a fundamental role in the precipitation of carbonates, conditioning mineralogy and morphology (e.g., Given and Wilkinson 1985; Burton 1993). The fluid chemistry, in particular Mg^{2+} and sulfate concentrations and the Mg/Ca ratio influence carbonate precipitation (Burton 1993). Calcite precipitation is hindered by the fact that Mg^{2+} ions are preferentially introduced into the crystal lattice of calcite. The so-called 'poisoning effect' of Mg^{2+} ions is caused by the strong hydration of the small Mg^{2+} ion, which results in a kinetical barrier for precipitation. It is consequently a selective factor favoring aragonite instead of calcite precipitation (Mucci and Morse 1983; Morse et al. 2007). Recently, it has been suggested that elevated Sr^{2+} concentrations in solution may also inhibit calcite precipitation (Wasylenki et al. 2005). The preservation of metastable aragonite in most of the serpentinites is due to sluggish conversion to calcite by dissolution and re-precipitation at low temperatures like those characterizing bottom seawater in contact with exposed serpentinites (Berndt and Seyfried 1999). Furthermore, high Mg^{2+} concentration of seawater and the stabilizing effect of the Sr^{2+} ion in aragonite (Katz et al. 1972) inhibit conversion to calcite.

These constraints indicate that precipitation and preservation of aragonite in LHF and GR serpentinites and LHF sulfides result from interactions with seawater (high Mg^{2+} and sulfate concentrations) at low temperatures. High $\delta^{18}O$ values of aragonite samples ranging from +1.3 to +5.3‰ reflect precipitation at low temperatures (Fig. 3.9). These values for the serpentinite-hosted aragonite are higher than values reported from the upper oceanic crust (Staudigel et al. 1981), and lower oceanic crust (Hart et al. 1994), but similar to aragonite reported from serpentinites from the Mid-Atlantic ridge (Bonatti et al. 1980; Ribeiro da Costa et al. 2008). $\delta^{13}C$ values of the serpentinite-hosted aragonite represent a marine carbon signal (−1.6 to +2.7‰), suggesting that aragonite precipitation was abiogenic, whereas sulfide-hosted aragonite exhibits $\delta^{13}C$ values as high as +3.6‰. The high $\delta^{13}C$ values may indicate a carbon source other than seawater, possibly residual carbon dioxide in the zone of methanogenesis (Irwin et al. 1977; see discussion below on dolomite).

Fluids that favored calcite precipitation, on the other hand, presumably had low Mg^{2+} and sulfate ion concentrations. Such fluids are typically generated by serpentinization

(Charlou et al. 2002). Thus, calcite precipitation in serpentinites of the LHF probably occurred under the influence of fluids other than seawater at higher temperatures. Calcite formation at high temperatures is indicated by low $\delta^{18}O$ values, varying between −20.0 to −16.1‰ (Fig. 3.9). A $\delta^{18}O$ value of −20‰ corresponds to a formation temperature of 186°C assuming seawater oxygen isotope composition of the fluid (cf., Kim and O'Neil 1997). Similarly, $\delta^{13}C$ values of serpentinite-hosted calcite (−5.8 to −4.5‰) agree with a contribution of mantle-derived carbon dioxide as in high-temperature hydrothermal fluids associated with serpentinites (Charlou et al. 2002). Calcite in serpentinites of the Iberian margin, on the other hand, is believed to have formed at low temperatures (13 to 15°C) (Agrinier et al. 1996).

The opaque and brown minerals in aragonite veins in modern serpentinites (Fig. 3.3b, 3.3e, 3.3f) likely precipitated from a fluid of similar composition as the vein-filling aragonite. Since the main constituent elements of those phases (Fe, Mn, Si, and Ni) are difficult to mobilize, their enrichment in the vein fill suggests rock-dominated conditions, perhaps due to restricted fluid flow.

Frankenwald Carbonates. The Late Devonian basalts and serpentinites of the Frankenwald now only contain calcite. However, it is possible that the basalt-hosted botryoidal crystal aggregates (Fig. 3.8b) were originally aragonitic suggesting early formation at low temperatures similar to the modern counterparts from the Mid-Atlantic ridge. Similarly, calcite hosted in the associated serpentinites may have formed at higher temperatures. It needs to be addressed whether the $\delta^{18}O$ and $\delta^{13}C$ values of calcite hosted the Frankenwald basalts and serpentinites are primary or were modified during diagenesis and metamorphic overprinting. The $\delta^{18}O$ values of basalt-hosted calcite ranging from −12.9 to −9.2‰ would indicate calcite formation between 65 to 95°C (Fig. 3.9). These temperatures are higher than most temperatures for basalt-hosted calcite reported from the upper ocean crust (Staudigel et al. 1981). Consequently, it seems most likely that the low $\delta^{18}O$ values reflect diagenetic and metamorphic overprinting. The obtained $\delta^{18}O$ values of serpentinite-hosted calcite (−16.0 to −14.6‰) similarly reflect increasing temperatures during the Variscan orogeny (cf., Franke 1989). Negative $\delta^{18}O$ values have also been reported for ophicalcites from South Pennine thrust nappes of eastern Switzerland (Weissert and Bernoulli 1984), and Mesozoic ophicalcites

from the north-central Apennines (Barbieri et al. 1979). The relatively uniform $\delta^{18}O$ values for the serpentinite-hosted calcite may reflect maximum temperatures during metamorphism. Apart from that, Postvariscan metamorphism influencing $\delta^{18}O$ values cannot be excluded (pers. comm. W. Franke, Frankfurt).

$\delta^{13}C$ values of the basalt-hosted calcite (around 0‰) indicate contribution of seawater-derived dissolved inorganic carbon (cf., Zeebe and Wolf-Gladrow 2005). The obtained $\delta^{13}C$ values are similar to those of Devonian carbonates of the Saxothuringian zone (Buggisch and Joachimski 2006). The $\delta^{13}C$ values of most serpentinite-hosted calcites are similar to the mantle carbon isotopic composition (–6 to –7‰; Fig. 3.9; Table 3.1), albeit extending to lower values. Serpentinite-hosted veins from modern spreading ridges either show seawater carbon isotopic composition (e.g., Bonatti et al. 1980) or somewhat lower (–6‰; Früh-Green et al. 2003) or higher values (as high as +4.5 ‰; Alt and Shanks 2003). Deviations from seawater are commonly interpreted as a result of methane formation (creating high $\delta^{13}C$ values; Alt and Shanks 2003) or oxidation of methane or other organic compounds (creating low $\delta^{13}C$ values; Früh-Green et al. 2003). For our samples, it cannot be excluded that the low $\delta^{13}C$ values reflect oxidation of complex organic matter, but methane is known to be abundant in environments influenced by serpentinization (Charlou et al. 2002), suggesting that methane is a more likely carbon source. In contrast to the Frankenwald and Lost City serpentinite-hosted carbonates, the ^{13}C content of ophicalcites from the Alps and the Apennines agrees with seawater-derived dissolved inorganic carbon as the carbon source (Barbieri et al. 1979; Weissert and Bernoulli 1984).

3.7. Hints for Biogenicity of Mineral Phases from the Logatchev Hydrothermal Field

Given the interesting textures of secondary carbonate phases in the ocean-floor hard rocks analyzed (Fig. 3.5c, 3.6, 3.7) one question is whether there is microbial influence on carbonate precipitation.

Clotted Carbonate. The term clotted carbonate is used for an aggregate of irregular, microcrystalline clots and carbonate cement, which fills space left by clots. The widely used term ‘clotted micrite’ implies that the clots are essentially formed of

microcrystalline calcite (Peckmann et al. 2002). In contrast, the clotted microfabrics in the LHF are formed of aragonite. Clots in seep carbonates of the Black Sea are formed of high Mg-calcite (Peckmann et al. 2001). Thus, a specific mineralogy is not crucial for its genesis. It is widely accepted that clotted fabrics are primary (e.g., Peckmann et al. 2002). Considering their primary nature, clotted fabrics of different scales are regarded as typical features of microbial carbonates (Burne and Moore 1987). The irregular shape may result from microenvironments caused by microbial metabolism. This fabric represents circumstantial, but not unequivocal, evidence for microbial mediation in carbonate precipitation.

Formation of Dolomite Dumbbells and Methanogenesis. Although dolomite is the thermodynamically stable carbonate phase in seawater, the presence of even minor amounts of dissolved sulfate are believed to suppress its formation (Baker and Kastner 1981). The high sulfate concentration of seawater (28 mM) is consequently thought to be responsible for the scarcity of dolomite in marine environments. Several studies have shown that sulfate-reducing bacteria mediate dolomite precipitation under anoxic conditions (Vasconcelos et al. 1995; Warthmann et al. 2000). The metabolism of sulfate-reducing bacteria favors dolomite formation in at least four ways: (1) removal of sulfate as an kinetic inhibitor, (2) increased availability of Mg^{2+} due to sulfate removal, (3) concentration of Ca^{2+} and Mg^{2+} in bacterial extracellular polymeric substances, and (4) increase of alkalinity as a consequence of the remineralization of organic matter (e.g., van Lith et al. 2003). However, apart from sulfate reducers, methanogens have been suggested to be able to induce dolomite precipitation (e.g., Mazzullo et al. 1995; Warren 2000; Roberts et al. 2004).

It is widely accepted that hydrogen is released during serpentinization in ultramafic environments (Bach et al. 2006; Schulte et al. 2006). In contrast to basalt-hosted hydrothermal environments, hydrogen concentrations in the LHF are extremely high (12 to 19 mmol/kg), but similar to the ultramafic-hosted Rainbow field (Charlou et al. 2002; Schmidt et al. 2007). Consequently, hydrogen is a potential energy source for microbial metabolism in the LHF (cf., Perner et al. 2007). Hydrogen is the electron donor for a number of chemoautotrophic biochemical processes, including methanogenesis (Berndt et al. 1996; Schulte et al. 2006).

High and low $\delta^{13}C$ values of authigenic carbonates indicate metabolic processes and hence argue for the presence of prokaryotes (Irwin et al. 1977). The high $\delta^{13}C$ values of LHF dolomite dumbbells may point to lithotrophic reduction of carbon dioxide by methanogens that produce methane from hydrogen and carbon dioxide. During this biological mediated process methane becomes enriched in ^{12}C, and thus the residual carbon dioxide becomes enriched in ^{13}C (Irwin et al. 1977). The $\delta^{13}C$ values of dolomite dumbbells are at the lower end of the compositional range of sedimentary methanogenic dolomite ($\delta^{13}C$ as high as +14‰) recovered from the Gulf of California (Kelts and McKenzie 1982). Based on the carbon isotope composition alone, a methanogenic origin of the dolomite cannot be concluded. However, $\delta^{18}O$ values of LHF dolomite (−9.2 to −7.0‰) indicate dolomite formation at elevated temperatures (83 to 100°C), and Sr isotope data indicate a small contribution of hydrothermal fluids (Eickmann et al., unpub. data). Any possible contribution of ^{13}C-depleted magmatic CO_2, such as in the LHF vent fluids (Charlou et al. 2002), would make the case for methanogenesis stronger. Furthermore, the LHF environment of dolomite formation appears to be more controlled by advective transport than in typical marine sediments so that a build-up of a methanogenic signal in the dissolved inorganic carbon pool of the pore waters is more difficult. While the isotopic evidence is inconclusive, the supposed formation temperatures for dolomite are consistent with the temperature range of thermophilic methanogens. Interestingly, methanogens also occur in hydrothermal settings including hydrothermal vent sediments from the Guaymas Basin, Gulf of California where members of the genus *Methanococcus* have been detected (Jones et al. 1989). A biogenic origin of the dolomite dumbbells is further supported by their intense autofluorescence, indicating a high content of organic matter and the crystal habit, which is typical of microbial dolomites (e.g., Peckmann et al. 1999; Warthmann et al. 2000; van Lith et al. 2003).

3.8. Conclusions

Authigenic carbonates from the Logatchev hydrothermal field (LHF) and the Gakkel ridge (GR) reflect precipitation at different temperatures and from different fluids spanning from ambient temperatures and seawater to hydrothermal conditions. Aragonite is the most abundant carbonate mineral found in both serpentinites (LHF and

GR) and massive sulfides (LHF). The precipitation and preservation of aragonite is believed to have resulted from contact with seawater being typified by high Mg^{2+} and sulfate concentrations. High $\delta^{18}O$ values of aragonite reflect precipitation at low temperatures. $\delta^{13}C$ values of serpentinite-hosted aragonite agree with a marine carbon signal, whereas high $\delta^{13}C$ values (as high as +3.6‰) of sulfide-hosted aragonite may reflect residual carbon dioxide in the zone of methanogenesis as carbon source. In contrast, fluids that favored calcite precipitation in the LHF supposedly had low Mg^{2+} and sulfate concentrations. Such fluids are typically generated by serpentinization. High temperature formation of calcite is supported by low $\delta^{18}O$ values, ranging from −20.0 to −16.1‰. Its low $\delta^{13}C$ values (as low as −5.8‰) agree with a contribution of magmatic carbon, presumably mantle-derived carbon dioxide.

In contrast to their counterparts from many modern sedimentary environments, clotted microfabrics of the LHF are formed of aragonite. Clotted carbonate fabrics of different scales are in accord with microbial mediation in precipitation. High $\delta^{13}C$ values, the crystal habit, and the intense autofluorescence of dolomite dumbbells from the LHF indicate that this phase formed as a result of microbial activity. Within the LHF, hydrogen concentrations have been reported to be extremely high, favoring methanogenesis. The high $\delta^{13}C_{dolomite}$ values may consequently reflect an enrichment of ^{13}C in the residual pool of carbon dioxide during methanogenesis. $\delta^{18}O_{dolomite}$ values indicate formation at elevated temperatures (83 to 100°C), consistent with the known temperature range of known thermophilic methanogens.

Late Devonian basalts and serpentinites of the Frankenwald contain different calcite phases. Among those, basalt-hosted botryoidal crystal aggregates possibly were primarily aragonite, suggesting early formation at low temperatures. Low $\delta^{18}O$ values of calcite phases reflect diagenetic and metamorphic overprinting during the Variscan orogeny. $\delta^{13}C$ values of basalt-hosted calcite point to seawater-derived dissolved inorganic carbon as the main carbon source. $\delta^{13}C$ values for serpentinite-hosted calcite, on the other hand, indicate at least two carbon sources: (1) mantle-derived carbon dioxide (for values as low as −6‰), and (2) a contribution of amagmatic carbon (for values as low as −8.6‰), presumably methane.

Acknowledgments

We thank D. Birgel (Bremen, Germany) and E. Hellebrand (Hawaii, USA) for providing samples from the Logatchev hydrothermal field and the Gakkel ridge, T. Heinrichs (Göttingen, Germany) for his support during FE-SEM studies, C. Vogt (Bremen, Germany) for help with XRD, B. Mader (Kiel, Germany) for help with electron microprobe work, M. Segl (Bremen, Germany) for stable isotope analyses, as well as J.L. Goedert (Wauna, WA, USA), two anonymous reviewers, and the editor D.B. Rowley (Chicago, USA) for providing comments that helped to improve the manuscript. Nico Augustin (Kiel, Germany) is gratefully acknowledged for the preparation of Figure 2. Anna Ksienzyk and Boonraksa Srisawang helped collecting the Frankenwald samples. The work was financed by grants from the Special Priority Program 1144 “From Mantle to Ocean: Energy-, Material- and Life-cycles at Spreading Axes” and the Excellence Cluster MARUM, Bremen of the Deutsche Forschungsgemeinschaft. This is publication no. 32 of the priority program 1144.

4. Geochemical constraints on the modes of carbonate formation in peridotites from the Logatchev Hydrothermal Vent Field and Gakkel Ridge

Benjamin Eickmann[a], Wolfgang Bach[a], Martin Rosner[a,b,#], Jörn Peckmann[a]

[a]MARUM – Zentrum für Marine Umweltwissenschaften, Universität Bremen, Leobener Straße, D-28334 Bremen, Germany

[b]Fachbereich Geowissenschaften, Freie Universität Berlin, Malteserstr. 74-100, D-12249 Berlin, Germany

[#]present adress: Bundesanstalt für Materialforschung und-prüfung, Unter den Eichen 87, D-12205 Berlin, Germany

Chemical Geology; in review

The ultramafic-hosted Logatchev Hydrothermal Field (LHF) at 15°N on the Mid-Atlantic Ridge and the Arctic Gakkel Ridge (GR) feature carbonate precipitates (aragonite, calcite, dolomite) in voids and fractures of different types of host rocks. We present chemical and Sr isotopic compositions of these different carbonates to examine the conditions that led to their formation. Our data reveal that different processes led to the formation of carbonates in the various settings. Seawater-like $^{87}Sr/^{86}Sr$ ratios of aragonite in serpentinites (0.70909 to 0.70917) from LHF are similar to those of aragonite from the GR (0.70912 to 0.70917) and indicate aragonite formation from seawater at ambient conditions at both sites. Aragonite veins in sulfide breccias from LHF also have seawater-like Sr isotope compositions (0.70909 to 0.70915), however, the rare earth element patterns show a clear positive europium (Eu) anomaly indicative of small (<1%) proportions of hydrothermal fluids. In contrast to aragonite, dolomite from the LHF precipitated at much higher temperatures (~100°C). Yet $^{87}Sr/^{86}Sr$ ratios of dolomite are only slightly lower than those of aragonite. Even higher formation temperatures are calculated for deformed calcite veins in serpentine-talc fault schist form north of the LHF. These samples show unradiogenic $^{87}Sr/^{86}Sr$ ratios (0.70460 to 0.70499) indicative of formation from evolved hydrothermal fluids. A simple mixing model based on Sr mass balance and enthalpy conservation indicates strongly variable conditions of fluid mixing and heat transfers involved in carbonate formation. Dolomite precipitated from a mixture of 97% seawater

and 3% hydrothermal fluid that should have had a temperature of approximately 14°C assuming that no heat was transferred. The much higher apparent formation temperatures based on oxygen isotopes hence indicate conductive heating, probably of seawater prior to mixing. The hydrothermal calcite in the fault schist formed from a mixture of 67% hydrothermal fluid and 33% seawater, which should have had an isenthalpic mixing temperature of ~250°C. The significantly lower temperatures calculated from oxygen isotopes are likely due to conductive cooling of hydrothermal fluid effusing along a fault. Rare earth element (REE) patterns corroborate the results of the mixing model, since the hydrothermal calcite samples that formed from waters with the greatest hydrothermal contribution have REE patterns that closely resemble those of vent fluids from the LHF. Our results demonstrate, for the first time, that (1) precipitation from pure seawater, (2) conductive heating of seawater, and (3) conductive cooling of hydrothermal fluids in the subseafloor all can lead to carbonate formation within a single ultramafic-hosted hydrothermal system.

4.1. Introduction

Seawater circulation within the ocean crust and associated water-rock interactions have profound consequences for the chemical and isotopic composition of both the aging ocean crust and seawater (e.g. Elderfield and Schulz, 1996). During the transformation of seawater to a hydrothermal fluid, calcium (Ca) concentration increases while magnesium (Mg) and sulfate concentrations decrease (e.g. von Damm, 1990). These changes are due to Ca-Mg exchange reactions and the precipitation of carbonate, anhydrite, and hydrous magnesium-silicates (Mottl, 1983; Seyfried, 1987; Teagle et al., 1998). High-temperature vent fluids discharge at or near the axis of mid-ocean ridges is manifested by the formation of black smokers and massive sulfide deposits (Von Damm, 1990; Tivey, 2007). In contrast, low-temperature alteration follows a different reaction path, characterized by the formation of palagonite, clay minerals and carbonate minerals (e.g. Staudigel et al., 1981; Alt, 1995). Even at low temperatures (<60°C), seawater looses Mg while it leaches Ca from the rock (Elderfield et al., 1999; Wheat et al., 2000). The increase in Ca in seawater is matched by the decrease in Mg, so that the overall reaction does not significantly change the pH of the circulating seawater. Calcite and

aragonite precipitate during low-temperature seawater-rock interactions and represent useful indicators for the determination of water-rock reactions and fluid mixing processes within the ocean crust (Hart et al. 1994; Coggon et al., 2004; Amini et al., 2008). Several previous studies of hydrothermal environments along the Mid-Atlantic Ridge (MAR) report that the carbonates have exclusively formed at low temperatures from virtually unmodified seawater (e.g., Bonatti et al., 1980; Blusztajn and Hart, 1996; Ribeiro da Costa et al., 2008). Despite the apparent dominance of carbonates formed at ambient seafloor conditions, there is also evidence for aragonite and calcite that precipitated at elevated temperatures from mixtures of ambient seawater and discharging hydrothermal fluids (Früh-Green et al., 2003; Pichler and Veizer, 2004; Ludwig et al., 2006; Amini et al., 2008). The main subject of this study are carbonate minerals from the Logatchev Hydrothermal Field (LHF) at the MAR at 14°45'N. Aragonite hosted in serpentinites from the Gakkel Ridge (GR) in the Arctic Ocean was also included in the study. This paper investigates the chemical aspects of precipitation of carbonate minerals at both sampling sites using Sr isotopes ($^{87}Sr/^{86}Sr$) and minor and trace element concentration of aragonite, calcite and dolomite formed during water-rock interaction. Our previous study revealed that $\delta^{18}O$ and $\delta^{13}C$ values agree with aragonite formation at low-temperatures similar to weathering environments (Bonatti et al., 1980) and moderate-temperature hydrothermal sites (Kelley et al., 2005). Contrary, low $\delta^{18}O$ and $\delta^{13}C$ values of serpentinites-hosted calcite from the LHF indicate precipitation from hydrothermal solutions dominated by magmatic CO_2 (Eickmann et al., in press). The study of LHF carbonate minerals consequently provides the extraordinary opportunity to investigate both calcite formation at high temperatures and aragonite formation at low temperatures within one hydrothermal field. Here, we demonstrate that calcite was precipitated from conductively cooled hydrothermal fluids, while dolomite has been precipitated from conductively heated seawater. Although aragonite formed from seawater, rare earth elements reveal a minor hydrothermal influence during its precipitation.

4.2. Geological background

Both the slow-spreading MAR and the ultraslow-spreading GR (Fig. 4.1) are characterized by the exposure of upper mantle rocks along detachment faults (Cannat, 1993; Tucholke and Lin, 1994; Dick et al., 2003).

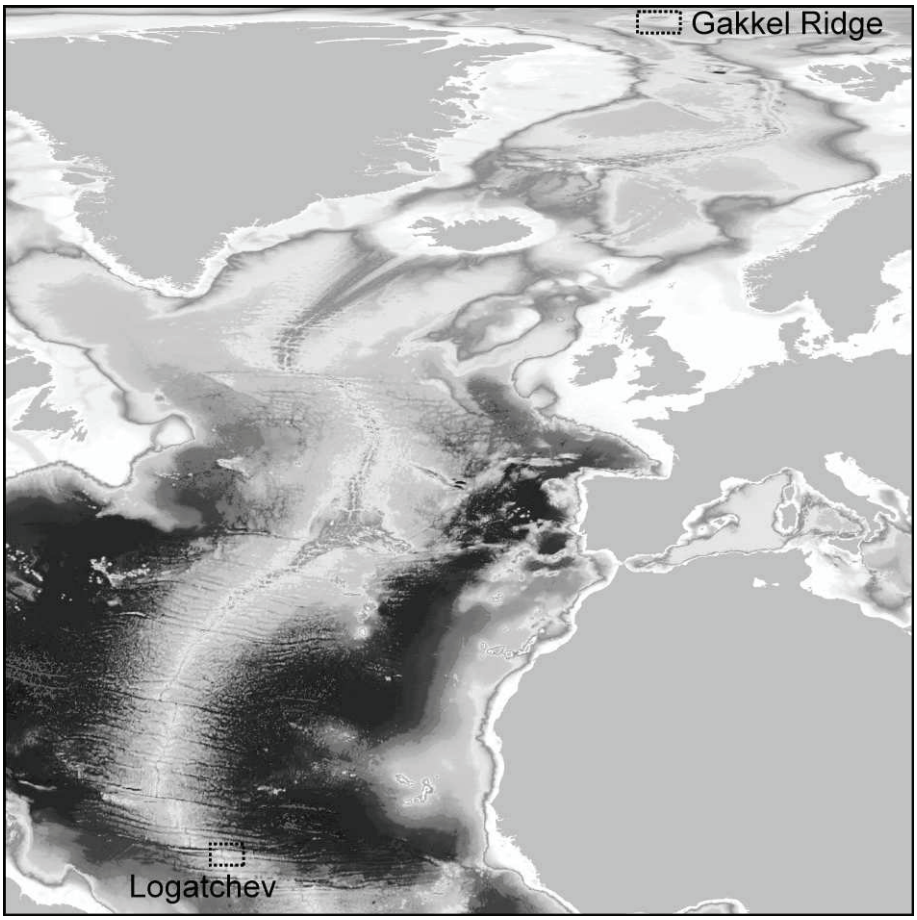

Fig. 4.1. Locations of the Logatchev hydrothermal field (LHF) at the Mid-Atlantic Ridge (14°45'N) and the Gakkel Ridge (GR) in the Arctic Ocean.

The area south of the Fifteen-Twenty Fracture Zone is typified by extensive exposure of peridotite and gabbroic rocks on both flanks along the spreading axis of the MAR (Cannat et al., 1997; Fujiwara et al., 2003). Widespread fluid-rock interaction in the sub seafloor is evident from extensive methane and hydrogen anomalies in the water column and high-temperature fluid discharge in the LHF (Charlou et al., 1998, 2002; Schmidt et al., 2007). The LHF is located at the rift valley wall of the MAR (Fig. 4.2) at a water depth of 3060 m to 2900 m. Several active and inactive sites are arranged in a NW-SE direction. The active LHF comprises seven high-temperature vent sites (Fig. 4.2),

including two black smokers (Irina II and Site 'A'), and five smoking craters (Quest, Site 'B', Irina, Anna-Louise and Candelabra). Basement rocks mainly consist of serpentinized and steatized peridotites, coarse-grained magmatic cumulates, and subordinate basalts and gabbros (Augustin et al., 2008). Furthermore, the LHF comprises abundant copper and iron sulfide mineralization (Gablina et al., 2006). Measured temperatures at different vent sites exhibit a wide range (Schmidt et al., 2007) with maximum temperatures of 353°C (Douville et al., 2002).

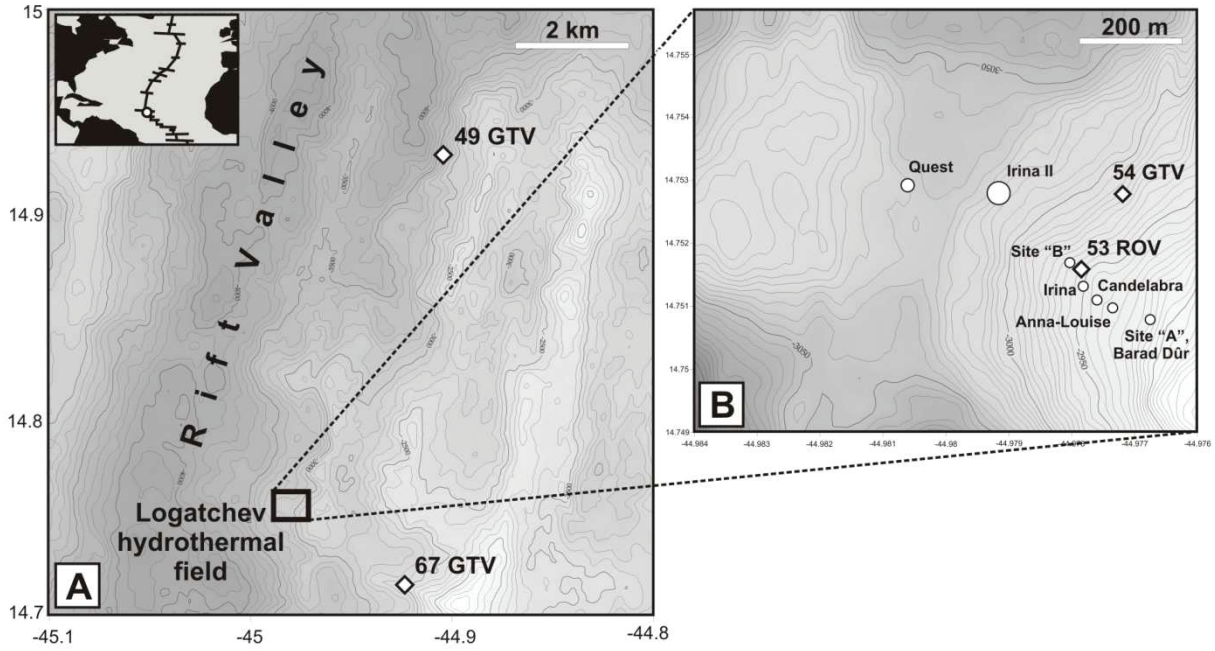

Fig. 4.2. Detailed map of the Logatchev hydrothermal field (LHF) showing the hydrothermal vents and sampling sites within the hydrothermal field.

The GR stretches 1800 km across the eastern Arctic Basin from the Lena Trough eastward to the Laptev Sea (Michael et al., 2003). It has been recently identified as an ultraslow-spreading ridge that is characterized by the absence of transform faults, long-lived low-angle faults defining the rift valley walls, and long stretches of seafloor where mantle peridotite is emplaced directly to the seafloor with little or no volcanic cover between widely spaced isolated magmatic centers (Michael et al., 2003; Dick et al., 2003). Michael et al. (2003) divided the GR into three magmato-tectonic segments; two of them are typified by abundant volcanism. Our samples have been dredged from the middle segment (005°36.2''E to 005°44.0''E and 014°43.6''E to 014°59.7''E), which is

volcanically starved. Despite its tectonically dominated ultraslow-spreading type, there is growing evidence for hydrothermal venting on the GR (Edmonds et al., 2003; Baker et al., 2004), which is localized near volcanic centers and, recently, even explosive volcanism has been documented (Sohn et al., 2008).

4.3. Samples and analytical methods

4.3.1. Samples

Samples were collected during METEOR cruise M60/3 in 2003 (LHF) and POLARSTERN cruise AMORE 1 in 2001 (GR). Serpentinite-hosted aragonite and calcite, sulfide-hosted aragonite, and dolomite hosted in talus breccia from the LHF have been studied. The sulfide-hosted aragonite samples and the dolomite were sampled in close proximity to active vent sites in the LHF, while serpentinite-hosted aragonite was sampled south of the active LHF sites (Fig. 4.2). Serpentinite-hosted calcite has been dredged 7 km north of the LHF in a detachment fault environment. The calcite veins show evidence of folding indicating that their formation started synkinematically within a chlorite-amphibole-serpentinie rock that probably represents a detachment fault (cf. Jöns et al., 2008). Sulfide-hosted aragonite fills the pore space between the sulfide minerals. From the GR only aragonite hosted in serpentinites was analyzed in order to compare serpentinte-hosted aragonite from both sites. At both sites, serpentinite-hosted aragonite occurs in veins of variable width that cut the porphyroclastic rock texture, postdating the emplacement and serpentinization of the upper mantle rocks (Eickmann et al., in press).

4.3.2. Analytical methods

For strontium (Sr) isotope analyses carbonate vein material collected by micro-drilling (2 – 20 mg) was twice cleaned in water (18.2 MΩ) before the carbonate was dissolved in acetic acid leaving any silicates and oxides un-dissolved. The Sr-bearing supernatant was separated from the un-dissolved residue by centrifugation and then dried in Savillex beakers at 120°C. For ion chromatographic separation of Sr, mini-columns made of polypropylene were loaded with 40-60µL Sr-resin (Sr-Spec from Eichrom®). The columns were cleaned and conditioned with four column volumes (2mL) of water and 3N HNO_3, respectively. The dried samples were re-dissolved in 0.5mL 3N HNO_3 and

loaded on the column. The matrix was then removed by passing three more column volumes of 3N HNO_3 through the column. Finally, Sr was eluted from the resin by adding three column volumes of water. Strontium procedure blanks were always well below 0.1% (as low as 0.001%) of the processed Sr of the samples and can therefore be regarded as unproblematic within the achieved analytical uncertainties (see below). For thermal ionization mass spectrometry (TIMS) 300 to 600ng Sr of the separated sample was loaded on out-gassed rhenium filaments and heated to about 2.1 A (beginning red heat). Strontium isotope analyses were made on a Finnigan MAT 261 mass spectrometer at the Freie Universität Berlin by static multi-collection. Interfering Rb was substracted using the measured Rb intensity on mass 85. The Rb-corrected $^{87}Sr/^{86}Sr$ ratio differs at maximum 0.005% from the un-corrected $^{87}Sr/^{86}Sr$ ratio showing that Rb-ionization within the Sr-isotope measurements was very low. Mass fractionation during TIMS was corrected using a $^{86}Sr/^{88}Sr$ ratio of 0.1194. Finally, the $^{87}Sr/^{86}Sr$ ratios were normalized to concurrently measured NIST SRM 987(0.710231 ±0.000069 2SD, n = 6) in the course of the study) using an $^{87}Sr/^{86}Sr$ ratio of 0.710245 to eliminate possibly existing instrumental mass discrimination effects. External reproducibility, including chemical preparation, can be estimated to be on the order of 0.00005 based on three individually processed aliquots of reference seawater IAPSO (batch P143) whereas internal precisions were always better than 0.00003 and typically below 0.00002. The mean $^{87}Sr/^{86}Sr$ ratio of the IAPSO aliquots of 0.70912 (±0.000049 2SD, n = 3) overlaps well within error with published $^{87}Sr/^{86}Sr$ ratios for modern seawater (0.70916; e.g., Banner, 2004).

Minor and trace elements were analyzed on polished thin sections (25 x 45 mm) by laser-ablation inductively coupled plasma mass spectrometry (LA-ICP-MS) at the University of Bremen using a ThermoFinnigan Element2 ICP-MS coupled with a NewWave UP193 laser (λ = 193 nm). In order to avoid surface contamination, each sample was preablated five times. Carbonate samples were ablated by a laser beam (irradiance: ~0.14 GW/cm^2) with a pulse rate of 5 Hz and a spot size of 100 µm. Data were calibrated against the NIST 612 glass standard reference using ^{43}Ca as internal standard and assuming a Ca concentration of 40.04 wt% for aragonite and calcite, as well as 21.8 wt% for dolomite. Standard reproducibility (RSD) for minor constituents (Mg, Mn, Sr) is < 0.1% and < 3.8% for rare earth elements. Precision of the analyses was checked by multiple analyses of standard samples. Total REE concentrations are given

as average values, their standard deviations are <10%. Ce/Ce* is $3Ce_N/(2La_N + Nd)$, while Eu/Eu* is $Eu_N(Sm_N + Gd_N)^{0,5}$, where $_N$ refers to normalization against the CI chondrite (Sun and McDonough, 1989).

4.3.3. Mixing model

The Sr isotope compositions ($^{87}Sr/^{86}Sr$) of secondary alteration phases like carbonates and hydrothermal fluids are powerful tracers of water-rock interactions because modern seawater (0.70916) and mid-ocean ridge basalt (~0.7025) is isotopically distinct (Hodell et al., 1990) and therefore can be used as a measure of the exchange between seawater and the cooling ocean crust. Furthermore, Sr isotopes provide a good proxy for fluid mixing as deeply rooted hydrothermal fluids display unradiogenic $^{87}Sr/^{86}Sr$ ratios very close to the Sr isotope compositions of the altered ocean crust (modeled $^{87}Sr/^{86}Sr$ ratio of the hydrothermal fluid endmember at LHF is 0.70344 ± 0.0004; Amini et al., 2008). We use Sr concentrations and isotope ratios to determine the fraction of seawater (F_{SW}) in hypothetic mixtures (*MIX*) of seawater (*SW*) and LHF vent fluids (*HF*) by simple mass balance:

$$\left(\frac{^{87}Sr}{^{86}Sr}\right)_{MIX} = \frac{F_{SW} C_{SW}^{Sr} \left(\frac{^{87}Sr}{^{86}Sr}\right)_{SW} + (1 - F_{SW}) C_{HF}^{Sr} \left(\frac{^{87}Sr}{^{86}Sr}\right)_{HF}}{F_{SW} C_{SW}^{Sr} + (1 - F_{SW}) C_{HF}^{Sr}}, \text{ hence}$$

$$F_{SW} = \frac{C_{HF}^{Sr} \left[\left(\frac{^{87}Sr}{^{86}Sr}\right)_{MIX} - \left(\frac{^{87}Sr}{^{86}Sr}\right)_{HF}\right]}{C_{SW}^{Sr} \left[\left(\frac{^{87}Sr}{^{86}Sr}\right)_{SW} - \left(\frac{^{87}Sr}{^{86}Sr}\right)_{MIX}\right] + C_{HF}^{Sr} \left[\left(\frac{^{87}Sr}{^{86}Sr}\right)_{MIX} - \left(\frac{^{87}Sr}{^{86}Sr}\right)_{HF}\right]}$$

Knowledge of the mixing proportions as well as composition and temperature of the endmember hydrothermal fluid and seawater allows us to determine the relative amounts of conductive cooling of hydrothermal solutions versus conductive heating of

seawater. For this approach we use isenthalpic mixing calculations, assuming that enthalpy is conserved like a non-reactive chemical property (here Sr isotopes). The heat capacity of a fluid that is near-boiling is much greater than that of a cooler fluid. Consequently, enthalpy and not temperature needs to be considered, because the latter is not an extensive property. We fit a fifth-order polynom to isobaric temperature-enthalpy relations (Bischoff and Rosenbauer, 1985). The enthalpy of the mixed fluid is then calculated ($H_{MIX} = F_{SW}H_{SW} + (1 - F_{SW})H_{HF}$), which in turn is used to calculate a temperature of the mixture.

4.4. Results

4.4.1. Strontium isotope ratios

Strontium isotope ratios of the carbonates from the LHF and the GR reveal precipitation from variably evolved fluids, with $^{87}Sr/^{86}Sr$ values ranging from 0.70460 to 0.70917 (Table 4.1). The lowest $^{87}Sr/^{86}Sr$ values were measured for the serpentinite-hosted calcite from the LHF, ranging from 0.70460 to 0.70499. In contrast, aragonite hosted in serpentinites and sulfides yielded the highest $^{87}Sr/^{86}Sr$ values. $^{87}Sr/^{86}Sr$ ratios for the serpentinite-hosted aragonite range from 0.70909 to 0.70917, and for the sulfide-hosted aragonite from 0.70909 to 0.70915. The Sr isotopic composition of aragonite from the LHF and the GR are indistinguishable from each other and similar to aragonite from hydrothermal settings along the MAR (Ribeiro da Costa et al., 2008). $^{87}Sr/^{86}Sr$ values for dolomite vary between 0.70896 and 0.70907. The extremely small variability of $^{87}Sr/^{86}Sr$ within the carbonate minerals (2σ = <0.00002) implies very similar formation conditions.

Table 4.1. Geochemistry of carbonate minerals. The standard deviation of $^{87}Sr/^{86}Sr$ is given as in-run precision. a; aragonite; c, calcite; d, dolomite.

Sample		Sr [ppm]	Mg [ppm]	Mn [ppm]	$^{87}Sr/^{86}Sr$	$2\sigma_m$	F_{SW}	$[Sr/Ca]_{CaCO3}$ (mmol/mol)	$[Mg/Ca]_{CaCO3}$ (mmol/mol)	$[Sr/Ca]_{fluid}$ (mmol/mol)	$[Mg/Ca]_{fluid}$ (mmol/mol)
LHF											
Site 49GTV											
49GTV-1C-S2	c	98	14767	5845	0.70495	0.00002	0.344	0.11	60.76	1.76	522.37
49GTV-1C-S3	c	98	3208	9358	0.70483	0.00001	0.320	0.11	13.20	1.75	123.35
49GTV-1C-S4	c	113	10630	8206	0.70460	0.00002	0.273	0.13	43.74	2.02	404.96
49GTV-1C-S5	c	108	8380	4932	0.70499	0.00002	0.353	0.12	34.48	1.85	400.91
Site 53ROV											
53ROV-2-S1	d	126	188973	608				0.14	777.51		
53ROV-2-S2	d	123	172752	256	0.70905	0.00002	0.984	0.14	710.77		
53ROV-2-S3	d	123	189121	751	0.70900	0.00001	0.978	0.14	778.12		
53ROV-2-S4	d	142	196325	630	0.70907	0.00002	0.986	0.16	807.76		
53ROV-2-S5	d	135	175482	434				0.15	722.00		
53ROV-2-S6	d	177	184305	500				0.20	758.30		
53ROV-2-S7	d	112	200989	633				0.13	826.95		
53ROV-2-S8	d	150	194803	1046				0.17	801.49		
Site 54GTV											
54GTV-2A-1-S1	a	8468	287	1				9.66	1.18	7.11	1180.83
54GTV-2A-1-S2	a	8646	314	2				9.87	1.29	7.08	1291.92
54GTV-2A-1-S3	a	8886	279	2				10.14	1.15	6.78	1147.91
54GTV-2A-1-S4	a	9527	561	5	0.70914	0.00001	0.995	10.87	2.31	7.21	2308.17
54GTV-2A-1-S5	a	7813	456	29				8.92	1.91	6.02	1956.55
54GTV-2A-1-S6	a	9780	536	3				11.16	2.21	7.53	2205.31
54GTV-2A-1-S7	a	9782	674	9	0.70915	0.00002	0.996	11.16	2.77	7.82	2773.09
54GTV-2A-4-S1	a	8917	381	1	0.70915	0.00002	0.996	10.18	1.57	6.81	1567.58
54GTV-2A-4-S2	a	10685	1594	9	0.70915	0.00002	0.996	12.19	6.56	8.98	6558.32
54GTV-2A-4-S3	a	10698	525	2				12.21	2.16	8.99	2160.05
54GTV-2A-4-S4	a	10130	778	5				11.56	3.20	8.84	3200.99
54GTV-2A-4-S5	a	9520	1350	48				10.86	5.55	7.30	5554.41
54GTV-2A-4-S6	a	10003	1497	33				11.42	6.16	7.74	6159.23
54GTV-2B-S1	a	10841	1716	24	0.70910	0.00001	0.991	12.37	7.06	8.50	7060.28
54GTV-2B-S2	a	9096	1177	5	0.70910	0.00001	0.991	10.38	4.84	7.27	4842.62
54GTV-2B-S3	a	10240	242	2				11.69	1.00	8.14	7001.56
54GTV-2B-S4	a	10392	857	3				11.86	3.53	8.92	3526.02
54GTV-2C-S1	a	10934	545	2				12.48	2.24	9.19	2242.34
54GTV-2C-S2	a	11202	904	6	0.70910	0.00001	0.990	12.78	3.72	9.31	3719.40
54GTV-2C-S3	a	9008	537	25	0.70911	0.00001	0.992	10.28	2.21	7.57	2209.42
54GTV-2C-S4	a	8047	749	38				9.18	3.08	6.34	3081.67
54GTV-2C-S5	a	7388	1163	2				8,43	4.79	5.74	4785.02
Site 67GTV											
67GTV-2C-S1	a	10271	143	1	0.70909	0.00001	0.989	11.72	0.59	7.84	588.36
67GTV-2C-S2	a	9038	90	1	0.70917	0.00001	0.999	10.31	0.37	6.67	370.29
GR											
Site PS 59											
PS 59-238-75-S1	a	8221	63	20	0.70917	0.00001	0.998	9.38	0.26	6.09	1053.28
PS 59-238-75-S2	a	9021	85	25	0.70912	0.00002	0.992	10.30	0.35	6.63	724.13
PS 59-238-75-S3	a	8396	433	9	0.70912	0.00001	0.992	9.58	1.78	6.07	798.19
PS 59-249-A63-S1	a	7922	239	36				9.04	0.98	5.78	1999.36

4.4.2. Minor and trace element contents

Elemental analyses reveal distinct minor and trace element concentrations for aragonite and calcite, which have significantly different average Sr and Mg concentrations (Table 4.1). Sr concentrations range from 98 to 113 ppm in calcite samples, whereas aragonite samples exhibit much higher Sr concentrations. They range from ~7800 to ~11200 ppm and are slightly higher for aragonite hosted in sulfides than for aragonite hosted in serpentinites. No differences in the Sr concentrations have been obtained for serpentinite-hosted aragonite from LHF and GR, suggesting precipitation under similar conditions and from similar fluids. Dolomite has intermediate Sr concentrations, vary between 112 to 150 ppm. Calcite has average Mg concentrations of ~9200 ppm, much higher than aragonite (~650 ppm). Mg concentrations for serpentinite-hosted aragonite from the GR are slightly higher (~205 ppm) then those from the LHF (~130 ppm), whereas Sr concentrations are similar. Aragonite hosted in sulfides from LHF yielded higher Mg concentrations (~1000 ppm) than aragonite in serpentinites. Similarly, Mn concentrations vary markedly between aragonite samples from different locations. Serpentinite-hosted aragonite from the LHF has very low Mn concentrations, while Mn concentrations for serpentinite-hosted aragonite from the GR are higher (~20 ppm). Mn concentrations for sulfide-hosted aragonite from the LHF are generally higher than those of serpentinites-hosted aragonite. Serpentinite-hosted calcite (~7100 ppm) and dolomite (~1100 ppm) exhibit higher Mn concentrations than aragonite samples. Sulfide-hosted aragonite has elevated Ba (~40 ppm) and Pb (~130 ppm) contents, whereas other carbonates contain trivial amounts of these elements.

Rare earth element (REE) concentrations of all carbonates from the LHF and the GR are reported in Table 4.2 and average chondrite-normalized concentrations are plotted in Fig. 4.3. The REE data show a remarkable variability in absolute concentrations as well as in pattern shape. Total REE concentrations are low (< 10 ppm) for serpentinites-hosted aragonite from both sampling sites and sulfide-hosted aragonite from the LHF. In contrast, serpentinite-hosted calcite and dolomite exhibit higher total REE concentrations (up to 70 ppm). Most of the carbonates from both sampling sites are mildly enriched in heavy REE (HREE), ranging from $Gd_N/Yb_N = 0.97$ for dolomite to $Gd_N/Yb_N = 2.25$ for serpentinite-hosted aragonite from the LHF. In contrast, REE patters for serpentinites-hosted calcite shows enrichment of light REE ($La_N/Sm_N = 9.97$) and depletion of heavy REE ($Gd_N/Yb_N = 3.08$).

Table 4.2. Chondrite-normalized rare earth element concentrations of carbonate minerals. Reported concentrations are given in parts per million (ppm).

	serpentinite-hosted aragonite	serpentinite-hosted calcite	sulfide-hosted aragonite	dolomite
La	0.16	20.85	0.53	2.36
Ce	0.08	13.19	0.14	1.89
Nd	0.11	5.37	0.23	3.31
Sm	0.11	2.27	0.27	3.85
Eu	0.09	48.60	0.85	26.66
Gd	0.08	1.57	0.19	4.06
Dy	0.09	1.15	0.18	4.40
Y	0.14	1.31	0.14	4.04
Er	0.09	0.99	0.18	4.39
Yb	0.08	0.93	0.35	4.51
Eu/Eu*	0.26	17.16	1.14	1.51
Ce/Ce*	0.39	0.84	0.37	0.74

Most of the serpentinite-hosted aragonite from the GR is depleted in light REE (La_N/Sm_N = 0.07 to 0.31) and enriched in heavy REE (Gd_N/Yb_N = 0.2 to 20.4). Dolomite is depleted in both, light REE (La_N/Sm_N = 0.4 to 0.98) and mid REE (Gd_N/Yb_N = 0.56 to 1.13). Serpentinite-hosted aragonite from both spreading centers do not show positive Eu anomalies (Eu/Eu* = 0.07 to 0.97), while sulfide-hosted aragonite and dolomite from the Logatchev field do exhibit positive Eu anomalies (Eu/Eu* = of up to 2.44). Strongly positive Eu anomalies have been obtained for serpentinite-hosted calcite from the Logatchev field (Eu/Eu* = 1.8 to 60). All studied carbonate minerals are characterized by negative Ce anomalies (Ce/Ce* = 0.34 to 0.74).

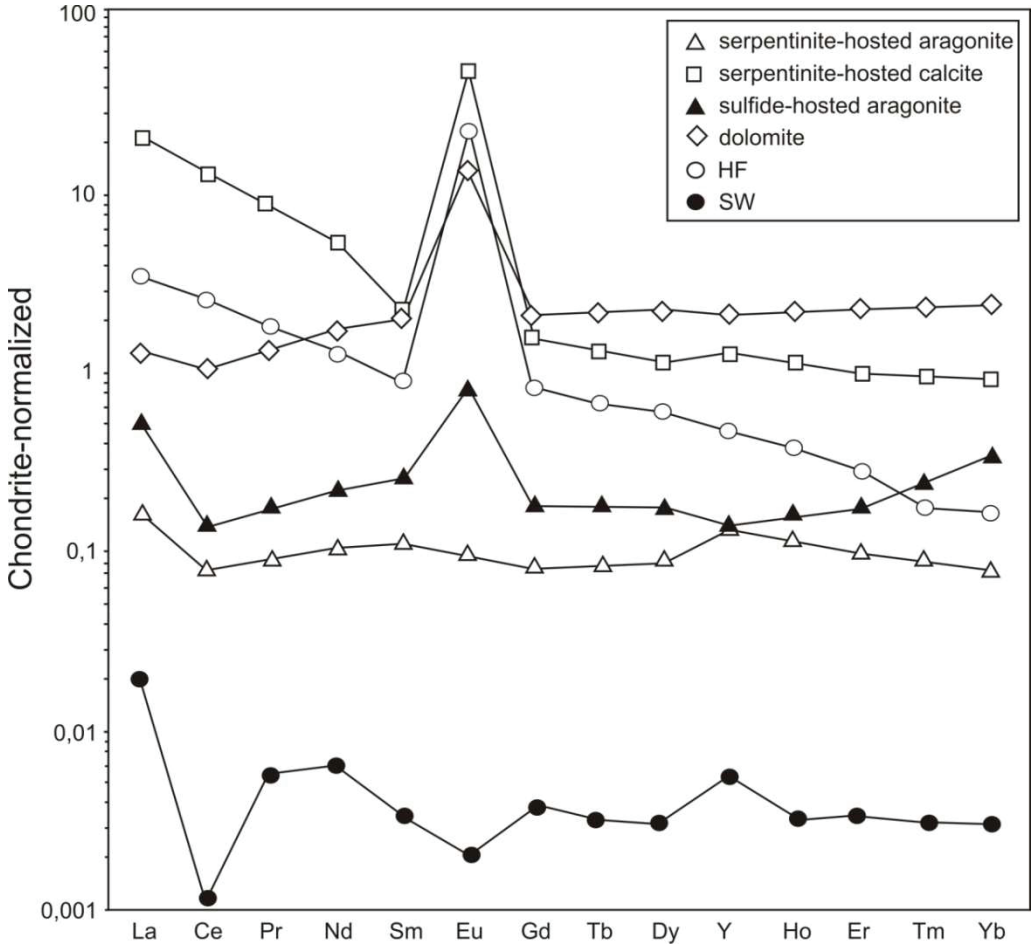

Fig. 4.3. Chondrite-normalized REE patterns for carbonate samples from the Logatchev hydrothermal field and the Gakkel ridge in comparison with hydrothermal fluids and seawater from the LHF. REE data for the hydrothermal fluid and seawater are from Schmidt et al. (2007) and were multiplied by a factor of 1000.

4.5. Discussion

4.5.1. Basement fluid evolution inferred from Sr isotope ratios and stable isotopes

Based on $\delta^{18}O$ and $\delta^{13}C$ values of aragonite from the LHF and the GR, formation from seawater at ambient seafloor temperatures has been proposed (Eickmann et al., in press). This finding is corroborated by the Sr isotope data, which reveal seawater $^{87}Sr/^{86}Sr$ ratios of the serpentinite-hosted aragonite from the GR and LHF. Moreover, the REE patterns of aragonite do not indicate any influence of hydrothermal or other sources (see section 4.5.2). The aragonite formed in a typical shallow weathering environment like the majority of serpentinite-hosted aragonite veins analyzed to date (Bonnatti et al., 1980; Agrinier et al., 1996; Bluzstajn and Hart, 1996; Ribeiro da Costa et

al., 2008). Since carbonate samples from the LHF formed within an active hydrothermal environment, it is of interest to examine the formation conditions in terms of hydrothermal influence with respect to temperature and chemistry. Sr isotopes provide insight into fluid mixing processes at hypothermal vents. $^{87}Sr/^{86}Sr$ ratios of carbonate minerals in hydrothermal environments primarily reflect mixing between seawater and hydrothermal fluids. Mid-ocean ridge basalts from the MARK area at the Mid-Atlantic Ridge have an average $^{87}Sr/^{86}Sr$ ratio of 0.7022 (Palmer, 1992). $^{87}Sr/^{86}Sr$ ratios of hydrothermal vent fluids reflect mixing between the two principle endmembers in hydrothermal environments; basalt-derived Sr and seawater (Albarède et al., 1981). To quantify mixing processes in the subseafloor basement, a simple mixing model (section 4.3.3) based on $^{87}Sr/^{86}Sr$ ratios and concentrations of seawater and hydrothermal vent fluids has been applied to estimate the fraction of seawater (F_{SW}) corresponding to a $^{87}Sr/^{86}Sr$ ratio measured in a carbonate sample (Fig. 4.4a). The value calculated for F_{SW} can be used to compute the temperature of a mixed fluid, assuming constant enthalpy in the system (section 4.3.3). The constant enthalpy assumption is false if a significant amount of heat was transferred by conduction, either by heating of seawater or by cooling of upwelling hydrothermal fluids. During mixing processes in the sub seafloor basement, the fluids are commonly subject to conductively cooling or heating (e.g., Seewald and Seyfried, 1990; Tivey et al., 1995). $^{87}Sr/^{86}Sr$ ratios of aragonite hosted in serpentinites and sulfides from LHF indicate that it precipitated from unmodified seawater, just like the aragonite from the GR (Fig. 4.4b). The $^{87}Sr/^{86}Sr$ ratios for aragonite from both sites are similar to $^{87}Sr/^{86}Sr$ ratios reported for aragonite in hydrothermal settings along the Mid-Atlantic Ridge (Ribeiro da Costa et al., 2008). To the best of our knowledge, the only aragonite samples that have been found to have precipitated from hydrothermal fluids are from a shallow-water hydrothermal system in Papua New Guinea (Pichler and Veizer, 2004). The aragonite samples from LHF are uninfluenced by hydrothermal activity in terms of their Sr isotope composition and resemble those

$^{87}Sr/^{86}Sr$ ratios of dolomite from the LHF are close to a typical radiogenic seawater Sr ratio, revealing only a minor influence of hydrothermal fluids (~2%). In contrast, calcite hosted in serpentinites from the LHF precipitated from a mixture of ~67% hydrothermal fluid and ~33% seawater. Ignoring other reactions in the system, calcite precipitation from the vent fluids can be reconciled by considering the low solubility of

calcite at high temperatures, leading to oversaturation ($\Omega_{calcite}$ = 40 to 49 at 170°C) with respect to calcite (Amini et al., 2008). According to their $^{87}Sr/^{86}Sr$ ratios and low $\delta^{18}O$ values the serpentinite-hosted calcite is similar to calcite samples from ODP Hole 1271A in the vicinity of LHF, which apparently precipitated directly from the hydrothermal fluid endmember based on their Sr isotope composition (Amini et al., 2008). The fluids from which LHF calcite precipitated had temperatures in the range of 129 to 186°C (calculated from O isotope compositions; Eickmann et al., in press), while the calculated batch mixing temperatures from conserving enthalpy and Sr mass balance suggests temperatures between 240 and 280°C. The mismatch between the calculated formation temperature and temperature expected from batch mixing can only be reconciled if the hydrothermal fluids underwent massive conductive cooling prior to precipitation of the calcite.

In contrast to carbonate minerals from the Juan de Fuca ridge (Coggon et al., 2004), a single temperature-$^{87}Sr/^{86}Sr$ trend for reported carbonates cannot be observed, suggesting carbonate precipitation either from fluids that experienced different chemical evolution or during mixing between different fluids (Fig. 4.4b). Aragonite hosted in serpentinites and sulfides from the LHF exhibits similar $^{87}Sr/^{86}Sr$ ratios (0.70909 to 0.70917), but O isotopes indicate that sulfide-hosted aragonite has formed at slightly higher temperatures (Fig 4.5). Measured $^{87}Sr/^{86}Sr$ ratios for dolomite is somewhat lower than those of aragonite (~0.70902), while their formation temperatures from O isotopes are markedly higher (~100°C). This suggests dolomite formation from conductively heated seawater. According to their unradiogenic $^{87}Sr/^{86}Sr$ isotope composition (Table 4.1), the calcite samples from the fault rock are derived from hydrothermal fluids. Simple mixing between seawater and hydrothermal fluids would lead to carbonate formation resembling the mixing trend. Aragonite samples resemble the theoretical mixing model of fluid evolution in the LHF (Fig. 4.4b), indicating direct precipitation from seawater. In contrast to aragonite, the formation of dolomite and calcite cannot be explained by simple mixing between seawater and hydrothermal fluids. The calculated formation temperatures for calcite samples are lower than the theoretical temperatures of the mixing model, while dolomite exhibits higher temperatures than predicted by the model. This indicates calcite formation during conductive cooling of a hydrothermal fluid, while dolomite has formed due to conductive heating of seawater.

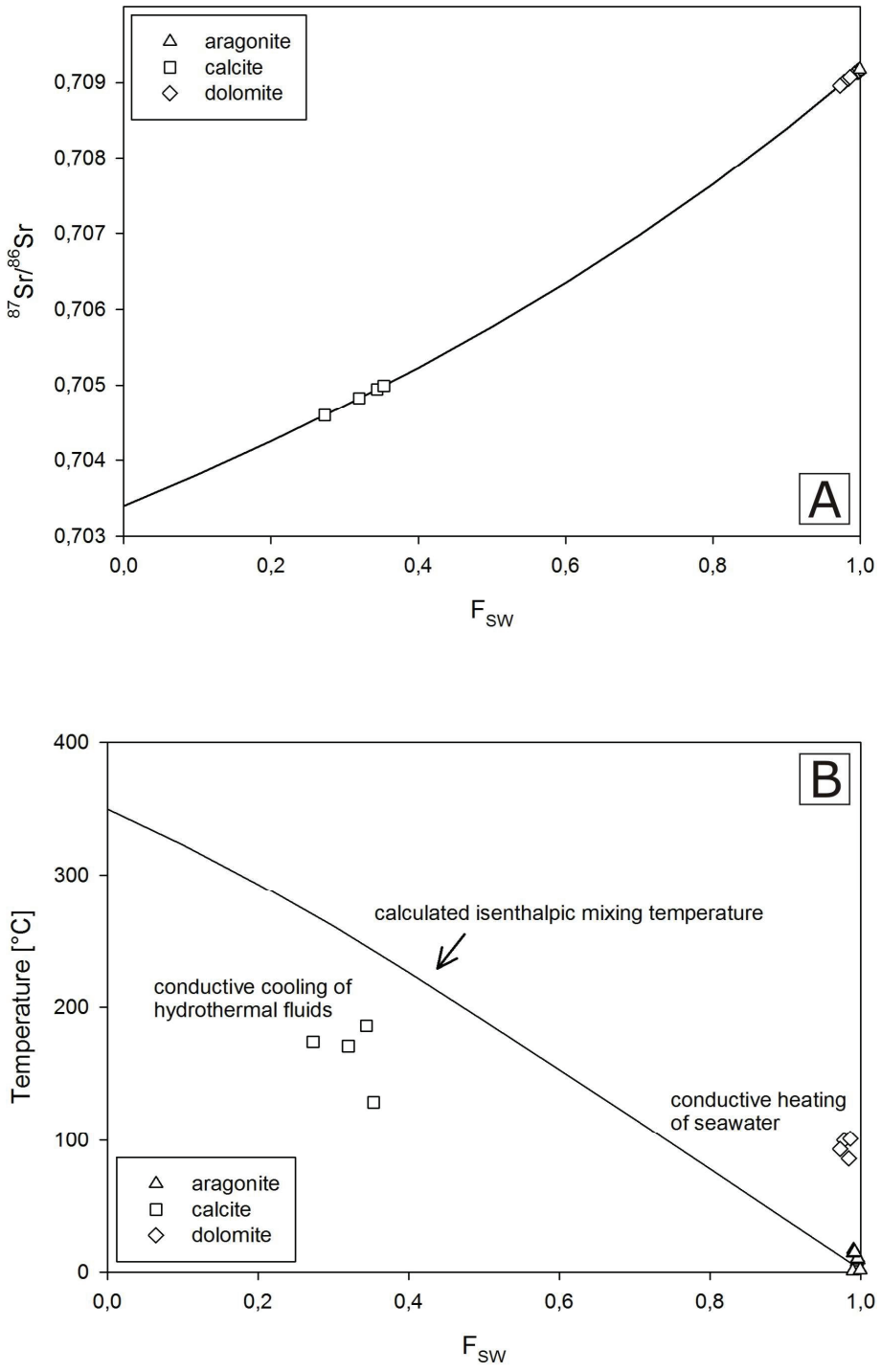

Fig. 4.4. Theoretical mixing model between seawater and hydrothermal fluids in the Logatchev hydrothermal field. (a) Sr isotope mass balance calculations provide the fraction of seawater in a mixture of seawater ($^{87}Sr/^{86}Sr$ = 0.70916, Sr = 90 µM; Palmer and Edmond, 1989) and Logatchev hydrothermal vent fluids ($^{87}Sr/^{86}Sr$ = 0.7034, Sr = 125 µM; Amini et al., 2008). (b) Isenthalpic mixing temperatures calculated using enthalpies of seawater and 350°C/300bar hydrothermal fluid from Bischoff and Rosenbauer (1985) in comparison with formation temperatures and F_{SW} values calculated from O and Sr isotopes, respectively. Minerals precipitating during batch mixing will plot on the line. Minerals formed from fluids that underwent conductive cooling plot below the line, while those formed from conductively heated seawater plot above the line.

4.5.2. Rare earth elements of carbonates at mid-ocean ridges

Rare earth element (REE) patterns of hydrothermal fluids issuing from basalt- and ultramafic-hosted environments exhibit enrichment of light rare earth elements with positive europium (Eu) anomalies (Allen and Seyfried, 2005; Douville et al., 1999). REE are greatly enriched in the LHF vent fluids relative to seawater, similar to those of other hydrothermal fluids from basaltic and ultramafic systems (Schmidt et al., 2007). Since yttrium (Y) has a geochemical behavior similar to that of REE, especially to that of holmium (Ho), it is integrated in the REE pattern between dysprosium (Dy) and Ho (Bau et al., 1991). Despite its trivalent oxidation state in hydrothermal solutions, cerium (Ce) is the only REE that can readily be oxidized to the (+IV) state. Strong negative Ce anomalies have been extensively observed in deep-sea seawater (German et al., 1995). It should be noted that the oxidation state of Ce may be stabilized by alkalinity and the presence of humic acid (Möller and Bau, 1993; Pourret et al., 2008).

The REE patterns of the serpentinite-hosted aragonite from the LHF and the GR are similar to each other (Table 4.2). Like seawater, they display a negative Ce and a positive Y anomaly (Fig. 4.3), suggesting that these aragonite veins have precipitated directly from oxygenated seawater. Although the sulfide-hosted aragonite from the LHF are low temperature precipitates (Eickmann et al., in press), they display positive Eu anomalies similar to those of dolomite that appear to have formed at temperatures around 100°C. Positive Eu anomalies in fluids point to a contribution of reduced hydrothermal fluids (Bau, 1991). The apparent contradiction between precipitation from hydrothermal fluids and precipitation at low temperatures can be explained when the magnitude of the Eu-enrichment in the LHF vent fluids (about 5 orders of magnitude enriched relative to seawater) is considered. A 0.01% contribution of vent fluid would not be apparent in Sr and O isotope composition, but 90% of the Eu in that mix would be derived from the vent fluid. A mixing model similar to that discussed in section 4.3.3 examines the development of Eu anomalies during mixing processes in the sub seafloor basement (Fig. 4.5b). We use REE concentrations, Sr isotope composition and concentration as well as temperature of seawater and hydrothermal fluid, to calculate Eu/Eu*, $^{87}Sr/^{86}Sr$, and isenthalpic temperatures of mixed fluids for values for F_{SW} that range from 0 to 1. This allows us to compute the co-evolution of Eu/Eu* and temperatures during mixing between seawater and hydrothermal fluids in the LHF. The results of this mixing model indicate that sulfide-hosted aragonite and dolomite formed from a mixed fluid with

similar REE and Sr isotope characteristics (Fig. 4.5a). The sulfide-hosted aragonite lie on a simple mixing trend between seawater and hydrothermal fluid, indicating that they precipitated from seawater dominated fluid with a small contribution of hydrothermal vent solution. The position of dolomite in the Eu/Eu* -temperature plane cannot be explained without involving considerable amounts of conductive heating of seawater or mixed fluids prior to dolomite precipitation.

In contrast to the low total REE contents of aragonite, calcite and dolomite samples exhibit higher REE contents, indicating precipitation from fluids other than seawater (Douville et al., 1999; Shields and Webb, 2004). Carbonate precipitation from solutions with significant hydrothermal vent fluid input is indicated by strong positive Eu anomalies (Fig. 4.3) and by results of the Sr isotope mass balance (Fig. 4.3b). The most pronounced hydrothermal REE pattern with an enrichment of the light REE and a prominent positive Eu anomaly were identified for the synkinematic serpentinite-hosted calcite from north of the LHF (Fig. 4.3). Its REE pattern are in good agreement with unradiogenic $^{87}Sr/^{86}Sr$ ratios (Fig. 4.5a) and previously discussed negative $\delta^{18}O$ and $\delta^{13}C$ values (cf. Eickmann et al., in press), indicating calcite precipitation from LHF-like hydrothermal fluids within the detachment fault.

The serpentinite-hosted calcite were sampled 7 km north of the active LHF (Fig. 4.2), but they apparently precipitated from fluids with $^{87}Sr/^{86}Sr$ ratios and REE patterns similar to the LHF vent fluids. We therefore suggest that the fluids migrating within the detachment fault were reminiscent of LHF vent fluids. They are similar in $^{87}Sr/^{86}Sr$ isotopic composition to calcite veins from serpentine-talc-tremolite schists in ODP Hole 1271A (Amini et al., 2008) located 40 km north of the LHF, indicating that calcite formation from hydrothermal fluids within detachment faults may be a common processes in the 15°20'N Fracture Zone area.

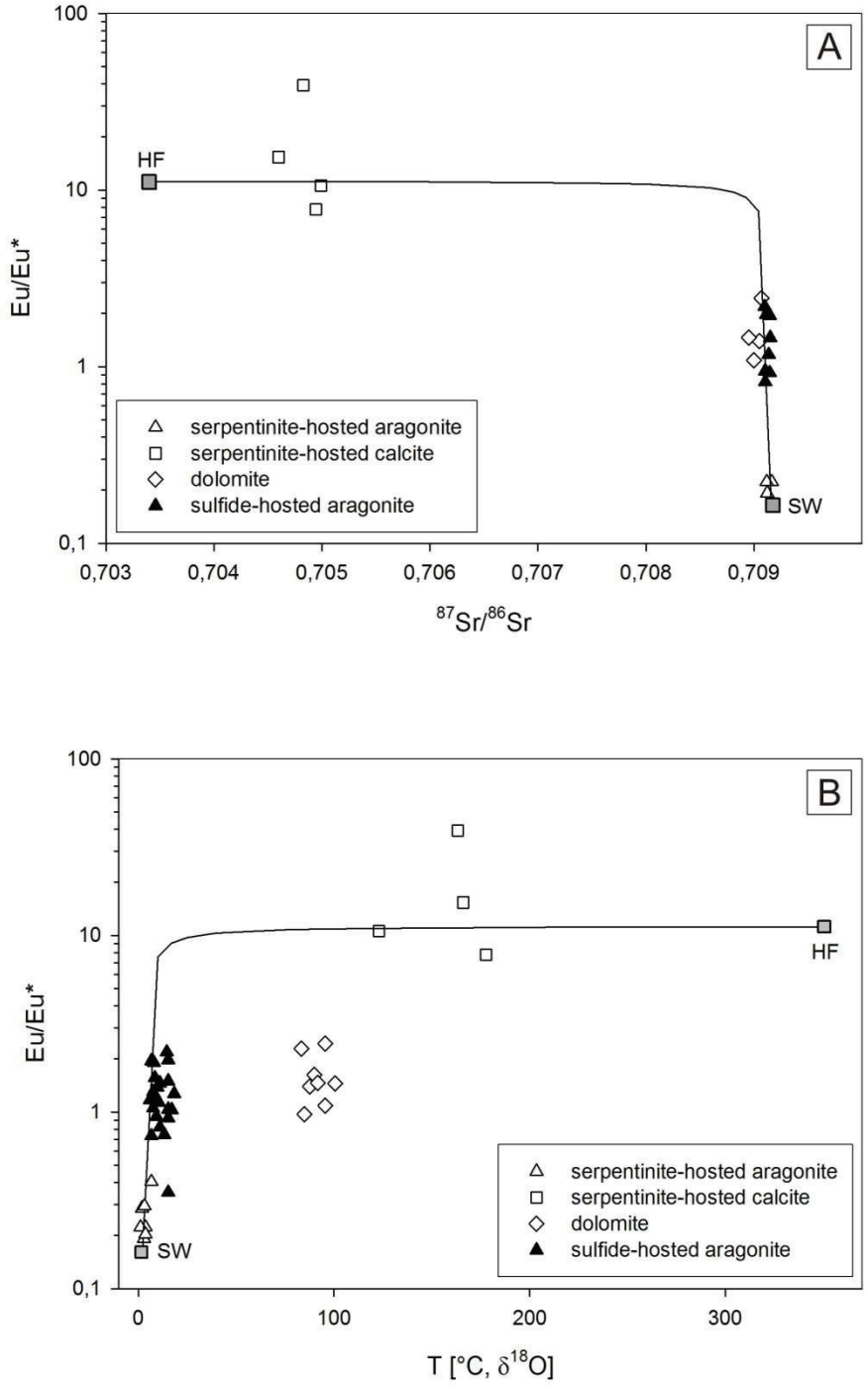

Fig. 4.5 Europium anomalies of carbonate samples plotted versus measured $^{87}Sr/^{86}Sr$ ratios (a) and oxygen isotope-derived formation temperature (b). The solid lines indicates a mixing model for europium anomaly between seawater (SW, Eu/Eu* = 0.032, T = 2°C, $^{87}Sr/^{86}Sr$ = 0.70916, [Sr] = 90µM) and hydrothermal fluid (HF, Eu/Eu* = 11.199, T = 350°C, $^{87}Sr/^{86}Sr$ = 0.70344, [Sr] = 125µM) within the Logatchev hydrothermal field. REE data for seawater and hydrothermal fluid are from Schmidt et al. (2007) and Amini et al. (2008). The effect of hydrothermal contribution to carbonate formation is not expressed in O and Sr isotopes, whereas Eu/Eu* is elevated in carbonates precipitated from fluids with minor proportions of vent fluid mixed in.

4.5.3. Compositional evolution of carbonates and calculated composition of sub seafloor fluids

Changes in element concentrations of carbonate minerals are affected by the chemical evolution of the fluids from which the carbonates precipitated. Calculated $[Sr/Ca]_{fluid}$ and $[Mg/Ca]_{fluid}$ ratios higher than seawater may also indicate prolonged exposure of the carbonates to seawater and subsequent incorporation of seawater-derived Sr and Mg, similar to carbonates from the Lost City field at the Mid-Atlantic Ridge (Ludwig et al., 2006). Most of the Mg/Ca ratios, however, are much lower than predicted for precipitation from seawater. Evidently, Mg/Ca and Sr/Ca ratios in carbonate are affected by precipitation kinetics (e.g., Cicero and Lohman, 2001; Morse et al., 2007). Nonetheless, Coggon et al. (2004) demonstrated that the precipitation of carbonate faithfully records the evolution of seawater during interactions with basaltic basement at T<65°C. As seawater interacts with basement, Mg is removed and Ca is added to the fluids (e.g., von Damm, 1995). Even at temperatures of 60°C and lower, Mg concentrations approach concentrations of 2 mmol/kg, while Ca concentrations increase to 60 mmol/kg (Elderfield et al., 1999; Wheat and Mottl, 2000). It is hence likely that fluid evolution paths in the sub seafloor away from hydrothermal upflow and mixing zones deviates from simple mixing scenarios such as discussed above. To test if processes other than mixing played a role in the formation of the carbonate veins under investigation, we calculated the compositions of the fluids from which they precipitated and compared these compositions with those of known simple mixtures. It is apparent that the majority of aragonite veins have lower Mg/Ca ratios than seawater (Fig. 4.6a), indicating that notable Mg loss and Ca gain of the seawater-derived fluids took place prior to precipitation (Amini et al., 2008). Those exchange reactions apparently took place in the absence of significant Sr isotope exchange. Such a lack of Sr isotope exchange is to be expected at the low formation temperatures of aragonite. Apparently, the Mg/Ca and Sr/Ca ratios are more readily affected by interactions with the basement than the Sr isotope composition (Fig. 4.6b). Isotope systems more sensitive to low-intensity basement-seawater interactions (e.g., Li, B, Ca) may be useful to better quantify to the effects of low-temperature exchange.

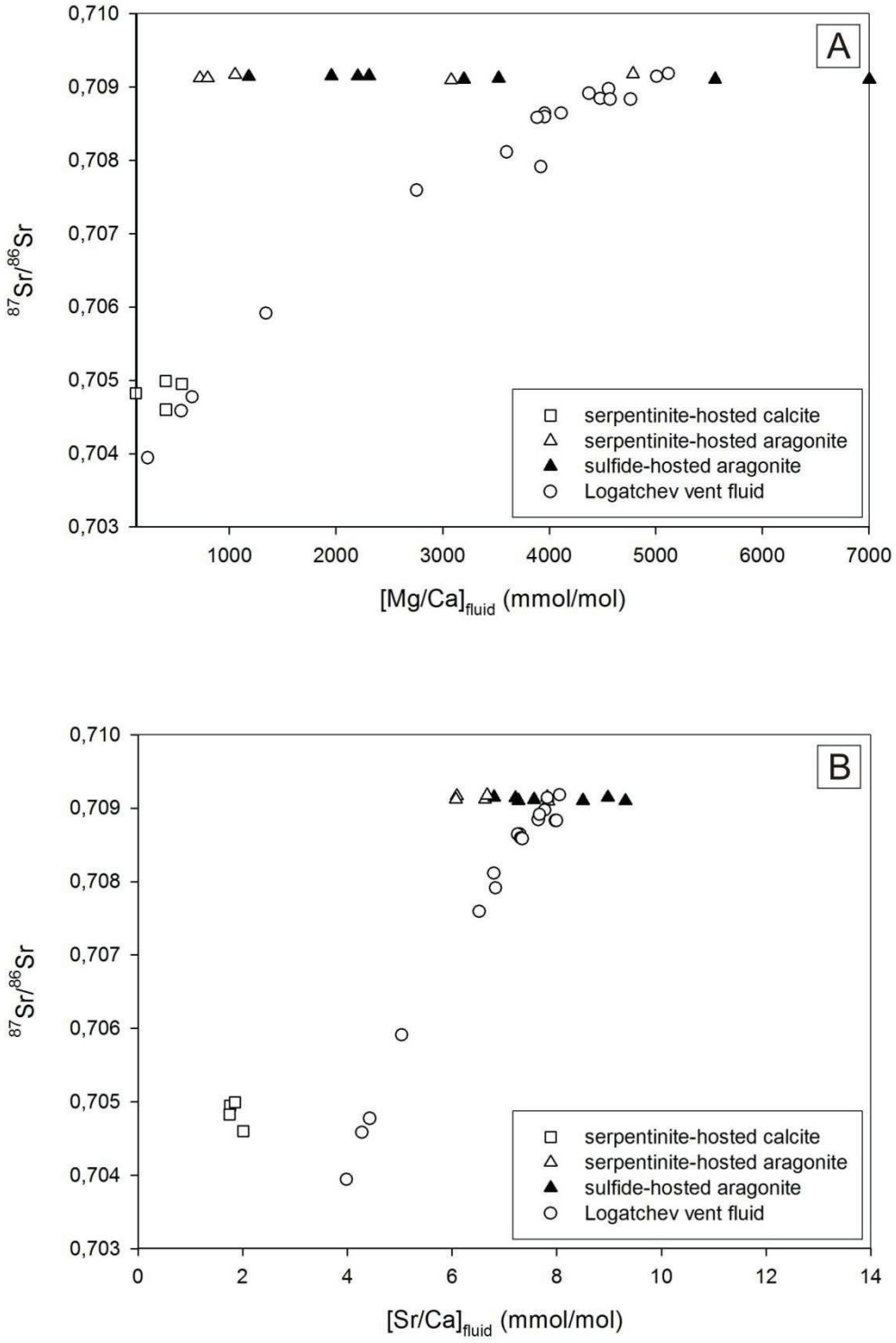

Fig. 4.6. Comparison between carbonate samples from the Logatchev hydrothermal field (LHF) and compositions of fluids from LHF that represent mixtures of hydrothermal vent fluid and seawater (Amini et al., 2008). (a) Calculated Sr/Ca ratios of formation fluids compared to strontium isotope composition. (b) Calculated Mg/Ca ratios of formation fluids compared to the corresponding $^{87}Sr/^{86}Sr$ ratios. Calculations of the Sr/Ca and Mg/Ca ratios of the fluids from carbonate compositions were conducted following Coggon et al. (2004). Note that some of the aragonite samples have Mg/Ca ratios much lower than predicted for seawater precipitates, while the Sr isotope composition is that of seawater.

4.6. Conclusions

Major and trace elements and $^{87}Sr/^{86}Sr$ ratios for carbonate minerals from the Logatchev hydrothermal field (LHF) at the Mid-Atlantic Ridge (MAR) and the ultraslow-spreading arctic Gakkel Ridge (GR) show different modes of formation. $^{87}Sr/^{86}Sr$ ratios and trace element (Mg, Sr, REE) compositions of serpentinite-hosted aragonite from the LHF and the GR indicate precipitation from seawater that had undergone very limited exchange with the host rock. These aragonite samples have REE patterns that lack europium anomalies consistent with precipitation from seawater without hydrothermal input. Similarly $^{87}Sr/^{86}Sr$ ratios and Sr/Ca and Mg/Ca ratios for sulfide-hosted aragonite from the LHF point to the precipitation from seawater at low temperatures. Sulfide-hosted aragonite, however, shows distinct positive Eu anomalies, which point to a contribution of reduced hydrothermal fluids. The apparent contradiction of formation from hydrothermal fluids at low temperatures indicates the sensitivity of europium in tracing even minimal contribution of hydrothermal input. Some aragonite samples from the LHF show higher Sr/Ca and Mg/Ca ratios than the seawater at the respective sampling sites, indicating prolonged exposure at the seafloor and subsequent incorporation of strontium and magnesium into aragonite. Dolomite in the LHF has $^{87}Sr/^{86}Sr$ ratios slightly lower than modern seawater (0.70896 to 0.70907), but show apparent formation temperatures of ~100°C (based on oxygen isotopes). A simple mixing model based on Sr and enthalpy balance indicates that these temperatures and Sr isotope compositions can only by reconciled if the dolomite formed from conductively heated seawater (Fig 3b), with only 3% of hydrothermal fluids. This formation scenario also explains the REE characteristics of the dolomite. Unradiogenic $^{87}Sr/^{86}Sr$ ratios (0.70483 to 0.70499) and calculated formation temperatures up to ~180°C for the serpentinite-hosted calcite from the LHF reveal precipitation from hydrothermal fluids in the sub seafloor basement. This hydrothermal origin is confirmed by REE patterns. The enrichment of light REE and strong positive Eu anomalies are similar to REE patterns of the LHF vent fluids. The Sr mass balance indicates that calcite precipitated from a mixture of ~67% hydrothermal fluid and ~33% seawater. The isenthalpic temperatures predicted from mixing 350°C hydrothermal fluids and seawater in these proportions would be much higher than the temperatures indicated from O isotope thermometry. In contrast to dolomite formation, the hydrothermal calcite was hence formed from fluids that underwent significant conductive cooling. Our results

demonstrate that useful information on the physicochemical conditions of carbonate formation within ocean hard rocks can be obtained from geochemical data.

Acknowledgments

We thank D. Birgel (Bremen, Germany) and E. Hellebrand (Hawaii, USA) for providing samples from the LHF and the GR. The help and assistance of H. Anders and A. Klügel (Bremen, Germany) with LA-ICP-MS analyses is gratefully acknowledged. This study was financed by grants from the Special Priority Program 1144 “From Mantle to Ocean: Energy-, Material- and Life-cycles at Spreading Axes” and the Excellence Cluster MARUM, Bremen of the Deutsche Forschungsgemeinschaft. This is publication no. X of the priority program 1144.

5. Widespread cryptoendolithic life in Devonian pillow basalts

Benjamin Eickmann[a], Wolfgang Bach[a], Steffen Kiel[b], Joachim Reitner[c], Jörn Peckmann[a,]

[a]MARUM – Center for Marine Environmental Sciences, University of Bremen, Leobener Straße, 28359 Bremen, Germany

[b]Department of Geosciences, University of Kiel, Ludewig-Meyn-Straße 10, 28114 Kiel, Germany

[c]Geoscience Center, University of Göttingen, Goldschmidtstraße 3, 37077 Göttingen, Germany

Palaeogeography, Palaeoclimatology, Palaeoecology; to be submitted

Late Devonian (Frasnian) pillow basalts from the Frankenwald and Thüringer Wald within the Saxothuringian zone in Germany were found to contain abundant putative biogenic filaments, indicating that the volcanic rocks once harboured microbial life. The mineralized filaments are found in vesicles, so-called amygdules, where they started to form on internal surfaces after seawater ingress. The filaments postdate an early fibrous carbonate cement but predate later equant calcite spar, revealing syngenetic formation. A biogenic origin of filaments is indicated by their size and morphology resembling modern microorganisms, their independence of crystal faces and cleavage plans, complex branching patterns, and internal segmentation. The filamentous microorganisms represent cryptoendoliths that lived in structural cavities of the basalt. They became preserved upon microbial clay authigenesis similar to the encrustation of modern prokaryotes in iron-rich environments. Filaments consist of clay minerals with the endmember composition berthierine-chamosite and illite-glauconite. Based on the discovery of fossilized filamentous microorganisms in Late Devonian pillow basalts of the Saxothurigian zone that mimic filaments previously found in Middle Devonian pillow basalts of the Rhenohercynian zone, it is apparent that cryptoendolithic life was more widespread than previously recognised. Structural cavities within seafloor basalt may thus represent a common, perhaps universal niche for life in the oceanic crust.

5.1. Introduction

Since the discovery of traces of microbial activity in the outer glassy margins of volcanic rocks, there is growing consensus that microbial activity contributes to the alteration of volcanic rocks (Thorseth et al., 1992; Staudigel et al., 2008). Bioalteration of pillow lavas has been documented from all ocean basins (e.g. Thorseth et al., 1995; Fisk et al., 1998; Furnes and Staudigel, 1999; Staudigel et al., 2006; Furnes et al., 2007), and in ancient pillow basalts extending back to ~3.5 Ga (Furnes et al., 2004; Banerjee et al., 2006; 2007). Evidence for bioalteration includes elevated amounts of elements such as carbon, phosphorous, nitrogen, potassium, and sulphur relative to the volcanic glass, highly negative and positive $\delta^{13}C$ values, and putative DNA associated with tubular and granular alteration textures in basaltic glass (Furnes et al., 2001; Banerjee and Muehlenbachs, 2003). The dissolution of basaltic glass is commonly accompanied by the precipitation of authigenic clay minerals, iron hydroxides, zeolites, and titanite (Storrie-Lombardi and Fisk, 2004; Banerjee et al., 2006; Furnes et al., 2007). Bioalteration is found to dominate over abiotic alteration of basaltic glass in the upper 250 m of the oceanic crust, steadily declining in importance to a maximal depth of ~550 m (Furnes and Staudigel, 1999).

Despite of the consensus that microbial activity contributes to the alteration of basaltic glass, the microorganisms involved in this process and their metabolism are poorly constrained. Phylogenetic analyses reveal that the basalt-hosted biosphere is dominated by Bacteria, with Proteobacteria being particularly abundant (Thorseth et al., 2001; Lysnes et al., 2004; Santelli et al., 2008), while Archaea seem to dominate the biosphere in deep-sea sediments (Lipp et al., 2008). In contrast to most studies suggesting the dominance of Bacteria in marine basalt, Fisk et al. (2003) identified mostly archaeal nucleic acid sequences in Hawaiian subsurface basalt. Quantitative polymerase chain reaction (qPCR) measurements of basaltic glass indicate total bacterial and archaeal cell densities in the range of ~ 6×10^5 to ~ 1×10^9 cells per g rock, 3 to 4 orders of magnitude greater than in overlying seawater (Einen et al., 2008; Santelli et al., 2008).

Microorganisms attached to external surfaces of rocks are termed epiliths, while organisms dwelling in the interior of rocks are referred to as endoliths (Golubic et al., 1981). Among different types of endoliths (Fig. 5.1), cryptoendoliths dwell within structural cavities (Golubic et al., 1981). With respect to volcanic rocks, most previous

studies focused on endolithic microbial activity in the glassy rim of pillow basalts. These rims are commonly bored by microorganisms, which are apparently capable of dissolving volcanic glass (e.g. Thorseth et al., 1995). Microorganisms actively penetrating rocks are referred to as euendoliths (Golubic et al., 1981; McLoughlin et al., 2007). Putative cryptoendolithic microorganisms that dwelled in volcanic rocks have only been recently recognized in Middle Devonian pillow basalts of the Rhenohercynian zone, Germany (Peckmann et al., 2008).

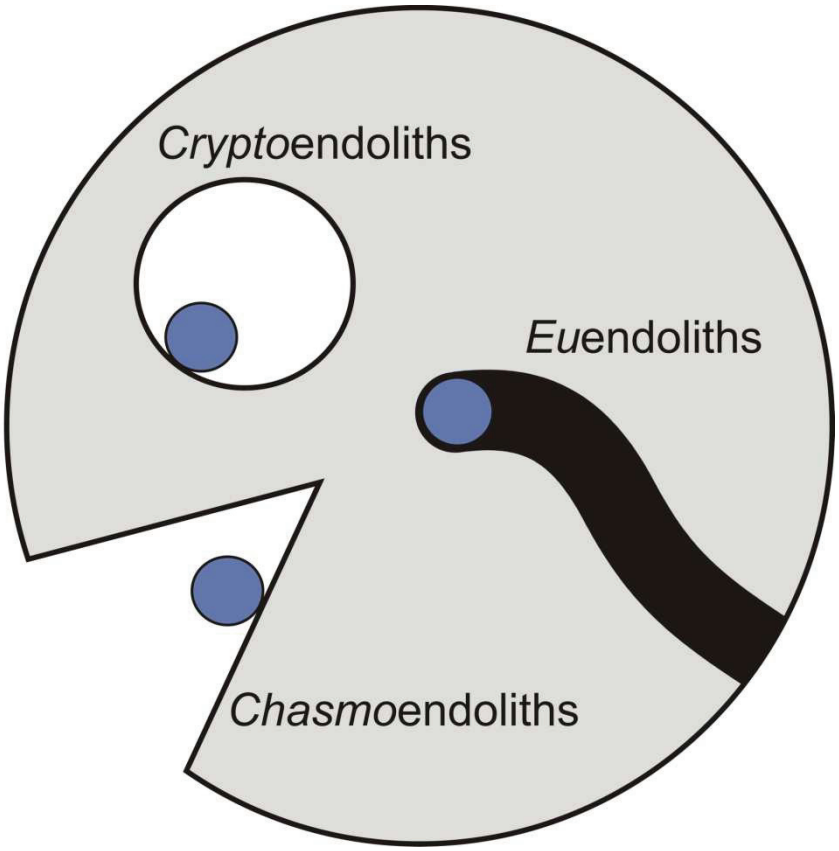

Fig. 5.1. Sketch illustrating the different endolithic habitats within rocks. Modified after Golubic et al. (1981).

Here, we report the presence of fossil cryptoendoliths within Late Devonian (Frasnian) pillow basalts from two sampling sites within the Saxothuringian zone, Germany. Our new findings indicate that a cryptoendolithic mode of life in volcanic rocks has been more widespread than previously recognized.

5.2. Geological setting

The studied Devonian pillow basalts are from two active quarries in south-east Germany (Fig. 5.2), part of the Saxothuringian basin of the Palaeozoic Variscan orogen (Franke, 1989). One quarry is located in the north-western part of the Frankenwald in northern Bavaria, on the northern slope of the Grundberg Hill (50°10'09.07''N, 11°31'37.55''E), approximately 2 km northwest of the town of Stadtsteinach. This part of the Saxothuringian zone is a north-east trending belt of rocks situated at the north-western margin of the Bohemian Massif (Franke et al., 1995). The other quarry is situated in the eastern part of the Thüringer Wald, approximately 3 km south of the town of Schleiz in eastern Thuringia (50°37'28.61''N, 11°50'30.67''E). Intraplate volcanism was common during the Late Devonian (Frasnian) of the Saxothuringian basin, recording a brief yet prominent interval of renewed rifting (Falk et al., 1995). The submarine extrusion of lava in the Frasnian led to the formation of thick piles of bedded volcanic rocks locally reaching more than 200 m in thickness in both study areas. This magmatic event was related to the subduction of Gondwana in the course of the closure of the Rheic Ocean (Linnemann, 2004).

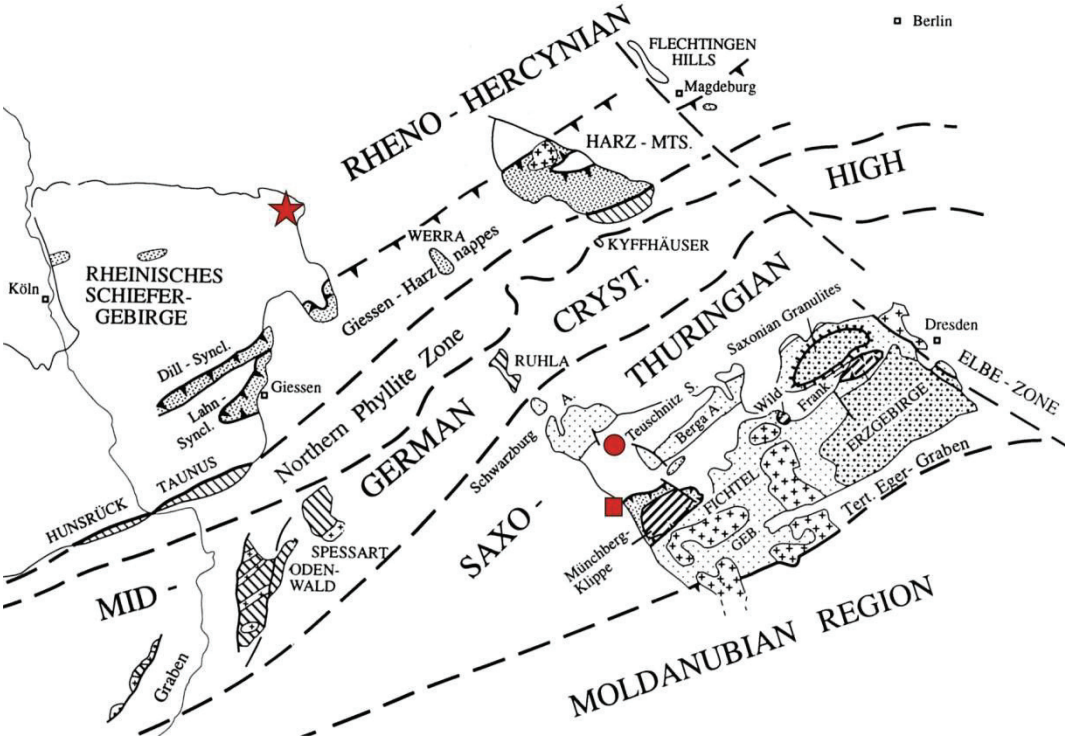

Fig. 5.2. Sketch map of the Variscan orogen of Central Europe showing the sampling sites in the Frankenwald and the Thüringer Wald of the Saxothuringian zone in south-west Germany (modified after Franke, 1995). Square, Frankenwald; circle, Kahlleite; star, Arnstein (Peckmann et al., 2008).

5.3. Methods

Standard petrographic microscopy was performed on thin sections (100 × 75 and 48 × 28 mm), which were partly stained with a mixture of potassium ferricyanide and alizarin red dissolved in 0.1% hydrochloric acid (Dickson, 1966). Petrographic microscopy was carried out with a Zeiss Axioskop 40 A Pol equipped with a Zeiss AxioCam MRc digital camera. Electron microprobe analyses were performed at the University of Kiel using a Jeol JXA 8900R instrument (Jeol, Tokyo, Japan). Analytical conditions were 15 kV accelerating potential, 20 nA probe current, and 1 µm beam diameter. Oxide standards were used for calibration, and data were corrected for matrix effects by the phi-rho-z method. Laser-ablation ICP-MS (inductively coupled plasma mass spectrometry) was carried out at the University of Bremen using a ThermoFinnigan Element2 coupled with a NewWave UP193 solid state laser ablation system (λ = 193 nm). In order to avoid surface contamination, each sample was preablated five times. Calibration was against NIST 612 glass standard using ^{43}Ca as internal standard, and assuming a calcium content of 40.04 wt%.

5.4. Results

The Late Devonian (Frasnian) pillow basalts from the Frankenwald and the Thüringer Wald are typified by abundant carbonate amydgules representing vesicles that formed upon extrusion of volatile-rich lava on the seafloor (Fig. 5.3). After cooling and seawater circulation through the pillows, two generations of carbonate cements precipitated in the vesicles, which also enclose filamentous minerals (Fig. 5.4). The time of formation of these filaments is confined by the paragenetic sequence of carbonate cements. The first carbonate cement is a fibrous rim cement that partially shows botryoidal crystal habits. It is recrystallized to different degrees and its mineralogy is now calcite. In all studied pillow basalts, filaments have never been found within this early cement. Filaments originate on the walls of amygdules (Fig. 5.5) or on the fibrous rim cement (Fig. 5.4). Later equant calcite spar completely filled the amygdules. Surrounding the filaments, equant calcite spar postdates filament formation. Calcite veins of variable widths and lengths crosscut the basalt matrix, but do not contain filaments. The occurrence of filaments is not pervasive. Filaments are most abundant close to the margin of pillows.

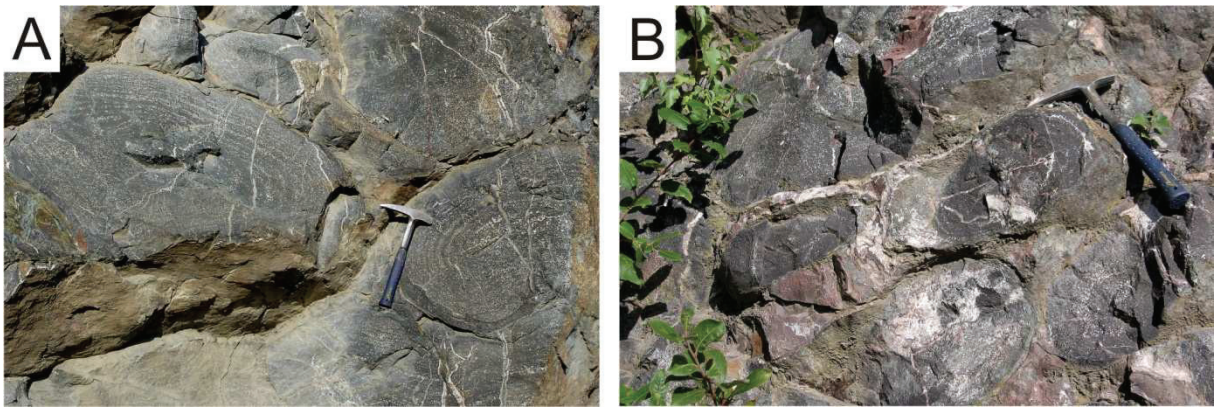

Fig. 5.3. Late Devonian pillow basalts. (A) Frankenwald, Grundberg Hill quarry. (B) Thüringer Wald, Kahlleite quarry.

Most filaments are not branching, are curved, and are of uniform width along their length (Fig. 5.5). Some filaments exhibit central swellings (Fig. 5.6). Another type of filaments is branching, occasionally resulting in dense networks. Some filaments of this type reveal internal segmentation (Fig. 5.7). Depending on the type of filaments, width varies from 3 µm (Fig. 5.5) to 10 µm (Fig. 5.7).

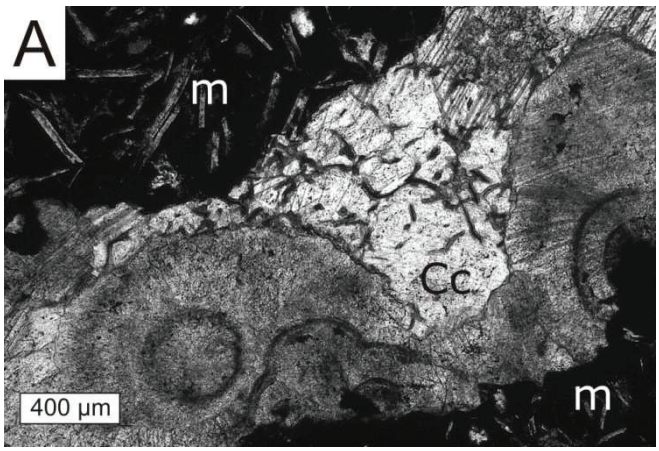

Fig. 5.4. Photomicrograph of filaments. Plane polarized light; m, basaltic matrix; Cc, calcite; fCc, fibrous rim cement. Filaments originate on the fibrous rim cement.

Most filaments consist of authigenic clay minerals, forming a composite fabric (Fig. 5.5; 5.6). Filaments with central swellings and complex branching patterns are made of unidentified phases, probably iron minerals. Because the mineralogy of the clay phases from the Frankenwald and the Thüringer Wald pillow basalts is very similar, they are

not described separately. Electron microprobe analyses indicate that the central portion of filaments consists of a clay mineral with a composition between chamosite and illite, with minor contribution of glauconite (Fig. 5.8A). The bright green phase (Fig. 5.5C) has a composition between chamosite and glauconite with minor contribution of illite.

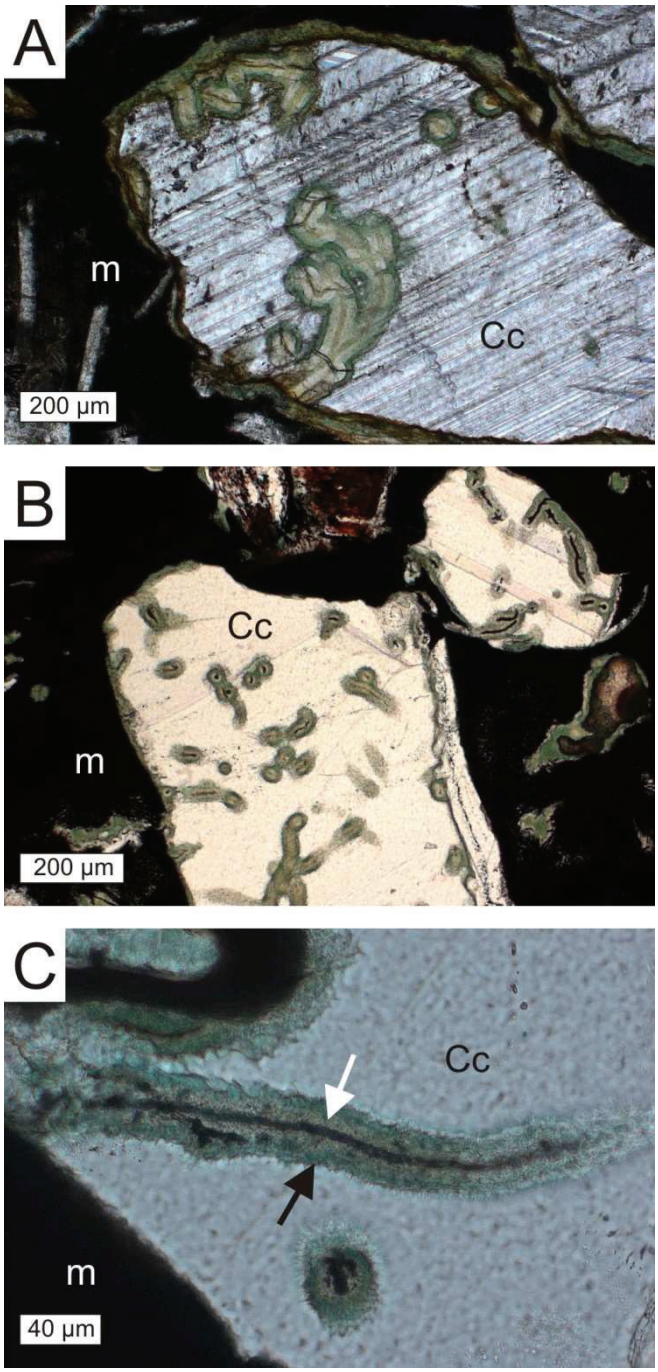

Fig. 5.5. Photomicrograph of secondary clay minerals forming filaments. Plane-polarized light; m, basaltic matrix; Cc, calcite. (A) Filaments project into a former vesicle, Frankenwald. (B) and (C) Mineralized filaments from the Thüringer Wald. The central portion of the filaments (chamosite/illite) is surrounded by chamosite/glauconite (white arrow) and illite/glauconite (black arrow).

Calculated mineral formulas are close to ideal endmember compositions of chamosite and glauconite or mixtures of them (Figs. 5.8A; 5.8B). The dark green phase (Fig. 5.5C) shows a composition between glauconite and illite, with minor contribution of chamosite. The most prominent difference between the three phases is the content of TiO_2, which varies from average values of 0.25 wt% (n = 46) for the bright green phase to 0.56 wt% (n = 47) for the dark green phase. In contrast, TiO_2 contents of the central filaments range from 0 to 74.5 wt% (n = 31). Central filaments with high TiO_2 contents show low FeO contents and vice versa.

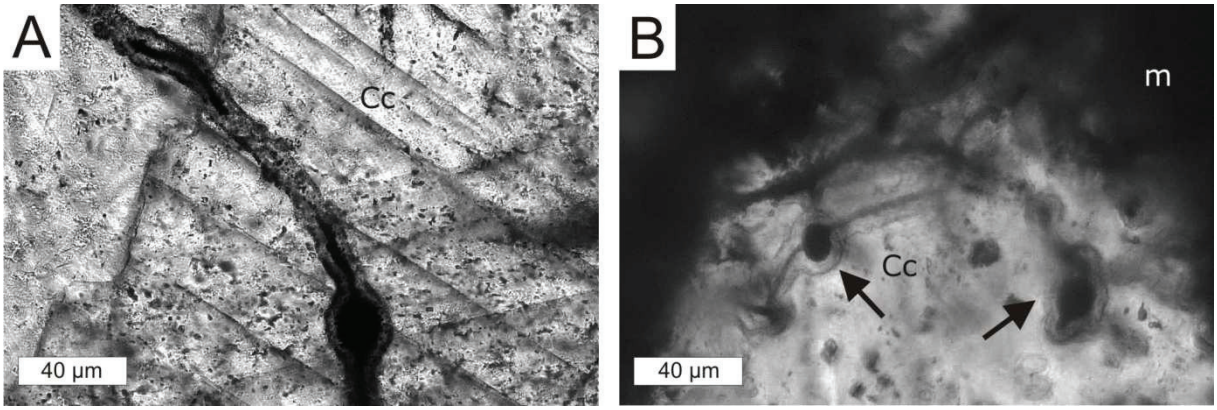

Fig. 5.6. Filaments with central swellings. (A) Thüringer Wald. (B) Arnstein (Peckmann et al., 2008). Plane-polarized light; m, basaltic matrix; Cc, calcite.

The bright green phase and the central filaments are similar to clay minerals that form filaments in carbonate amygdules of Middle Devonian pillow basalts of the Arnstein locality in the Rheinisches Schiefergebirge (cf. Peckmann et al., 2008). However, all Late Devonian authigenic clay minerals exhibit higher Fe contents than their Middle Devonian equivalents.

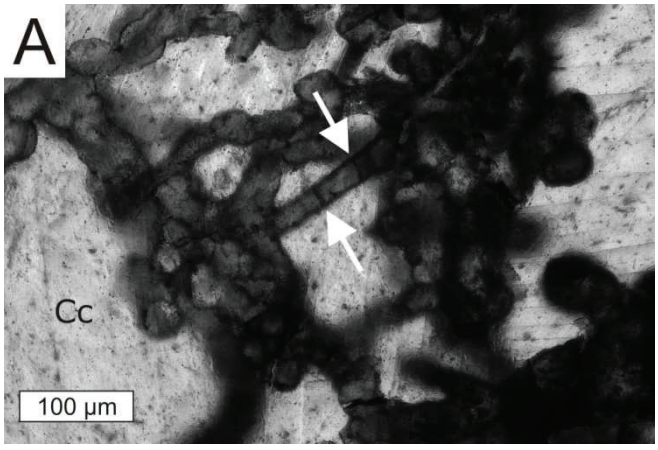

Fig. 5.7. Branching filaments. Plane-polarized light; Cc, calcite. The white arrows indicate internal segmentation.

5.5. Discussion

5.5.1. Volcanic rocks as a niche of life

Putative microbial textures have been identified worldwide in volcanic glass from modern and ancient seafloor environments (Thorseth et al., 1992; 1995; 2003; Furnes et al., 2001; Staudigel et al., 2008). The granular and tubular borings represent trace fossils, which may represent the earliest fossils on Earth (Furnes et al., 2004; Banerjee et al., 2005). In contrast to the filaments in Devonian pillow basalts described here, the textures in the glassy rim of pillows lavas are traces of euendoliths (Fig. 5.1; cf. Golubic et al., 1981; Staudigel et al., 2008). Recent findings suggest that microbial activity is not restricted to the glassy rim of pillow basalts. Ivarsson et al. (2008) reported putative microbial textures attached to phillipsite surfaces in pillow lavas from the Emperor Seamounts in the Pacific. Mineralization patterns of filaments in amygdules of Late Devonian pillow basalts from the Saxothuringian zone described here, closely resemble filaments in amygdules of Middle Devonian pillow basalts from the Rhenohercynian zone, which have been interpreted to represent microorganisms that became fossilized upon microbial clay authigenesis (Peckmann et al., 2008). This suggests that cryptoendolithic basalt-hosted ecosystems were probably common in the past.

Several lines of evidence indicate that the filaments enclosed in carbonate amygdules of the Saxothuringian zone represent fossilized microorganisms. (1) Size of filaments, (2) independence of crystal faces or cleavage plans, (3) constant diameter of filaments, (4) characteristic swellings possibly representing specialized cells (cf. Peckmann et al., 2008), and (5) internal segmentation of some filaments suggest biogenicity. The fact that the filaments occur in amygdules, which are filled by marine carbonate cement, reveals that these vesicles were open to circulating seawater, allowing the introduction of microorganisms or their resting stages. Based on element patterns, Peckmann et al. (2008) showed that the carbonate phases pre- and postdating the filaments formed from marine waters during the Devonian, confirming the syngenicity of filaments. The filaments within the amygdules originate on vesicle walls or on the early fibrous rim cement. This can be explained by growth of microorganisms on mineral surfaces and agrees with the observation that filamentous microorganisms are often attached to the surface of minerals like phillipsite in pillow lavas (Ivarsson et al., 2008). We suggest that the filaments in the Frankenwald and Thüringer Wald basalts represent cryptoendoliths

analogous to the Middle Devonian fossils from the Arnstein quarry of the Rhenohercynian zone (cf. Peckmann et al., 2008).

Like the Middle Devonian filaments, the Late Devonian filaments were fossilized by microbial clay authigenesis. Progressive mineralization led to the complete encrustation of filaments by clay minerals, similar to microbial clay authigenesis in modern environments (Konhauser and Urrutia, 1999). The most pristine filaments at both sites contain chamosite, indicating that the encrustation of microbial cells proceeded from poorly ordered (Fe, Al) silicates towards a crystalline form of chamosite (cf. Ferris et al., 1987; Peckmann et al., 2008). Such a mineralization pattern is consistent with the preferential binding of iron to cell walls and extracellular polymeric substances, which subsequently served as nucleation site for the formation of more complex authigenic minerals (cf. Ferris and Beveridge, 1986; Konhauser et al., 1994).

The observation that some of the filaments show branching patterns and internal segmentation (Fig. 5.7) sheds some light on the phylogenetic affiliation of the putative microorganisms. Interestingly, similar filamentous microorganisms with supposed septa, also occurring in amygdules of marine basalt – but interpreted to represent euendoliths – have been suggested to represent fungi (Schumann et al., 2004). As the Late Devonian branching filaments and filaments with internal segmentation do not consist of clay minerals like the majority of filaments, it seems feasible that different types of microorganisms dwelled within the amygdules of Late Devonian basalt.

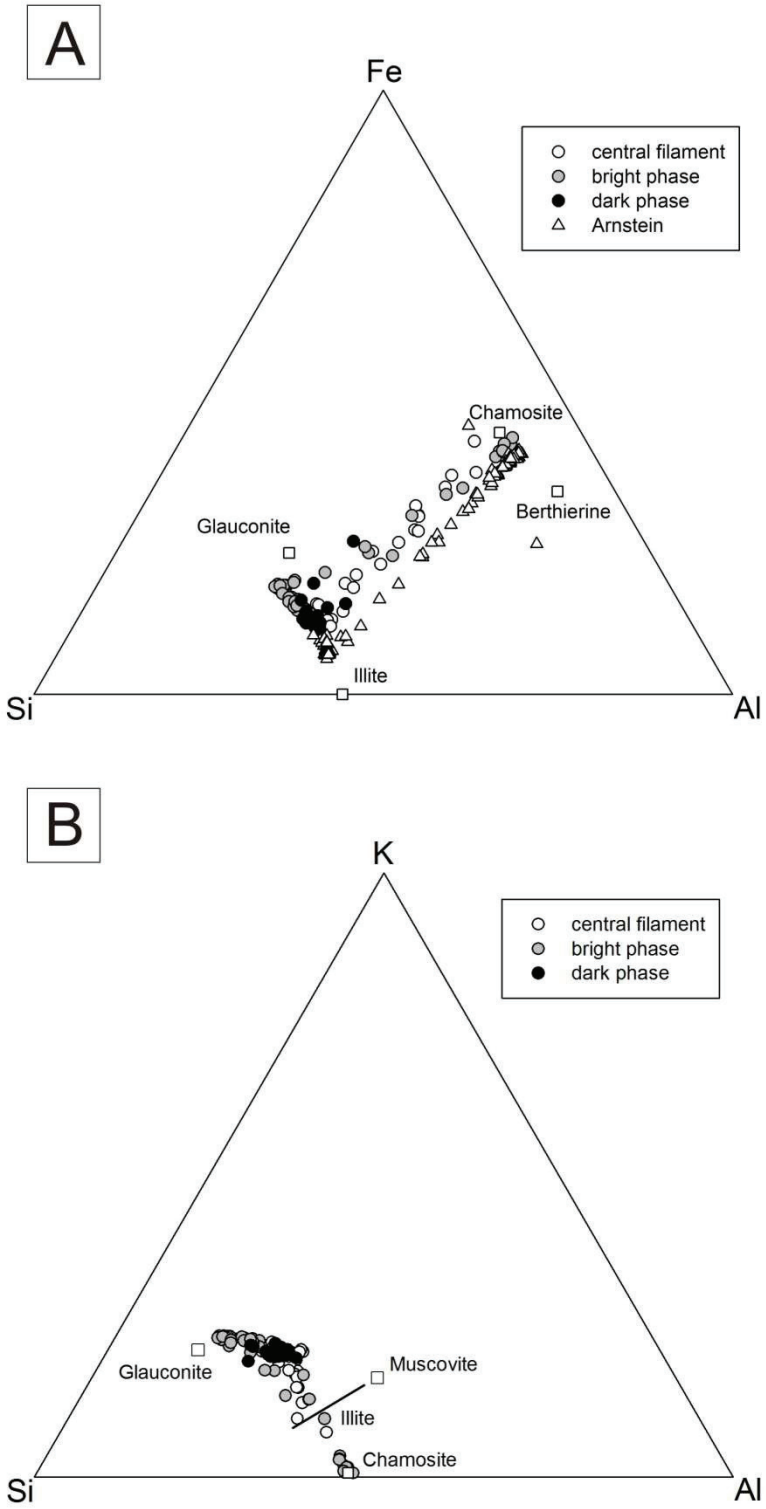

Fig. 5.8. (A) Composition of clay minerals in a Si-Al-Fe ternary. The two endmembers are bethierine-chamosite and glauconite-illite. Compositions of biogenic clay minerals encrusting cryptoendoliths from Peckmann et al. (2008) are included. (B) Composition of clay minerals in a Si-Al-K ternary. Most of the filaments have a composition between illite and glauconite. Compositions of biogenic clay minerals are from Konhauser and Urrutia, 1999.

5.5.2. How widespread were basalt-hosted ecosystems?

The discovery of cryptoendoliths in ancient pillow basalts fuels speculation on the global extent of bioalteration of the oceanic crust. Bioalteration of volcanic glass by euendoliths has been identified in pillow lavas in all ocean basins. It possibly dates back to 3.5 Ga, revealing its worldwide significance and likely impact on seawater composition throughout Earth history (Staudigel et al., 2008). Based on evidence for alteration of basalt by cryptoendoliths (Peckmann et al., 2008), bioalteration is not restricted to volcanic glass, but probably more diverse than previously assumed. This assumption is now strengthened with the recognition of the same type of cryptoendoliths in Late Devonian pillow basalts from two outcrops in the Saxothuringian zone. Since seawater ingress into structural cavities of pillow basalt commonly leads to alteration at low temperatures, such ecosystems may have been widely distributed in Earth history and probably still occur today.

The energy source of the cryptoendoliths is unknown, but submarine basalt contains sufficient quantities of reduced iron and sulphur to support microbial ecosystems (Bach and Edwards, 2003). It has been shown that the oxidation of iron at low temperatures plays an important role in supporting modern basalt-hosted microbial ecosystems (Edwards et al., 2005), but the key microbial organisms involved in alteration have not yet been identified. Although iron oxidation may be a feasible source of energy in basalt, we are unable to constrain its significance for the basalt-hosted ecosystems in the shallow subsurface of the Devonian seafloor (cf. Peckmann et al., 2008).

5.6. Conclusions

Late Devonian (Frasnian) pillow basalts from the Saxothuringian zone of Germany exhibit abundant carbonate-filled vesicles (amygdules) that contain filamentous clay minerals. These filaments project into the vesicles, originating on the basaltic matrix of vesicle walls and early fibrous carbonate cement. Equant calcite spar, which filled up the remaining vesicle space, is surrounding the filaments. Several observations point to the biogenicity of the filaments including (1) size and morphology resembling modern microorganisms, (2) independence of crystal faces and cleavage plans, (3) constant diameter of filaments, (4) characteristic swellings possibly representing specialized cells (cf. Peckmann et al., 2008), and (5) internal segmentation of some filaments. Filaments

preferentially occur close to the margins of pillows, suggesting that microorganisms or their resting stages entered the structural cavities during seawater ingress. Syngenicity of the filaments is revealed by the paragenetic sequence of carbonate cements: filaments postdate the early fibrous rim cement, but predate the later equant calcite spar. The preservation of filaments by clay mineral authigenesis occurred analogous to the encrustation of modern prokaryotes, which is known to be initiated on cell walls and in extracellular polymeric substances. After recognition of fossilized cryptoendolithic microorganisms in Middle Devonian pillow basalt (Peckmann et al., 2008), the new examples of the same type of fossils in Late Devonian pillow basalt suggest that this mode of life was widespread in the shallow subsurface of the Devonian seafloor. It seems unlikely that cryptoendolithic life in volcanic rocks is limited to the Devonian period. More work is needed to constrain the antiquity and longevity of this unusual ecosystem and to identify the respective microorganisms and their metabolism.

Acknowledgements

We thank S. Flotow for preparation of thin sections and assistance during the collection of the samples from the Kahlleite quarry, H. Anders (both Bremen, Germany) for help with LA-ICP-MS analyses, as well as B. Mader (Kiel, Germany) for assistance during microprobe work. The guidance of H. Blumenstengel (Jena, Germany) during field work in the Kahlleite quarry is gratefully acknowledged. This study was supported by the Deutsche Forschungsgemeinschaft within the priority program 1144 ‘From Mantle to Ocean: Energy-, Material- and Life-cycles at Spreading Axes’ and the Excellence Cluster MARUM, Bremen.

IV. GENERAL CONCLUSIONS AND OUTLOOK

GENERAL CONCLUSIONS

This thesis demonstrates that authigenic carbonates from the Logatchev hydrothermal field (LHF) and the Gakkel ridge (GR) reflect precipitation at different temperatures and from different fluids spanning from ambient temperatures and sweater to hydrothermal conditions. Aragonite is the most abundant carbonate mineral found in both serpentinites (LHF and GR) and massive sulfides (LHF), because its preservation is believed to have resulted from contact with seawater being typified by high magnesium and sulfate concentrations. High $\delta^{18}O$ values and radiogenic $^{87}Sr/^{86}Sr$ ratios of aragonite reflect precipitation at low temperatures. These aragonite samples have rare earth element (REE) patterns that lack europium anomalies consistent with precipitation from seawater without hydrothermal input. Serpenitnite-hosted aragonite from the LHF and GR indicate precipitation from seawater that had undergone very limited exchange with the host rock. $\delta^{13}C$ values of serpentinite-hosted aragonite agree with a marine carbon signal, whereas high $\delta^{13}C$ values of sulfide-hosted aragonite may reflect residual carbon dioxide in the one of methanogenesis. Similar $^{87}Sr/^{86}Sr$ ratios of sulfide-hosted aragonite from the LHF point to the precipitation from seawater at low temperatures. Sulfide-hosted aragonite, however, shows distinct positive Eu anomalies, which point to a contribution of reduced hydrothermal fluids. This apparent contradiction of formation from hydrothermal fluids at low temperatures indicates the sensitivity of Eu in tracing even minimal contribution (<1%) of hydrothermal input. Some aragonite samples from the LHF show higher Sr/Ca and Mg/Ca ratios than seawater, indicating prolonged exposure at the seafloor and subsequent incorporation of strontium and magnesium into aragonite.

$\delta^{13}C$ values of dolomite hosted in talus breccias in the LHF, similar to those of sulfide-hosted aragonite, may indicate residual carbon dioxide in the zone of methanogenesis. $^{87}Sr/^{86}Sr$ ratios are slightly lower than modern seawater (0.70896 to 0.70907), but show apparent formation temperatures of ~100°C (based on oxygen isotopes). A simple mixing model based on strontium and enthalpy balance indicates that these temperatures and $^{87}Sr/^{86}Sr$ ratios can only be reconciled if the dolomite formed from conductively heated seawater, with only 3% of hydrothermal fluids. This hydrothermal input also explains the REE patterns with its strong positive Eu anomalies of the dolomite.

Calcite veins from the LHF have low $\delta^{18}O$ values (as low as −20.0‰), indicative of precipitation from hydrothermal fluids. Its low $\delta^{13}C$ values (as low as −5.8‰) agree with a contribution of magmatic carbon, presumably mantle-derived carbon dioxide. Unradiogenic $^{87}Sr/^{86}Sr$ ratios (0.70483 to 0.70499) and calculated formation temperatures up to ~180°C reveal precipitation from hydrothermal fluids in the sub seafloor basement. This hydrothermal origin is confirmed by REE patterns. The enrichment of light REE and strong positive Eu anomalies are similar to REE patterns of the LHF vent fluids. Strontium mass balance indicates that calcite precipitated from a mixture of ~67% hydrothermal fluid and ~33% seawater. Further, the isenthaphic temperatures predicted from mixing 350°C hydrothermal fluids and seawater in these portions would be much higher than the temperatures indicated from oxygen isotopes. Hence, the hydrothermal calcite was formed from fluids that underwent significant conductive cooling. Fluids that favored calcite formation in the LHF have low Mg/Ca, Sr/Ca ratios and sulfate concentrations. Such fluids are typically generated by serpentinization.

Late Devonian (Frasnian) calcite hosted in serpentinites and basalts from the Saxothuringian zone contain different calcite phases. Among those, basalt-hosted botryoidal crystal aggregates possibly were primarily aragonite, suggesting early formation at low temperatures. Low $\delta^{18}O$ values of calcite reflect diagenetic and metamorphic overprinting during the Variscan orogeny. $\delta^{13}C$ values of basalt-hosted calcite reflects seawater-derived dissolved inorganic carbon as the main carbon source. In contrast, $\delta^{13}C$ values for serpenitnite-hosted calcite indicate at least two carbon souces: (1) mantle-derived carbon dioxide, and (2) a contribution of amagmatic carbon, presumably methane. Pillow basalts exhibit abundant carbonate-filled vesicles that contain filamentous clay minerals. These filaments project into the vesicles, originating on the basaltic matrix of vesicle walls and early fibrous rim cement. Several observations point to the biogenicity of the filaments including (1) size and morphology resembling modern microorganisms, (2) independence of mineralogy, (3) constant diameter of filaments, (4) characteristic swellings possibly representing specialized cells, and (5) internal segmentation of some filaments. The syngenicity of the filaments is revealed by the paragenetic sequence of carbonate cements: filaments postdate the early fibrous rim cement, but predate the later equant calcite spar. This suggests that microorganisms or their resting stages entered the structural cavitites during seawater ingress. The

preservation of filaments by clay mineral authigenesis occurred analogous to the encrustation of modern prokaryotes, which is known to be initiated on cell walls and in extracellular polymeric substance. The same type of fossilized cryptoendolithic microorganisms were found in Middle Devonian pillow basalt and suggest that this mode of life was widespread in the shallow subsurface of the Devonian seafloor. It seems unlikely that cryptoendolithic life in volcanic rocks is limited to the Devonian period.

OUTLOOK

In order to progress the understanding of carbonate formation in serpentinite-hosted environments, several additional inorganic and organic geochemical methods would help to verify those processes. Since this study provides evidence that carbonates precipitate from seawater or hydrothermal fluids within a single hydrothermal system, isotope systems more sensitive to low-intensity seawater-rock interactions may be useful to better quantify the effects of low-temperature exchange. Lithium (Li) is a good indicator of seawater-rock interaction because at low temperatures Li is taken into secondary minerals and at high temperatures it is leached from the host rocks (Chan et al., 2002). Within this thesis it was demonstrated that the carbonates formation associated with serpentinites is due to reactions between seawater and upper mantle peridotite producing alkaline fluids having a pH value between 9 and 12 (Palandri and Reed, 2004). To quantify the pH-dependent carbonate formation, it is of great interest whether different carbonate minerals precipitate at different pH values. Here, the boron (B) isotopic composition of carbonate may provide useful insights. The boron isotope fractionation is due to the preferential incorporation of ^{11}B in the $B(OH)_3$-species, while ^{10}B is incorporated in the $B(OH)_4^-$-species (Palmer and Swihart, 1996). The abundance of $B(OH)_3$ and $B(OH)_4^-$ in fluids is a function of the pH that mainly controls the distribution of ^{11}B and ^{10}B. At low pH values $B(OH)_3$ is the dominant species, whereas $B(OH)_4^-$ is dominant at high pH values (Foster, 2008). A more detailed understanding of carbonate formation at high and low temperatures under hydrothermal conditions to can be obtained by analyzing the sulfur isotopic composition of structurally substitutes sulfate (SSS) in carbonate minerals (Kampschulte and Strauss, 2004). Since the sulfur cycle at

hydrothermal systems is characterized by the principle endmembers seawater-derived sulfur ($\delta^{34}S$ = 21.5 ‰) and mantle-derived sulfur ($\delta^{34}S$ =~ 0‰) with well distinct sulfur isotopic compositions, the contribution of this two endmembers are of great interest in quantifying chemical fluxes in hydrothermal environments.

To get a deeper understanding of the carbonate precipitation in serpentinite-hosted environments, biomarker analyses of authigenic carbonate minerals would help to provide useful insights. Serpentinization of peridotites generates fluids with high concentrations of methane and hydrogen (e.g. Charlou et al., 2002). The reduction of iron could serve as an energy source for biology through the production of hydrogen, the electron donor for a number of chemoautotrophic biochemical processes, including methanogenesis (e.g. Schulte et al., 2006). Since this vast amount of energy may drive chemoautotrophic communities, it is of great interest whether microorganisms trigger the precipitation of carbonates. One could think of a process similar to the anaerobic oxidation of methane (AOM), a process responsible for the formation of authigenic carbonates at cold seeps (e.g. Peckmann et al. 2001). Here, the anaerobic oxidation of methane is mediated by a consortium of methanotrophic Archaea and sulfate-reducing Bacteria (Hinrichs et al., 1999). Carbonates precipitated via the anaerobic oxidation of methane yield low $\delta^{13}C$ values reflecting methane as the principle carbon source. This methane, either biogenic or thermogenic is strongly depleted in ^{13}C resulting in low $\delta^{13}C$ values (Whiticar, 1999). There are several characteristic ^{13}C-depleted biomarkers in ancient cold seep environments, which help to identify the microorganisms involved in the formation of authigenic carbonates (Peckmann and Thiel, 2004). A promising target area to investigate whether the serpentinite-hosted carbonates are mediated by microorganisms is the Mariana Trench. The Mariana Trench is characterized by abundant serpentinite mud volcanoes with carbonate chimneys forming atop the seamounts, similar to the carbonate chimneys in the Lost City field (Haggerty, 1991). Recently, Mottl et al. (2003) showed that fluids emanating from the seamounts have high pH values (12.5). Further, Archaea are found to dominate the microbial community operating at pH, oxidizing the methane to carbonate ion, while reducing sulfate to bisulfate. There is a huge potential that this reaction may drive the formation of carbonate minerals atop the serpentinite mud volcanoes. If this is so, the analyses of biomarker in this authigenic carbonates would help to get further insights in the mechanisms triggering the carbonate formation. Additionally, $\delta^{13}C$ values for the

carbonates from the Mariana Trench are as low as −21.2‰ (Haggerty, 1991), suggesting that seawater-derived dissolved inorganic carbon can be excluded as the carbon source. Those low $\delta^{13}C$ values are similar to seep carbonates, indicative of methane as the principle carbon source (e.g.Peckmann and Thiel, 2004). I postulate that a comprehensive study of carbonates at the Mariana Trench, including specific biomarker analyses would provide detailed insights in the carbonate formation in serpentinite-hosted environments.

V. REFERENCES

Agrinier, P., Cornen, G., and Beslier, M.-O. 1996. Mineralogical and oxygen isotopic features of serpentinites recovered from the ocean/continent transition in the Iberia abyssal plain. In Whitmarsh, R. B., Sawyer, D. S., Klaus, A., and Mason, D. S., (Eds.), Proc. ODP, Sci. Results, 149, 541-552

Albarède, F., Michard, A., Minster, J.-F., and Michard, G. 1981. $^{87}Sr/^{86}Sr$ ratios in hydrothermal waters and deposits from the East Pacific Rise at 21°N. Earth and Planetary Science Letters 55, 229-236

Allen, D. E., and Seyfried, W. E. 2003. Compositional controls on vent fluids from ultramafic-hosted hydrothermal systems at mid-ocean ridges: an experimental study at 400°C, 500 bar. Geochimica et Cosmochimica Acta 67, 1531-1542

Allen, D. E., and Seyfried, W. E. 2005. REE controls in ultramafic hosted MOR hydrothermal systems: An experimental study at elevated temperature and pressure. Geochimica et Cosmochimica Acta 69, 675-683

Alt, J. C., and Shanks, W. C. 1998. Sulfur in serpentinized oceanic peridotites: Serpentinization processes and microbial sulfate reduction. Journal of Geophysical Research 103, 9917-9929

Alt, J. C., and Shanks, W. C. 2003. Serpentinization of abyssal peridotites from the MARK area, Mid-Atlantic Ridge: Sulfur geochemistry and reaction modeling. Geochimica et Cosmochimca Acta 67, 641–653

Alt, J. C., and Teagle, D. A. H. 1999. The uptake of carbon during alteration of ocean crust. Geochimica et Cosmochimica Acta 63, 1527-1535

Alt, J. C., and Teagle, D. A. H. 2003. Hydrothermal alteration of upper oceanic crust formed at a fast-spreading ridge: mineral, chemical, and isotopic evidence from ODP Site 801. Chemical Geology 201, 191-211

Alt, J. C., and Bach, W., 2006. Oxygen isotope composition of a section of lower oceanic crust, ODP Hole 735B. Geochemistry Geophysics Geosystems 7, doi:10.1029/2006GC001385

Amini. M., Eisenhauer, A., Böhm, F., Fietzke, J., Bach, W., Garbe-Schönberg, D., Rosner, M., Bock, B., Lackschewitz, K., and Hauff, F. 2008. Calcium isotope ($\delta^{44/40}Ca$) fractionation along hydrothermal pathways, Logatchev field (Mid-Atlantic Ridge. 14°45'N). Geochimica et Cosmochimica Acta 72, 4107-4122

Augustin, N., Lackschewitz, K. S., Kuhn, T., and Devey, C.W. 2008. Mineralogical and chemical mass changes in mafic and ulramafic rocks from the Logatchev hydrothermal field (MAR 15°N). Marine Geology 256, 18-29

Bach, W., and Edwards, K. J. 2003. Iron and sulfide oxidation within the basaltic ocean crust: Implications for chemolithoautotrophic microbial biomass production. Geochimica et Cosmochimica Acta 67, 3871-3887

Bach, W., Paulick, H., Garrido, C. J., Ildefonse, B., Meurer, W. P., and Humphris, S. 2006. Unravelling the sequence of serpentinization reactions: petrography, mineral chemistry, and petrophysics of serpentinites from MAR 15°N (ODP Leg 209, Site 1274). Geophysical Research Letters 33, L13306

Baker, P. A., and Kastner, M. 1981. Constraints on the formation of sedimentary dolomite. Science 213, 214-216

Baker, E. T., Edmonds, H. N., Michael, P. J., Bach, W., Dick, H. J. B., Snow, J. E., Walker, S. L., Banerjee, N. R., and Langmuir, C. H. 2004. Hydrothermal venting in magma deserts: The ultraslow-spreading Gakkel and Southwest Indian Ridges. Geochemistry Geophysics Geosystems 5, doi:10.1029/2004GC000712

Banerjee, N. R., Furnes, H., Muehlenbachs, K., Staudigel, H., and de Wit, M. 2006. Preservation of ~3.4 – 3.5 Ga microbial biomarkers in pillow lavas and hyaloclastites from the Barberton Greenstone Belt, South Africa. Earth and Planetary Science Letters 241, 707-722

Banerjee, N.R., Simonetti, A., Furnes, H., Muehlenbachs, K., Staudigel, H., Heaman, L., Van Kranendonk, M.J. 2007. Direct dating of Archaean microbial ichnofossils: Geology 35, 487-490

Banner, J.L. 2004. Radiogenic isotopes: systematics and applications to earth surface processes and chemical stratigraphy. Earth Science Reviews 65, 141-191

Barbieri, M., Masi, U, and Tolomeo, L. 1979. Stable isotope evidence for a marine origin of ophicalcites from the north-central Apennines (Italy). Marine Geology 30, 193-204

Bau, M. 1991. Rare-earth element mobility during hydrothermal and metamorphic fluid-rock interaction and the significance of the oxidation state of europium. Chemical Geology 93, 219-230

Berndt , M. E., Allen, D. E., and Seyfried, W. E. 1996. Reduction of CO_2 during serpentinization of olivine at 300°C and 500 bar. Geology 24, 351-354

Berndt, M. E., and Seyfried, W. E. 1999. Rates of aragonite conversion to calcite in dilute aqueous fluids at 50°C to 100°C: Experimental calibration using Ca-isotope attenuation. Geochimica et Cosmochimica Acta 63, 373-381

Bischoff, J. L., and Rosenbauer, R. J. 1985. An empirical equation of state for hydrothermal seawater (3.2 percent NaCl). American Journal of Science 285, 725-763

Blusztajn, J., and Hart, S. R. 1996. Sr and O isotopic ratios of aragonite veins from site 895. In Mével, C., Gillis, K.M., Allan, J.F., Meyer, P.S. (Eds.), Proceedings of the Ocean Drilling Program, Scientific Results, Vol. 147, 311-313

Bonatti, E., Lawrence, J. R., Hamlyn, P. R., and Berger, D. 1980. Aragonite from deep sea ultramafic rocks. Geochimica et Cosmochimica Acta 44, 1207-1214

Buggisch, W., and Joachimski, M. M. 2006. Carbon isotope stratigraphy of the Devonian of Central and Southern Europe. Palaeogeography Palaeoclimatology Palaeoecology 240, 68-88

Burke, W. H., Denison, R. E., Hetherington, E. A., Koepnick, R. B., Nelson, H. F. and Otto, J. B. 1992. Variation of seawater $^{87}Sr/^{86}Sr$ throughout Phanerozoic time. Geology 10, 516-519

Burne, R. V., and Moore, L. S. 1987. Microbialites: organosedimentary deposits of benthic microbial communities. Palaios 2, 241-254

Burton, E. A. 1993. Controls on marine carbonate cement mineralogy: review and reassessment. Chemical Geology 105, 163-179

Butterfield, D. A., Nelson, B. K., Wheat, G. W., Mottl, M. J., and Roe, K. K. 2001. Evidence for basaltic Sr in mid-ocean ridge-flank hydrothermal systems and implications for the global oceanic Sr isotope balance. Geochimica et Cosmochimica Acta 65, 4141-4153

Cannat, M. 1993. Emplacement of mantle rocks in the seafloor at mid-ocean ridges. Journal of Geophysical Research 98, 4163-4172

Cannat, M., Lagabrielle, Y., de Coutures, N, Bougault, H., Casey, J., Dmitriev, L, and Fouquet, Y. 1997. Ultramafic and gabbroic exposures at the Mid-Atlantic Ridge: geological mapping in the 15°N region. Tectonophysics 279, 193-213

Chan, L.-H., Alt, J. C., and Teagle, D. A. H. 2002. Lithium and lithium isotope profiles through the upper oceanic crust: a study of sweater-basalt exchange at ODP Sites 504B and 896A. Earth and Planetary Science Letters 201, 187-201

Charlou, J. L., Fouquet, Y., Bougault, H., Donval, J. P., Etoubleau, J., Jean-Baptiste, P., Dapoigny, A., Appriou, P., and Rona, P. A. 1998. Intense CH_4 plumes generated by serpentinization of ultramafic rocks at the intersection of the 15°20'N fracture zone on the Mid-Atlantic Ridge. Geochimica et Cosmochimica Acta 62, 2323-2333

Charlou, J. L., Donval, J. P., Fouquet, Y., Jean-Baptiste, P, and Holm. N. 2002. Geochemistry of high H_2 and CH_4 vent fluids issuing from ultramafic rocks at the Rainbow hydrothermal field (36°14'N, MAR). Chemical Geology 191, 345-359

Cicero, A. C., and Lohman, K. G. 2001. Sr/Mg variation during rock-water interaction: Implications for secular changes in the elemental chemistry of ancient seawater. Geochimica et Cosmochimica Acta 65, 741-761

Coggon, R. M., Teagle, D. A. H., Cooper, M. J., and Vanko, D.A. 2004. Linking basement carbonate vein compositions to porewater geochemistry across the eastern flank of the Juan de Fuca Ridge, ODP Leg 168. Earth and Planetry Science Letters 219, 111-128

Dick, H. J. B., Lin, J., and Schouten, H. 2003. An ultraslow-spreading class of ocean ridge. Nature 426, 405-412

Dickson, J. A. D. 1966. Carbonate identification and genesis as revealed by staining. J. Sedimentary Petrology 36, 491-505

Douville, E., Bienvenu, P., Charlou, J. L., Donval, J. P., Fouquet, Y., Appriou, P., and Gamo, T. 1999. Yttrium and rare earth elements in fluids from various deep-sea hydrothermal systems. Geochimica et Cosmochimica Acta 63, 627-643

Douville, E., Charlou, J. L., Oelkers, E. H., Bienvenu, P., Jove Colon, C. F., Donval, J. P., Fouquet, Y., Prieur, D., and Appriou, P. 2002. The rainbow vent fluids (36°14'N, MAR): the influence of ultramafic rocks and phase separation on trace metal content in Mid-Atlantic Ridge hydrothermal fluids. Chemical Geology 184, 37-48

Edmonds, H. N., Michael, P. J., Baker, E. T., Connelly, D. P., Snow, J. E., Langmuir, C. H., Dick, H. J. B., Mühe, R., German, C. R., and Graham, D. W. 2003. Discovery of abundant hydrothermal venting on the ultraslow-spreading Gakkel ridge in the Arctic Ocean. Nature 421, 252-256

Edwards, K. J., Bach, W., and McCollom, T. M. 2005. Geomicrobiology in oceanography: mineral-microbe interactions in the deep-sea. Trends in Microbiology 13, 449-456

Eickmann, B., Bach, W., and Peckmann, J. in press. Authigenesis of carbonate minerals in modern and Devonian ocean-floor hard rocks. The Journal of Geology, doi:10.1086/597362

Einen, J., Thorseth, I. H., and Øvreås, L. 2008. Enumeration of Archaea and Bacteria in seafloor basalt using real-time quantitative PCR and fluorescence microscopy. FEMS Microbiology Letters 282, 182-187

Elderfield, H, and Schultz, A. 1996. Mid-ocean ridge hydrothermal fluxes and the chemical composition of the ocean. Annual Reviews of Earth and Planetary Sciences 24, 191-224

Elderfield, H., Wheat, C. G., Mottl, M. J., Monnin, C., and Spiro, B. 1999. Fluid and geochemical transport through oceanic crust: a transect across the eastern flank of the Juan de Fuca Ridge. Earth and Planetary Science Letters 172, 151-165

Falk, F., Franke, W., and Kurze, M. 1995. Stratigraphy. In Dallmeyer, R. D., Franke, W., and Weber, K., (Eds.), Pre-Permian geology of Central and Eastern Europe. Springer-Verlag, Berlin-Heidelberg, 221-234

Feigl, F. 1958. Spot test in inorganic analysis. Fifth enlarged and revised English edn. Elsevier, Amsterdam

Ferris, F. G., Fyfe, W. S., and Beveridge, T. J. 1987. Bacteria as nucleation sites for authigenic minerals in a metal-contaminated lake sediment. Chemical Geology 63, 225-232

Fisk, M. R., Giovannoni, S. J., and Thorseth, I. H. 1998. Alteration of oceanic volcanic glass: textural evidence of microbial activity. Science 281, 978-980

Fisk, M. R., Storrie-Lombardi, M. C., Douglas, S., Popa, R., McDonald, G, and Di Meo-Savoie, C. 2003. Evidence of biological activity in Hawaiian subsurface basalts. Geochemistry, Geophysics, Geosystems, 4, doi: 10.1029/2002GC000387

Fortin, D., Ferris, F. G., and Scott, S. D. 1998. Formation of Fe-silicates and Fe-oxides on bacterial surfaces in samples collected near hydrothermal vents on the Southern Explorer Ridge in the northeast Pacific Ocean. American Mineralogist 83, 1399-1408

Foster, G. L. 2008. Seawater pH, pCO_2 and $[CO_3^{2-}]$ variations in the Caribbean Sea over the last 130 kyr: a boron isotope and B/Ca study of planktic foraminifera. Earth and Planetary Science Letters. doi:10.1016/j.epsl.2008.04.015

Foustoukos, D. I. and Seyfried, W. E. Jr. 2004. Hydrocarbons in hydrothermal vent fluids: the role chromium-bearing catalysts. Science 304, 1002-1005

Franke, W. 1989. Variscan plate tectonicsin Central Europe-current ideas and open questions. Tectonophysics 169, 221-228

Franke, W., Kreuzer, H., Okrusch, M., Schüssler, U., and Seidel, E. 1995. Structure. In Dallmeyer, R. D., Franke, W., and Weber, K. eds. Pre-permian geology of Central and Eastern Europe, 177-294

Früh-Green, G. L., Kelley, D. S., Bernasconi, S. M., Karson, J. A., Ludwig, K. A., Butterfield, D. A., Boschi, C., and Proskurowski, G. 2003. 30,000 Years of hydrothermal activity at the Lost City Vent Field. Science 301, 495-498

Früh-Green, G. L., Connolly, J. A. D., Plas, A, Kelley, D. S., and Grobéty, B. 2004. Serpentinization of oceanic peridotites: implications for geochemical cycles and biological activity. In The subseafloor biosphere at mid-ocean ridges, Geophysical monograph series 144, Wilcock, W. S. D, DeLong, E. F., Kelley, D. S., Baross, J. A., and Carry, S. C. (Eds.), American Geophysical Union, Washington, 119-136

Furnes, H., and Staudigel, H. 1999. Biological mediation in ocean crust alteration: how deep is the deep biosphere? Earth and Planetary Science Letters 166, 97-103

Furnes, H., Muehlenbachs, K., Tumyr, O., Torsvik, T., and Xenophontos, C. 2001. Biogenic alteration of volcanic glass from the Troodos ophiolite, Cyprus. Journal of the Geological Society, London 158, 75-84

Furnes, H., Banerjee, N. R., Staudigel, H., and de Witt, M. 2004. Early life recorded in Archean pillow lavas. Science 304, 578-581

Furnes, H., Dilek, Y., Muehlenbachs, K., and Banerjee, N. R. 2006. Tectonic control of bioalteration in modern oceanic crust as evidenced by carbon isotopes. Island Arc 15, 143-155

Fujiwara, T., Lin, J., Matsumoto, T., Kelemen, P. B., Tucholke, B. E., and Casey, J. F. 2003. Crustal evolution of the mid-Atlantic Ridge near the Fifteen-Twenty Fracture Zone in the last 5 Ma. Geochemistry Geophysics Geosystems 4, doi: 10.1029/2002GC000364

Gablina, I. F., Semkova, T. A., Stepanova, T. V., and Gor'kova, N. V. 2006. Diagentic alterations of copper sulfides in modern ore-bearing sediments of the Logatchev-1 hydrothermal field (Mid-Atlantic Ridge 14°45'N). Lithology and Mineral Resources 41, 27-44

German, C. R., Masuzawa, T., Greaves, M. J., Elderfield, H., and Edmond, J. M. 1995. Dissolved rare earth elements in the Southern Ocean: cerium oxidation and the influence of hydrography. Geochimica et Cosmochimica Acta 59, 1551-1558

Given, R. K., and Wilkinson, B. H. 1985. Kinetic control of morphology, composition, and mineralogy of abiotic sedimentary carbonates. Journal of Sedimentary Petrology 55, 109-119

Golubic, S., Friedmann, I., and Schneider, J. 1981. The lithobiontic ecological niche, with special reference to microorganisms. Journal of Sedimentary Petrology 51, 475-478

Haggerty, J. A. 1991. Evidence from fluid seeps atop serpentine seamount in the Mariana forearc: clues for emplacement of the seamounts and their relationship to forearc tectonics. Marine Geology 102, 293-309

Hardie, L. A. 2003. Secular variations in Precambrian seawater chemistry and the timing of Precambrian aragonite seas and calcite seas. Geology 31, 785-788

Hart, S. R., Blusztajn, J., Dick, H. J. B., and Lawrence, J. R. 1994. Fluid circulation in the oceanic crust: Contrast between volcanic and plutonic regimes. Journal of Geophysical Research 99, 3163-3173

Hellebrand, E., Snow, J. S., and Mühe, R. 2002. Mantle melting beneath Gakkel Ridge (Arctic Ocean): abyssal peridotite spinel compositions. Chemical Geology 182, 227-235

Hinrichs, K.-U., Hayes, J. M., Sylva, S. P., Brewer, P. G., and DeLong, E. F. 1999. Methane-consuming archaebacteria in marine sediments. Nature 398, 802-805

Hodell, D. A., Mead, G. A., and Mueller, P. A. 1990. Variation in the strontium isotopic composition of seawater (8 Ma to present): Implications for chemical weathering rates and dissolved fluxes to the oceans. Chemical Geology 80, 291-307

Hoefs, J. 2004. Stable isotope geochemistry. Springer-Verlag

Hunter, A.G., Kempton, P. D. and Greenwood, P. 1999. Low-temperature fluid-rock interaction – an isotopic and mineralogical perspective of upper crustal evolution, eastern flank of the Juan de Fuca Ridge (JdFR), ODP Leg 168. Chemical Geology 155, 3-28

Irwin, H., Curtis, C., and Coleman, M. 1977. Isotopic evidence for source of diagenetic carbonates formed during burial of organic-rich sediments. Nature 269, 209-213

Ivarsson, M., Lindblom, S., Broman, C., and Holm, N. G. 2008. Fossilized microorganisms associated with zeolite-carbonate interfaces in sub-seafloor hydrothermal environments. Geobiology 6, 155-170

Jöns, N., Bach, W., and Schroeder, T. 2008. Formation and alteration of plagiogranites in an ultramafic-hosted detachment fault at the Mid-Atlantic Ridge (ODP Leg 209). Contribution to Mineralogy and Petrology, doi:10.1007/s00410-008-0357-2

Jones, W. J., Stugard, C. E., and Jannasch, H. W. 1989. Comparison of thermophilic methanogens from submarine hydrothermal vents. Archives of Microbiology 151, 314-318

Kampschulte, A. and Strauss, H. 2004. The sulfur isotopic evolution of Phanerozoic seawater based on the analysis of structurally substituted sulfate in carbonates. Chemical Geology 204, 255-286

Karson, J. A., Früh-Green, G. L., Kelley, D. S., Williams, E. A., Yorger, D. R. and Jakuba, M. 2006. Detachment shear zone of the Atlantis Massif core complex, Mid-Atlantic Ridge, 30°N. Geochemistry Geophysics Geosystems 7, doi:10.1029/2005GC001109

Katz, A., Sass, E., and Starinsky, A. 1972. Strontium behavior in the aragonite-calcite transformation: an experimental study at 40-98°C. Geochimica et Cosmochimica Acta 36, 481-496

Kelley, D. S., Karson, J. A., Früh-Green, G. L., Yoerger, D. R., Shank, T. M., Butterfield, D. A., Hayes, J. M., Schrenk, M. O., Olson, E. J., Proskurowski, G., Jakuba, M., Bradley, A., Larson, B., Ludwig, K., Glickson, D., Buckman, K., Bradley, A. S., Brazelton, W. J., Roe, K., Elend, M. J., Delacour, A., Bernasconi, S. M., Lilley, M. D., Baross, J. A., Summons, R. E., and Sylva, S. P. 2005. A serpentinite-hosted ecosystem: The Lost City Hydrothermal Field. Science 307, 1428-1434

Kelts, K., and McKenzie, J. A. 1982. Diagenetic dolomite formation in Quarternary anoxic diatomaceous muds of Deep Sea Drilling Project Leg 64 , Gulf of California. *In* Curray, J. R., Moore, D. G., et al. eds. Initial Reports. DSDP, 64, 553-569

Kim, S. T., and O'Neil, J. R. 1997. Equilibrium and nonequilibrium oxygen isotope effects in synthetic carbonates. Geochimica et Cosmochimica Acta 61, 3461-3475

Kim, S. T., O'Neil, J. R., Hillaire-Mercel, C., and Mucci, A. 2007. Oxygen isotope fractionation between synthetic aragonite and water: Influence of temperature and Mg^{2+} concentration. Geochimica et Cosmochimica Acta 71, 4704-4715

Konhauser, K. O., Schultze-Lam, S., Ferris, F. G., Fyfe, W. S., Longstaffe, F. J., and Beveridge, T. J. 1994. Mineral precipitation by epilithic biofilms in the Speed River, Ontario, Canada. Applied and Environmental Microbiology 60, 549-553

Konhauser, K. O., and Urrutia, M. M. 1999. Bacterial clay authigenesis: a common biogeochemical process. Chemical Geology 161, 399-413

Li, Y., Takahashi, T., and Broecker, W. S. 1969. Degree of saturation of $CaCO_3$ in the oceans. Journal of Geophysical Research 74, 5507-5525

Linnemann, U., 2004, Sedimentation and geotectonic setting of the basin development of Saxo-Thuringia (Neoproterozoic – Lower Carboniferous): In Linnemann, U., Das Saxothuringikum, 71-110

Lipp, J. S., Morono, Y., Inagaki, F., and Hinrichs, K.-U. 2008. Significant contribution of Archaea to extant biomass in marine subsurface sediments. Nature 454, 991-994

Ludwig, K. A., Kelley, D. S., Butterfield, D. A., Nelson, B. K., and Früh-Green, G. 2006. Formation and evolution of carbonate chimneys at the Lost City Hydrothermal Field. Geochimica et Cosmochimica Acta 70, 3625-3645

Lysnes, K., Thorseth, I. H., Steinsbu, B. O., Øvreås, L., Torsvik, T, and Pedersen, R. B. 2004. Microbial community diversity in seafloor basalt from the Arctic spreading ridges. FEMS Microbiology Ecology 50, 213-230

Mazullo, S. J., Bischoff, W. D., and Teal, C. S. 1995. Holocene shallow-subtidal dolomitization by near-normal seawater, northern Belize. Geology 23, 341-344

McLoughlin, N., Brasier, M. D., Wacey, D., Green, O. R., and Perry, R. S. 2007. On biogenicity criteria for endolithic microborings on early Earth and beyond. Astrobiology 7, 10-26

Michael, P. J., Langmuir, C. H., Dick, H. J. B., Snow, J. E., Goldstein, S. L., Graham, D. W., Lehnert, K., Kurras, G., Jokat, W., Mühe, R., and Edmonds, H. N. 2003. Magmatic and amagmatic seafloor generation at the ultraslow-spreading Gakkel ridge, Arctic Ocean. Nature 423, 956-961

Möller, P., and Bau, M. 1993. Rare-earth patterns with positive cerium anomaly in alkaline waters from Lake Van, Turkey. Earth and Planetary Science Letters 117, 671-676

Moffett, J. W. 1990. Microbially mediated cerium oxidation in sea water. Nature 345, 421-423

Morse, J. W., Gledhill, D. K. and Millero, F. J. 2003. $CaCO_3$ precipitation kinetics in waters from the Great Bahama Bank: implications for the relationship between Bank. Geochimica et Cosmochimica Acta 67, 2819-2826

Morse, J. W., Arvidson, R. S., and Lüttge, A. 2007. Calcium carbonate formation and dissolution. Chemical Reviews 107, 342-381

Mottl, M. J. 1983. Hydrothermal processes at seafloor spreading centers: Application of basalt-seawater experimental results: In Rona, P. A., Bostrom, K., Laubier, L., Smith, K. L. (Eds.), Hydrothermal Processes at Seafloor Spreading Centers, 199-224

Mottl, M. J., and Wheat, C.G. 1994. Hydrothermal circulation through mid-ocean ridge flanks: fluxes of heat and magnesium. Geochimica et Cosmochimica Acta 58, 2225-2237

Mottl, M. J., Komor, S. C., Fryer, P. and Moyer, C. L. 2003. Deep-slap fluids fuel extremophilic Archaea on a Mariana forearc serpentinite mud volcano: Ocean Drilling Program Leg 195. Geochemistry Geophysics Geosystems 4, doi:10.1029/2003GC000588

Mucci, A., and Morse, J. W. 1983. The incorporation of Mg^{2+} and Sr^{2+} into calcite overgrowths: influences of growth rate and solution composition. Geochimica et Cosmochimica Acta 47, 217-233

Muehlenbachs, K., and Clayton, R. N. 1976. Oxygen isotope composition of the ocean crust and its bearing on seawater. Journal of Geophysical Research 81, 4365-4369

Palandri, J. E., and Reed, M. K. 2004. Geochemical models of metasomatism in ultramafic systems: Serpentinization, rodingitization, and sea floor carbonate chimney precipitation. Geochimica et Cosmochimica Acta 68, 1115-1133

Palmer, M. R., and Edmond, J.M. 1989. The strontium isotope budget of the modern ocean. Earth and Planetary Science Letters 92, 11-26

Palmer, M. R. 1992. Controls over the chloride concentration of submarine hydrothermal vent fluids: evidence from Sr/Ca and $^{87}Sr/^{86}Sr$ ratios. Earth and Planetary Science Letters 109, 37-46

Palmer, M. R. and Swihart, G. H. 1996. Boron isotope geochemistry: an overview. In Grew, E. S., and Anowitz, L. M. (Eds), Boron, Mineralogy, Petrology and Geochemistry, Review in Mineralogy 33, 845-862

Peckmann, J., Thiel, V., Michaelis, W., Clari, P., Gaillard, C., Martire, L., and Reitner, J. 1999. Cold seep deposits of Beauvoisin (Oxfordian, southeastern France) and Marmorito (Miocene, northern Italy): microbially induced authigenic carbonates. International Journal of Earth Sciences 88, 60-75

Peckmann, J., Reimer, A., Luth, U., Luth, C., Hansen, B. T., Heinicke, C., Hoefs, J., and Reitner, J. 2001. Methane-derived carbonates and authigenic pyrite from the northwestern Black Sea. Marine Geology 177, 129-150

Peckmann, J., Goedert, J. L., Thiel, V., Michaelis, W., and Reitner, J. 2002. A comprehensive approach to the study of methane-seep deposits from the Lincoln Creek Formation, western Washington State, USA. Sedimentology 49, 855-873

Peckmann, J. and Thiel, V. 2004. Carbon cycling at ancient methane-seeps. Chemical Geology 205, 443-467

Peckmann, J., Bach, W., Behrens, K., and Reitner, J. 2008. Putative cryptoendolithic life in Devonian pillow basalt, Rheinisches Schiefergebirge, Germany. Geobiology 6, 125-135

Perner, M., Kuever, J., Seifert, R., Pape, T., Koschinsky, A., Schmidt, K., Strauss, H., and Imhoff, J. F. 2007. The influence of ultramafic rocks on microbial communities at the Logatchev hydrothermal field, located 15°N on the Mid-Atlantic Ridge. FEMS Microbiology Ecology 61, 97-109

Pichler, T, and Veizer, J. 2004. The precipitation of aragonite from shallow-water hydrothermal fluids in a coral reef; Tutum Bay, Ambitle Island, Papua New Guinea. Chemical Geology 207, 31-45

Pourret, O., Davranche, M., Gruau, G., and Dia, A. 2008. New insights into cerium anomalies in organic-rich alkaline waters. Chemical Geology 251, 120-127

Proskurowski, G., Lilley, M. D., Seewald, J. S., Früh-Green, G. L., Olson, E. J., Lupton, J. E., Sylva, S. P., and Kelley, D. S. 2008. Abiogenic hydrocarbon production at Lost City hydrothermal field. Science. 319, 604-607

Ribeiro da Costa, I., Barriga, F. J. A. S., and Taylor, R. N. 2008. Late seafloor carbonate precipitation in serpentinites from the Rainbow and Saldanha sites (Mid-Atlantic Ridge). European Journal of Mineralogy 20, 173-181

Ridgwell, A. and Zeebe, R. E. 2005. The role of the global carbonate cycle in the regulation and evolution of the Earth system. Earth and Planetary Science Letters 234, 299-315

Roberts, J. A., Bennett, P. C., Gonzales, L. A., MacPherson, G. L., and Milliken, K. L. 2004. Microbial precipitation of dolomite in methanogenic groundwaters. Geology 32, 277-280

Rogers, J. R., and Bennett, P. C. 2004. Mineral stimulation of subsurface microorganisms: release of limiting nutrients from silicates. Chemical Geology 203, 91-108

Romanek, C. S., Grossman, E. L. and Morse, J. W. 1992. Carbon isotope fractionation in synthetic aragonite and calcite: effects of temperature and precipitation rate. Geochimica et Cosmochimica Acta 56, 419-430

Rubinson, M. and Clayton, R. M. 1969. Carbon-13 fractionation between aragonite and calcite. Geochimica at Cosmochimica Acta 33, 997-1002

Ryan, P. C., and Hillier, S. 2002. Bertherine/chamosite, corrensite, and discrete chlorite from evolved verdine and evaporate-associated facies in the Jurassic Sundance Formation, Wyoming. American Mineralogist 87, 1607-1615

Santelli, C. M., Orcutt, B. N., Banning, E., Bach, W., Moyer, C. L., Sogin, M. L., Staudigel, H., and Edwards, K. J. 2008. Abundance and diversity of microbial life in ocean crust. Nature 453, 653-657

Schmidt, K., Koschinsky, A., Garbe-Schönberg, D., de Carvalho, L. M., and Seifert, R. 2007. Geochemistry of hydrothermal fluids from the ultramafic-hosted Logatchev hydrothermal field, 15°N on the Mid-Atlantic Ridge: Temporal and spatial investigation. Chemical Geology 242, 1-21

Schulte, M., Blake, D., Hoehler T., and McCollom, T. 2006. Serpentinization and its implications for life on the early Earth and Mars. Astrobiology 6, 364-376

Schumann, G., Manz, W., Reitner, J., and Lustrino, M. 2004. Ancient fungal life in North Pacific Eocene oceanic crust. Geomicrobiology Journal 21, 241-246

Seewald, J. S., and Seyfried, Jr. W. E. 1990. The effect of temperature on metal mobility in subseafloor hydrothermal systems: constraints from basalt alteration experiments. Earth and Planetary Science Letters 101, 388-403

Shields, G. A., and Webb, G. E. 2004. Has the REE composition of seawater changed over geological time? Chemical Geology 204, 103-107

Sohn, R. A., Willis, C., Humphris, S., Shank, T. M., Singh, H., Edmonds, H. N., Kunz, C., Hedman, U., Helmke, E., Jakuba, M., Liljebladh, B., Linder, J., Murphy, C., Nakamura, K., Sato, T., Schlindwein, V., Stranne, C., Tausenfreund, M., Upchurch, L., Winsor, P., Jakobsson, M., and Soule, A. 2008. Explosive volcanism on the ultraslow-spreading Gakkel ridge, Arctic Ocean. Nature 453, 1236-1238

Staudigel, H., Muehlenbachs, K., Richardson, S. H., and Hart, S. R. 1981. Agents of low temperature ocean crust alteration. Contributions to Mineralogy and Petrology 77, 150-157

Staudigel, H., Hart, S. R., and Richardson, S. H. 1981. Alteration of the oceanic crust: processes and timing. Earth and Planetary Science Letters 52, 311-327

Staudigel, H., Furnes, H., Banerjee, N. R., Dilek, Y., and Muehlenbachs, K. 2006. Microbes and volcanoes: A tale from the oceans, ophiolites, and greenstone belts. GSA Today 16, 4-10

Staudigel, H., Furnes, H., McLoughlin, N., Banerjee, N. R. Connell, L. B., and Templeton, A. 2008. 3.5 billion years of glass bioalteration: Volcanic rocks as a basis for microbial life? Earth Science Reviews 89, 156-176

Stein, C. A. and Stein, S. 1994. Constraints on hydrothermal heat flux through the oceanic lithosphere from global heat flow. Journal of Geophysical Research 99, 3081-3095

Stetter, K. O. 2006. Hyperthermophiles in the history of life. Philosophical Transactions of the Royal Society B. 361, 1837-1843

Storrie-Lombardi, M. C., and Fisk, M. R. 2004. Elemental abundance distributions in suboceanic basalt glass: evidence of biogenic alteration. Geochemistry, Geophysics, Geosystems 5, doi: 10.1029/2004GC000755

Sun, S. S., and McDonough, W. F. 1989. Chemical and isotopic systematics of oceanic basalts: implications for mantle composition and processes. In Saunders, A.D., Norry, M.J. (Eds.), Magmatism of the ocean basins. Geological Society Special Publications 42, 313-345

Teagle, D. A. H., Alt, J. C., and Halliday, A. N. 1998. Tracing the chemical evolution of fluids during hydrothermal recharge: Constraints from anhydrite recovered in ODP Hole 504B. Earth and Planetary Science Letters 155, 167-182

Thorseth, I. H., Furnes, H., and Heldal, M. 1992. The importance of microbiological activity in the alteration of natural basaltic glass. Geochimica et Cosmochimica Acta 56, 845-850

Thorseth, I. H., Torsvik, T., Furnes, H., and Muehlenbachs, K. 1995. Microbes play an important role in the alteration of ocean crust. Chemical Geology 126, 137-146

Thorseth, I. H., Torsvik, T., Torsvik, V., Daae, F. L., Pedersen, R. B., and Keldysh-98 Scientific Party, 2001. Diversity of life in ocean floor basalt. Chemical Geology 194, 31-37

Thorseth, I. H., Pedersen, R. B., and Christie, D. M. 2003. Microbial alteration of 0-30 Ma seafloor and sub-seafloor basaltic glasses from the Australian Antarctic discordance. Earth and Planetary Science Letters 215, 237-247

Tivey, M. K., Hunphris, S. E., Thompson, G., Hannington, M. D., and Rona, P.A. 1995. Deducing patterns of fluid flow and mixing within the active TAG mound using mineralogical and geochemical data. Journal of Geophysical Research 100, 12527-12555

Tivey, M. K. 2007. Generation of seafloor hydrothermal vent fluids and associated mineral deposits. Oceanography 20, 50-65

Tucholke, B. E., and Lin, J. 1994. A geological model for the structure of ridge segments in slow spreading ocean crust. Journal of Geophysical Research 99, 11937-11958

Von Damm, K. L. 1990. Seafloor hydrothermal activity: Black smoker chemistry and chimneys. Annual Reviews of Earth and Planetary Sciences 18, 173-204

Van Lith, Y., Warthmann, R., Vasconcelos, C., and McKenzie, J. A. 2003. Sulphate-reducing bacteria induce low-temperature Ca-dolomite and high Mg-calcite formation. Geobiology 1, 71-79

Vasconcelos, C., McKenzie, J. A., Bernasconi, S., Grujic, D., and Tien, A. J. 1995. Microbial mediation as a possible mechanism for natural dolomite formation at low temperatures. Nature 377, 220-222

Vasconcelos, C., McKenzie, J. A., Warthmann, R., and Bernasconi, S. M. 2005. Calibration of the $\delta^{18}O$ paleothermometer for dolomite precipitated in microbial cultures and neutral environments. Geology 33, 317-320

Veizer, J. 1983. Trace elements and isotopes in sedimentary carbonates. In Reeder, R. J. Carbonates: Mineralogy and Chemistry 11, 265-300

Walton, A. W. 2008. Microtubules in basalt glass from Hawaii Scientific Drilling Project #2 phase 1 core and Hilina slope, Hawaii: evidence of the occurrence and behavior of endolithic microorganisms. Geobiology 6, 351-364

Warren, J. 2000. Dolomite: occurrence, evolution and economically important associations. Earth Science Reviews 52, 1-81

Warthmann, R., Van Lith, Y., Vasconcelos, C., McKenzie, J. A., and Karpoff, A. M. 2000. Bacterially induced dolomite precipitation in anoxic culture experiments. Geology 28, 1091-1094

Wasylenki, L. E., Dove, P. M., Wilson, D. S., and de Yoreo, J. L. 2005. Nanoscale effects of strontium on calcite growth: an in situ AFM study in the absence of vital effects. Geochimica et Cosmochimica Acta 69, 3017-3027

Weissert, H., and Bernoulli, D. 1984. Oxygen isotope composition of calcite in Alpine ophiocarbonates: a hydrothermal or Alpine metamorphic signal? Eclogae Geologae Helveticae 77, 29-43

Wheat, C. G., and Mottl, M. J. 2000. Composition of pore and spring waters from baby Bare: Global implications of geochemical fluxes from a ridge flank hydrothermal system. Geochimica et Cosmochimica Acta 64, 629-642

Wheat, C. G., Elderfield, H., Mottl, M. J., and Monnin, C. 2000. Chemical composition of basement fluids within an oceanic ridge flank: Implications for along-strike and across-strike hydrothermal circulation. Journal of Geophysical Research 105, 13437-13447

Whiticar, M. J. 1999. Carbon and hydrogen isotope systematics of bacterial formation and oxidation of methane. Chemical Geology 161, 291-314

Zeebe, R. E., and Wolf-Gladrow, D. 2005. CO_2 in seawater: equilibrium, kinetics, isotopes. Elsevier Oceanography Series 65

Zheng, Y. F. 1999. Oxygen isotope fractionation in carbonate and sulfate minerals. Geochemical Journal 33, 109-126

ACKNOWLEDGEMENTS

Although it is almost impossible to thank all the people who supported me during the last years, I would like to thank all these people for their continuous enthusiasm and for keeping me interesting.

First of all, I would like to thank Jörn Peckmann for giving me the opportunity to work on the interface between hard rock geology and geobiology and for creating a really nice atmosphere. I especially appreciated the trust, freedom and great enthusiasm during the years.

Many thanks to Wolfgang Bach for being my second supervisor, for all your support throughout the years, especially for the fruitful discussions and for introducing me to the world of thermodynamics.

There are many people who supported me during my analytical methods. I would like to start thanking Yuangao Qu, Matthias Gothieu and Sebastian Flotow for the continuous preparation of thin sections, which were the basis of my study. Furthermore, thanks to Andreas Klügel and Heike Anders for their laboratory assistance and for introducing me to the use of the LA-ICP-MS technique. Thanks to Till Heinrichs for help with FE-SEM analyses and Barbara Mader for assistance during electron microprobe analyses.

Special thanks to all the members of the Geobiology Group for all discussions and support. I'll never forget our activities beyond the science, especially the Boßel tours. I'm lucky to have done my PhD work in such a great working group. I really enjoyed the monthly breakfasts we had during the years.

Thanks to Jim and Jörn for the great trip to Oregon. I'll never forget how cold the nights could be in August!

Thanks to Julio, Arne, Simone, Antonie, Frauke, Simone, Nadine, Verena, Solveig, Julius, Lars, Tobias H., Florian, Marcus, Daniel, Marcos, Pamela, Esther, Yu-Shih, Kai, Birgit, Xavi, Sebastian, Tobias E., Matthias, Xiaolei, Florence, Henning, Boonraksa, Steffi L., Steffi T., Kai and Jörn for a nice time.

Many thanks to Frauke for a great time and … for everything. I'm glad that we met again here in Bremen – "mein lieber Herr Gesangsverein!."

Frieder, thanks for all activities beyond the university. I really enjoyed our great trip to Volcano Island …the best place for geologists.

My deepest thanks go to my family and my friends. Thank you for always being there for me!

ERKLÄRUNG

Name: Benjamin Eickmann **Datum:** 11.03.2009

Anschrift: Beim Steinernen Kreuz 7, 28203 Bremen

Hiermit versichere ich, dass ich

1. die Arbeit ohne unerlaubte fremde Hilfe angefertigt habe,
2. keine anderen als die von mir angebenden Quelle und Hilfsmittel benutzt habe und
3. die den benutzen Werken wörtlich oder inhaltlich entnommenen Stellen als solche kenntlich gemacht habe.

Bremen, den 11.03.2009

Benjamin Eickmann